2004

NUMERICAL INVESTIGATION OF THERMAL TRANSPORT MECHANISMS DURING ULTRA-FAST LASER HEATING OF NANO-FILMS USING 3-D DUAL PHASE LAG (DPL) MODEL

Illayathambi Kunadian
University of Kentucky, ikuna0@engr.uky.edu

ABSTRACT OF THESIS

NUMERICAL INVESTIGATION OF THERMAL TRANSPORT MECHANISMS DURING ULTRA-FAST LASER HEATING OF NANO-FILMS USING 3-D DUAL PHASE LAG (DPL) MODEL

Ultra-fast laser heating of nano-films is investigated using 3-D Dual Phase Lag heat transport equation with laser heating at different locations on the metal film. The energy absorption rate, which is used to model femtosecond laser heating, is modified to accommodate for three-dimensional laser heating. A numerical solution based on an explicit finite-difference method is employed to solve the DPL equation. The stability criterion for selecting a time step size is obtained using von Neumann eigenmode analysis, and grid function convergence tests are performed. DPL results are compared our results with classical diffusion and hyperbolic heat conduction models and significant differences among these three approaches are demonstrated. We also develop an implicit finite-difference scheme of Crank–Nicolson type for solving 1-D and 3-D DPL equations. The proposed numerical technique solves one equation unlike other techniques available in the literature, which split the DPL equation into a system of two equations and then apply discretization. Stability analysis is performed using a von Neumann stability analysis. In 3-D, the discretized equation is solved using δ-*form* Douglas and Gunn time splitting. The performance of the proposed numerical technique is compared with the numerical techniques available in the literature.

KEYWORDS: 3-D femtosecond laser heating, 3-D explicit finite-difference scheme, 3-D implicit finite-difference scheme, Douglas-Gunn time-splitting, von Neumann stability analysis

Illayathambi Kunadian
July 26, 2004

NUMERICAL INVESTIGATION OF THERMAL TRANSPORT MECHANISMS DURING ULTRA-FAST LASER HEATING OF NANO-FILMS USING 3-D DUAL PHASE LAG (DPL) MODEL

By

Illayathambi Kunadian

James M. McDonough, Ph.D.
Co-Director of Thesis

Kaveh A. Tagavi, Ph.D.
Co-Director of Thesis

George Huang, Ph.D.
Director of Graduate Studies

July 26, 2004

RULES FOR THE USE OF THESES

Unpublished theses submitted for the Master's degree and deposited in the University of Kentucky Library are as a rule open for inspection, but are to be used only with due regard to the rights of the authors. Bibliographical references may be noted, but quotations or summaries of parts may be published only with the permission of the author, and with the usual scholarly acknowledgments.

Extensive copying or publication of the thesis in whole or in part also requires the consent of the Dean of the Graduate School of the University of Kentucky.

THESIS

Illayathambi Kunadian

The Graduate School

University of Kentucky

2004

NUMERICAL INVESTIGATION OF THERMAL TRANSPORT MECHANISMS DURING ULTRA-FAST LASER HEATING OF NANO-FILMS USING 3-D DUAL PHASE LAG (DPL) MODEL

THESIS

A thesis submitted in partial fulfillment of the
requirements for the degree of Master of Science in Mechanical Engineering
in the College of Engineering at the University of Kentucky

By

Illayathambi Kunadian

Co-Directors: Dr. James M. McDonough, Professor of Mechanical Engineering and Mathematics
and Dr. Kaveh A. Tagavi, Professor of Mechanical Engineering

Lexington, Kentucky

2004

Acknowledgments

The author deeply appreciates the guidance and instructive comments of his adviser Dr. James M. McDonough, and co-adviser Dr. K. A. Tagavi throughout this work. This work would have been impossible without their support. He would like to thank Dr. M. P. Mengüç for taking the time to serve on the final examination committee. He would like to thank Dr. Yang for helpful discussions and continuous support of his work. He would like to thank his parents for their love, support and encouragement throughout his life. He also would like to thank his brother Dr. Babu Kunadian for supporting him to pursue graduate education at the University of Kentucky.

Contents

List of Figures

List of Tables

List of Files

IKthesis.pdf . . . . . 816 KB

Chapter 1
INTRODUCTION

In this chapter, a brief description of the challenges in microscale heat transfer [71] will be presented. Following this the objectives of this research and the framework of thesis will be discussed briefly.

1.1 Challenges in Microscale Heat Transfer

Heat transport requires sufficient collisions among energy carriers irrespective of the conducting medium. Electrons and phonons are the energy carriers in metals and phonons are the primary energy carriers in dielectric crystals, insulators, and semiconductors. The phonon gas is viewed as a group of "mass particles" that characterize the energy state of a metal lattice. The energy state of the metal lattice vibrating at a frequency ν at a certain temperature T, and hence the energy state of the phonon, is given by

$$E = h\nu, \tag{1.1}$$

where h is the Planck constant.

Energy transport from one lattice to the other occurs as a consequence of a series of phonon collisions in time history (see Fig. 1.1, reproduced from Tzou [71]). The mean free path can be defined as the algebraic mean of the distances traveled by a phonon between two successive collisions with other phonons and mean free time can be defined as the algebraic mean of the times traveled by a phonon between two successive collisions with other phonons. Sufficiently long time is required to have a statistically meaningful concept of mean free path and time for phonon collisions. The mean free time, or *relaxation time*, is of the order of

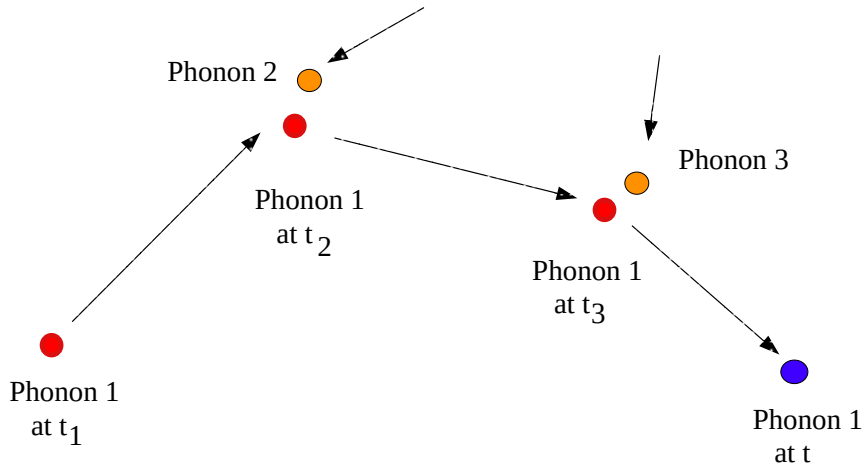

Figure 1.1 Energy transport through phonon collision. The mean free path for phonon 1 in successive collision is $(d_1 + d_2 + d_3)/3$. The mean free "time" for phonon 1 in successive collisions is $(t - t_1)/3$ (adapted from [71]).

picoseconds for metals and nanosecond to picoseconds for dielectric crystals and insulators. The mean free path for electrons is of the order of tens of nanometers ($10^{-8}m$) at room temperature.

Microscale heat transfer with response time shorter than a nanosecond has received special attention because the physical dimension in microscale heat transfer is of the same order of magnitude as the mean free path, and consequently, the response time in heat transport is of the same magnitude as the mean free time. In macroscopic heat transfer the temperature gradient may lose its physical meaning for a thin film of thickness of the same order of magnitude as the mean free path and the response time of the same order of magnitude as the mean free time; consequently the conventional way of defining the heat flux vector according to Fourier's law becomes questionable. Phonons propagate at the speed of sound depending on the type of solid medium, on average, which is of the order of 10^4 to $10^5 m/s$ at room temperature. Thus, a response time of the order of picoseconds implies a penetration depth

of the order of submicrons, necessitating a simultaneous consideration of the microscopic effect in space.

In order to ensure reliable performance and longevity of micro-electronic and photonic devices, it is imperative that effective means for heat removal at short times, based on the ultrafast transient responses in micro- and nano-scale, is ensured. In giga-hertz to tetra-hertz photonic devices, the response time enters the physical domain of the thermalization and relaxation time of the energy carriers resulting in excessively high temperature at short times, causing early-time thermal damage before steady state operations can occur. In order to ensure superior thermal performance of such micro-electronic and photonic devices detailed understanding of the micro- to nanoscale thermal transport mechanisms is very important.

1.2 Objectives

Recently, an increasing interest has developed in the use of short-pulse lasers in numerous applications related to microfabrication and material processing of thin film structures [10, 17, 56, 62], scientific research [46] (e.g. study of heat transfer behavior in micro-photonic or electronic devices) and medicine (laser surgery [13]). High power short-pulse lasers [12, 37, 40] (on the order of femtoseconds) have given rise to several innovative technologies and have brought considerable attention to the thermal transport mechanisms occurring in materials during and after short-pulse laser material interaction.

From a microscopic point of view, ultrafast laser heating of metals is composed of three processes: deposition of radiation energy on electrons, transport of energy by electrons and heating of the material lattice through electron-phonon interactions. In dielectric films, insulators and semiconductors, the process of heat transport is governed by phonon scattering.

Classical heat conduction theory, established on the macroscopic level fails for microscale conditions ($10^{-6} - 10^{-9}m$) because they describe macroscopic behavior averaged over many grains. During a relatively slow heating process, the deposition of radiation energy can be assumed to be instantaneous and can be modeled by Fourier conduction; but applicability of this approach to very short-pulse laser applications becomes questionable. We must look for non-Fourier models because the laser pulse duration is shorter than the thermalization time (time required for the phonons and electrons to reach thermal equilibrium) and relaxation time (characteristic time for the activation of the ballistic behavior in the electron gas) in the electron-phonon system [65, 66]. In the case of dielectric crystals, if the response time is of the same order of magnitude as the relaxation time of the Umklapp process (the characteristic time in which momentum is non-conserving in phonon collisions), the microscopic process describing the phonon scattering from the grain boundaries needs to be accomodated.

The Cattaneo-Vernotte (CV) wave equation in the thermal wave theory describes the inertial effect in the short-time transient, assuming a macroscopic behavior averaged over many grains. When the microstructural effects are predominant (resulting from shortening of response time), the concept of macroscopic average may lose its physical significance. Also, it has been shown that the hyperbolic heat conduction model (CV model) suffers from violation of the second law of thermodynamics, and physically unrealistic solutions are therefore unavoidable [5, 6, 69].

Kagnov et al. [52] described the microscopic exchange between electrons and phonons followed by the phenomenological two-step model [14] proposed by Anisimov describing the temperatures of the electron gas and metal lattice during short-pulse laser heating of metals.

Later, Qiu and Tien [65, 66] rigorously derived the two-step models from solution of the Boltzmann equation. Qiu and Tien [65] numerically solved the hyperbolic two-step model by considering a $96fs$ duration laser pulse irradiating a thin film of thickness $0.1\mu m$. The predicted temperature change of the electron gas during the picosecond transient agreed well with the experimental data, supporting the validity of the hyperbolic two-step model for describing the heat transfer mechanisms during short-pulse laser heating of metals.

Even though we have a microscopic model that works quite well, when investigating macroscopic effects a different model is required. Tzou proposed the dual phase lag model (DPL model) [71, 72, 73, 74] that has the capability of capturing a wide range of physical responses, from microscopic to macroscopic scales, in both space and time under special values of relaxation times associated, separately, with temperature gradient and heat flux.

The analytical solution for the DPL model is restricted to linear problems, but problems in most real life situations always involve nonlinear material properties and complex physical geometries. Due to these nonlinearities analytical solution of the DPL model can be impossible. Over the years, several finite-difference approaches have been successfully employed to solve the DPL equation. For example, femtosecond laser heating of thin metal films has been successfully modeled numerically using the DPL model in 3D [29]. Yet, three-dimensional aspects of laser heating of thin metal films have not been previously investigated. In this research ultra-fast laser heating of gold film will be investigated using an explicit finite difference scheme to solve the DPL model in three dimensions with laser heating at different locations of the film.

1.3 Framework of Thesis

A detailed summary of the various heat transfer models including macroscopic models (classical heat conduction model, hyperbolic heat conduction model or thermal wave model [76, 14]), microscale heat transfer models (microscopic two-step model or phonon-electron interaction model [4], phonon-scattering model [45] and phonon radiative transfer model [60]), and the dual phase lag model [71, 72, 73, 74] will be presented in Chapter II.

The classical problem of heat conduction in a solid bar will be investigated in Chapter III. Heat conduction in a semi-infinite solid slab starting from a stationary state subjected to a sudden temperature rise at the surface boundary will be investigated. An explicit finite difference scheme [75] is employed for this problem, and one-dimensional stability and convergence criteria derived using von Neumann stability analysis [2] is presented. The numerical results are compared with the available analytical solution. It is shown that the DPL model can be reduced to all of parabolic, hyperbolic, phonon scattering or phonon-electron interaction models under different values of relaxation times (corresponding to temperature gradient and heat flux). The problem involving heat conduction in a solid slab subjected to temperature rise at both ends of the slab will be also be examined. The problem of violation of second law of thermodynamics, causality and maximum principle by the hyperbolic heat conduction model will be explained with the help of this example.

In Chapter IV, numerical simulation of femtosecond pulse laser heating of sub-micron sized gold film will be examined using the DPL model [71, 72, 73, 74] under different values of relaxation times, and comparing the computed results with the experimental results by Brorson *et al.* [12], and Qiu and Tien [65, 66]. An explicit finite- difference scheme is

employed to solve the DPL equation, and one-dimensional stability criteria derived using von Neumann stability analysis [16] is presented. No energy loss is expected to occur during the picosecond transient, therefore both the front and rear surface boundaries are assumed to be thermally insulated. The energy absorption rate is used to model the femtosecond pulse laser heating. The normalized reflectivity change recorded in the experiments is converted into normalized temperature change by a direct correlation.

In continuing the investigation of the transient response on a sub-micron sized gold film, a three-dimensional formulation for the same problem, will be presented in Chapter V. We will also consider laser heating at different locations of the gold film. The finite-difference method for this problem is presented along with three-dimensional stability criteria derived using von Neumann stability analysis. The source term is modified to accomodate the three-dimensional laser heating at different locations of the gold film. The DPL model is reduced to parabolic and hyperbolic models under different values of relaxation times. Significant differences seen in the results among DPL, parabolic and hyperbolic models will be explained.

In Chapter VI, we will develop an implicit finite-difference scheme of the Crank–Nicolson type for solving the one-dimensional DPL equation. Grid function convergence tests will be performed to test the convergence of the numerical solution. Stability analysis will be performed using a von Neumann stability analysis. We will show that the proposed numerical technique is unconditionally stable. For the sake of comparison we will develop a numerical procedure for the semi-infinite slab problem considered in Chapter III. The numerical technique will be extended to three-dimensions and a numerical procedure for computing the transient temperature distribution during short pulse laser heating of thin films will be

presented. The discretized 3-D microscale DPL equation is then solved using using δ-*form* Douglas and Gunn time-splitting technique. The performance of the proposed numerical technique will be compared with the numerical techniques available in the literature.

Chapter 2
OVERVIEW OF DIFFERENT HEAT TRANSFER MODELS

In this chapter a detailed summary of the various heat transfer models including macroscopic models (classical heat conduction model, hyperbolic heat conduction model or thermal wave model [76, 14]), microscale heat transfer models (microscopic two-step model or phonon-electron interaction model [4], phonon-scattering model [45] and phonon radiative transfer model [60]), and the dual phase lag model [71, 72, 73, 74] will be presented. The various analytic and numerical models developed to solve the DPL equation will be discussed.

2.1 Introduction

The microscopic models namely the phonon-electron interaction model (two-step models) [4], the phonon scattering model [45], and the phonon radiative transfer model (PRT) [60] resulted from the solutions of semi-classical Boltzmann transport equation. The phonon-electron interaction model (two-step model) describes the microscopic heat transfer mechanism between phonons and electrons in metal. The phonon scattering model describes the heat transfer mechanism for phonon collisions in a pure phonon field. The phonon radiative transfer model describes the heat transfer mechanism in an acoustically thin medium. The acoustically "thin" or "thick" medium refers to the thickness of film structure relative to the phonon mean free path. For an acoustically thin medium, the thickness of the film is much less than the mean free path of phonons.

Other models include the Fourier diffusion model, the thermal wave model (CV wave) [14, 76], Jeffrey's heat flux equation [49, 50], the Gurtin-Pipkin model [44, 49], the frac-

tal model [35, 39, 42, 48], and the dual phase lag (DPL) model [71, 72, 73, 74]. Classical Fourier diffusion describes the relationship between the heat flux and the temperature gradient in macroscale heat transfer. The thermal wave model depicts a temperature disturbance propagating as a wave, with thermal diffusivity acting as a damping effect in heat propagation. Jeffrey's heat flux equation is used for describing thermal relaxation behavior, and the Gurtin-Pipkin model describes the thermal relaxation in both the heat flux and internal energy during fast transient response. The fractal model is employed for describing the conducting path in amorphous material and the scattering of fractons over the correlation length on a small scale. The DPL model includes the effects of delay times due to microscale effects on the transient response.

2.2 Heat Transfer Models

The following subsections provide details of various heat transfer models, demonstrating the physical and mathematical interpretations of each model. The problem of switching from one model to another, and complexity of studying microscale effects will be shown. The universality of the DPL model will be shown by comparing it with the other models.

2.2.1 Parabolic Heat Conduction Model

According to classical heat conduction theory heat flux is directly proportional to the temperature gradient (Fourier's law) in the form

$$\boldsymbol{q}(\boldsymbol{r}, t) = -k\nabla T(\boldsymbol{r}, t), \tag{2.1}$$

with $\boldsymbol{r}$ denoting the position vector of the material volume, t the physical time, $\boldsymbol{q}$ the heat flux vector and k the thermal conductivity. When the above equation is incorporated into

the first law of thermodynamics,

$$-\nabla \cdot \boldsymbol{q}(\boldsymbol{r}, t) = \rho C_p \frac{\partial T(\boldsymbol{r}, t)}{\partial t}, \tag{2.2}$$

a parabolic heat conduction equation for the temperature field is obtained:

$$\frac{\partial T}{\partial t} = \alpha \nabla^2 T, \tag{2.3}$$

with

$$\alpha = \frac{k}{\rho C_p}, \tag{2.4}$$

where α is the thermal diffusivity, ρ is the density and C_p is the volumetric heat capacity.

Although Fourier's law represents one of the best known models in mathematical physics, it possesses anomalies, the most predominant being its prediction that heat conduction is a diffusion phenomenon in which temperature disturbances will propagate at infinite velocities, implying that a thermal disturbance applied at a certain location in a solid medium can be sensed immediately anywhere else in the medium (violating precepts of special relativity).

The parabolic character of Fourier's law implies that the heat flow starts (vanishes) simultaneous with the appearance (disappearance) of a temperature gradient, thus violating the causality principle, which states that two events, which are causally correlated, cannot happen at the same time; but the cause must precede the effect, as noted by Cimmelli [19]. In situations dealing with transient heat flow for extremely short periods of time (e.g., applications involving laser pulses of nanosecond or less duration [65]), high heat fluxes, and at temperatures near absolute zero (heat conduction at cryogenic temperatures), Fourier's law fails to predict the correct temperature distribution [19].

2.2.2 Hyperbolic Heat Conduction Model

In order to address these discrepancies, a modified heat flux that accommodates the finite propagation speed of observed thermal waves was proposed by Vernotte [76] and Cattaneo [14] in 1958:

$$\boldsymbol{q}(\boldsymbol{r},t) + \tau \frac{\partial \boldsymbol{q}(\boldsymbol{r},t)}{\partial t} = -k\nabla T(\boldsymbol{r},t), \tag{2.5}$$

where τ is the relaxation time, which is the effective mean free path λ divided by the phonon speed (v, speed of sound in the medium). In the absence of relaxation time ($\tau = 0$), implying infinite phonon speed or zero mean free path, Eq. (2.5) reduces to the classical Fourier's law. When Eq. (2.5) is coupled with the energy Eq. (2.2) we obtain the conventional hyperbolic heat conduction equation (CHE);

$$\frac{1}{\alpha}\frac{\partial T}{\partial t} + \frac{1}{v^2}\,\frac{\partial^2 T}{\partial t^2} = \nabla^2 T, \tag{2.6}$$

with

$$V = \sqrt{\frac{\alpha}{\tau}}. \tag{2.7}$$

Eq. (2.6) is the thermal wave equation depicting a temperature disturbance propagating as a wave with thermal diffusivity appearing as a damping effect in heat propagation. The quantity v is the thermal wave speed which approaches infinity when $\tau \to 0$, reducing Eq. (2.6) to the classical diffusion equation.

The frequently cited experimental evidence for validity of hyperbolic heat conduction includes that of Kaminski [54] and Mitra et al. [61], who investigated wet sand and processed meat, respectively. But later investigations by Graβmann et al. [41] and Herwig et al. [47] clearly showed that the hyperbolic effect does not appear in the experiments for the materials

studied by Kaminski and Mitra et al. To date, there has been no clear experimental evidence supporting hyperbolic heat conduction although wave nature has been observed by Peshkov [64] using superfluid liquid helium at temperature near absolute zero. He referred to this phenomenon as second sound, because of similarity between observed thermal and ordinary acoustic waves. Also, the HHCE neglects the energy exchange between the electrons and the lattice, and so its applicability to short-pulse laser applications becomes questionable.

Over the years there has been some confusion over whether the conventional hyperbolic heat conduction equation (CHE) is compatible with the second law of thermodynamics. Barletta and Zanchini [6] pointed out that the CV wave equation is not compatible with the local equilibrium scheme. Within the scheme of local equilibrium, Clausius' inequality implies that the entropy production rate must be non-negative. This was checked by determining the entropy production rate per unit volume in a solid slab subjected to sudden temperature rise on its boundaries. It was found that the temperature rise in the interior of the slab was accompanied by negative values of entropy. Therefore no violation of second law occurs, because the local equilibrium scheme does not hold and the temperature field cannot be interpreted in the usual thermodynamic sense.

This phenomena was also observed by Taitel [69] who noted that the transient temperature rise may exceed the temperature of the boundaries as well as the initial temperature of the layer. He also notes that even though one may argue that thermodynamically (second law considerations) this solution is acceptable [53] it still seems to be unrealistic for gaseous material and possibly for most solids [9]. He concludes that the hyperbolic heat conduction equation is at most an approximation which is not valid for short periods of time, and in

this sense it is not much better than the conventional diffusion equation. It is therefore quite expected that both the equations (CV wave and parabolic) lead to physical distortion like infinite propagation speed (parabolic) and temperature overshoot (CV wave).

Korner and Bergmann [57] investigate CHE on a microscopic scale from a physical point of view starting from the Boltzmann transport equations. They find that the hyperbolic approach to the heat current density violates the fundamental law of energy conservation. They show that the modified Fourier's law given by Eq. (2.5) is based on an electron distribution function f which does not obey the law of conservation of energy. As a consequence, the CHE predicts physically impossible solutions with a negative local heat content. In order to compensate for the defects in the conventional HHCE, Bai and Lavine [5] modified the HHCE by simply adding terms to the energy balance while making no attempt to eliminate the unrealistic results.

Within nonequilibrium thermodynamics there are two schools of thought: one based on extended irreversible thermodynamics and the other based on rational thermodynamics [20]. Both schools allow that under nonequilibrium conditions, entropy production may depend on heat flux. Then, using CV equation for heat flux in the expression for entropy production rate, it has been shown that there are a variety of expressions for entropy that makes non-negative entropy production possible [51]. Thus, CHE itself is compatible with the second law. The extended irreversible thermodynamics argument ends there, concluding that the CHE is compatible with the second law of thermodynamics. However Coleman et al. [20] showed (in the context of nonequilibrium rational thermodynamics) that CHE is not consistent with the second law of thermodynamics, and presents a modified system also

called the "modified hyperbolic type heat conduction equation" or MHE.

CV Equation:

$$\tau(T)\frac{\partial q}{\partial t} + q + k(T)\frac{\partial q}{\partial x} = 0 \tag{2.8}$$

First Law:

$$\frac{\partial q}{\partial x} + \left[\rho c(T) + q^2 \frac{d}{dT} a(T)\right] \frac{\partial T}{\partial t} + 2a(T) q \frac{\partial q}{\partial t} = g \tag{2.9}$$

where q is the heat flux, and g is the heat source per unit volume. Coleman et al. [20, 21] showed that if the entropy depends upon heat flux, so must internal energy, and derived unique expressions for entropy and internal energy which allow the second law to be satisfied.

Bai and Lavine [5] have solved the MHE for a one-dimensional solid slab subject to a sudden temperature change on both sides. Initially the slab is at temperature T_0, and for $t > 0$, the temperature of both boundary surfaces (at $x = 0, l$) is dropped to T_W ($T_W < T_0$). Even though modification has been done to the energy equation to fix the problem of violation of the second law of thermodynamics, the MHE still violates the second law of thermodynamics and is not much different from the conventional hyperbolic heat conduction equation.

2.2.3 Phonon-Electron Interaction Model

Anisimov et al. [4] proposed a two-step model to describe the electron temperature T_e and the lattice temperature T_l during the short-pulse laser heating of metals. Later, Qiu and Tien [65, 66] rigorously derived the hyperbolic two-step model from the Boltzmann transport equation making the following assumptions:

1. electron-phonon interaction is the dominant scattering process for electrons;

2. conduction of heat by phonons is negligible, and

3. phonons and electrons have temperatures T_l and T_e, respectively.

The equation describing the heating of electrons is then given by

$$C_e \frac{\partial T_e}{\partial t} = \nabla \cdot \boldsymbol{q} - G(T_e - T_l), \tag{2.10}$$

and the equation describing heating of metal lattice is given by

$$C_l \frac{\partial T_l}{\partial t} = G(T_e - T_l). \tag{2.11}$$

C_l and C_e are the volumetric heat capacities of metal lattice and electron-gas in Eqs. (2.10) and (2.11), respectively.

The electron-phonon coupling factor, G, is the key parameter governing the rate of the electron-phonon thermal relaxation process and can be calculated from free electron theory [1, 52]. If the lattice temperature is not much smaller than the Debye temperature T_D, approximate expression for G can be written as

$$G = \frac{\pi^2 m_e n_e v^2}{6\tau(T_e) T_e}, \tag{2.12}$$

where $\tau(T_e)$ is the electron mean free time between collisions at temperature T_e, n_e is the number density of free electrons per unit volume, m_e is the mass of free electrons, v is the speed of sound, and T_e is the electron temperature. For pure metals at room temperature, τ is dominated by collisions between electrons and phonons, and is inversely proportional to T_e. Therefore, G depends weakly on T_e. G can be further expressed in terms of thermal conductivity as

$$G = \frac{\pi^4 (n_e v k_B)^2}{k}, \tag{2.13}$$

where k_B is the Boltzmann constant, and k is thermal conductivity. The speed of sound v is evaluated from T_D and the atomic number density n_a [55]

$$v = \frac{\kappa}{2\pi h}\left(6\pi^2 n_a\right)^{\frac{1}{3}} T_D, \tag{2.14}$$

where h is the Planck constant.

Qiu and Tien [65, 66] calculated the values for the electron-phonon coupling factor G for several common metals using Eq. (2.13) with reported physical constants [55] and compared them with the measured values from the literature [11, 38, 43]. They found that the calculated values of G generally agree with the measured values. Metals with higher free electron number density and higher T_D have larger G values and shorter thermal relaxation times. Substitution of Eq. (2.1) into Eq. (2.10) results in parabolic two-step model

$$C_e\frac{\partial T_e}{\partial t} = \nabla\cdot(\nabla T(\boldsymbol{r},t)) - G(T_e - T_l) \tag{2.15a}$$

$$C_l\frac{\partial T_l}{\partial t} = G(T_e - T_l), \tag{2.15b}$$

and substitution of Eq. (2.5) into Eq. (2.10) results in the hyperbolic two-step model:

$$C_e\frac{\partial T_e}{\partial t} = \nabla\cdot\boldsymbol{q} - G(T_e - T_l), \tag{2.16a}$$

$$C_l\frac{\partial T_l}{\partial t} = G(T_e - T_l) \tag{2.16b}$$

$$\boldsymbol{q}(\boldsymbol{r},t) + \tau\frac{\partial \boldsymbol{q}(\boldsymbol{r},t)}{\partial t} = -k\nabla T(\boldsymbol{r},t). \tag{2.16c}$$

Combining Eqs. (2.15a) and (2.15b) and eliminating the electron gas temperature T_e gives

$$\frac{1}{{C_E}^2}\frac{\partial^2 T_l}{\partial t^2} + \frac{1}{\alpha_E}\frac{\partial T_l}{\partial t} - \frac{\alpha_e}{{C_E}^2}\frac{\partial(\nabla^2 T_l)}{\partial t} = \nabla^2 T_l. \tag{2.17}$$

Similarly, eliminating the metal-lattice temperature T_l gives

$$\frac{1}{{C_E}^2}\frac{\partial^2 T_e}{\partial t^2} + \frac{1}{\alpha_E}\frac{\partial T_e}{\partial t} - \frac{\alpha_e}{{C_E}^2}\frac{\partial(\nabla^2 T_e)}{\partial t} = \nabla^2 T_e, \tag{2.18}$$

where

$$\alpha_e = \frac{k}{C_e + C_l}, \tag{2.19}$$

$$C_E = \sqrt{\frac{kG}{C_e C_l}}. \tag{2.20}$$

Qiu and Tien [65] numerically solved Eqs. (2.16a), (2.16b) and (2.16c) by considering a $96fs$ duration laser pulse irradiating a thin film of thickness $0.1\mu m$. The predicted temperature change of the electron gas during the picosecond transient agreed well with the experimental data, supporting the validity of the hyperbolic two-step model for describing the heat transfer mechanisms during short-pulse laser heating of metals. In the case that $\tau \to 0$ and $G \to \infty$, implying that either the number density of free electrons $\to \infty$ (see Eq. (2.13)) or the speed of sound $\to \infty$ (see Eq. (2.14)), Eq. (2.18) collapses to the classical diffusion equation and T_l becomes equal to T_e

2.2.4 Phonon Scattering Model

The heat transport process caused by phonon-phonon collision and scattering is described by the phonon scatering model. Guyer and Krumhansl [45] solved the linearized Boltzmann equation for the pure phonon field in dielectric crystals. They proposed a constitutive relation between the heat flux vector and the temperature gradient, neglecting heat conduction by the electrons and other interactions in which momentum is lost from phonon systems:

$$\frac{\partial \boldsymbol{q}}{\partial t} + \frac{c^2 C_p}{3}\nabla T + \frac{1}{\tau_{_R}}\boldsymbol{q} = \frac{\tau_{_N} v^2}{5}\left[\nabla^2 \boldsymbol{q} + 2\nabla(\nabla \cdot \boldsymbol{q})\right], \tag{2.21}$$

where v is the average speed of phonons; $\tau_{_R}$ stands for the relaxation time for the Umklapp processes (momentum relaxation occurs only by electron-electron scattering, i.e., a momentum non-conserving process); and $\tau_{_N}$ is the relaxation time (mean free time) for normal

processes in which momentum is conserved in the phonon system. Combining Eq. (2.21) with the energy equation (2.2) and eliminating the heat flux vector leads to the equation for the phonon scattering model:

$$\frac{9\tau_{_N}}{5}\frac{\partial}{\partial t}(\nabla^2 T) - \frac{3}{\tau_{_R} c^2}\frac{\partial T}{\partial t} - \frac{3}{c^2}\frac{\partial^2 T}{\partial t^2} = \nabla^2 T. \tag{2.22}$$

2.2.5 Phonon Radiative Transfer Model

The phonon radiative transfer model (PRT) proposed by Majumdar [60] employs the solution of the linearized Boltzmann transport equation. The PRT model describes the Stefan-Boltzmann radiative heat equation for an acoustically thin medium (thickness of film structure is less than mean free path of phonons) and the CV wave equation for an acoustically thick medium. Majumdar derived the PRT equation from Boltzmann transport equation by employing a relaxation time approximation. After summing all three phonon polarizations over the distribution function of the phonons with vibrational frequency ω, the phonon intensity function (I_ω) is obtained as

$$I_\omega(\theta, \phi, x, t) = \sum_p \boldsymbol{v}(\theta, \phi) f_\omega(x, t) h\omega D(\omega), \tag{2.23}$$

with $\boldsymbol{v}(\theta, \phi)$ denoting the velocity vector of phonons in the direction defined by (θ, ϕ) in a spherical coordinate system within a solid angle $d\Omega = sin\theta d\theta d\phi$, as shown in Fig. 2.1. Here h is the Planck constant, and $D(\omega)$ is the density of states per unit volume in the frequency domain of lattice vibrations. The PRT equation defined by Majumdar in 1-D is then

$$\frac{1}{\boldsymbol{v}}\frac{\partial I_\omega}{\partial t} + \mu\frac{\partial I_\omega}{\partial x} = \frac{I_\omega^o - I_\omega}{\tau \boldsymbol{v}}, \tag{2.24}$$

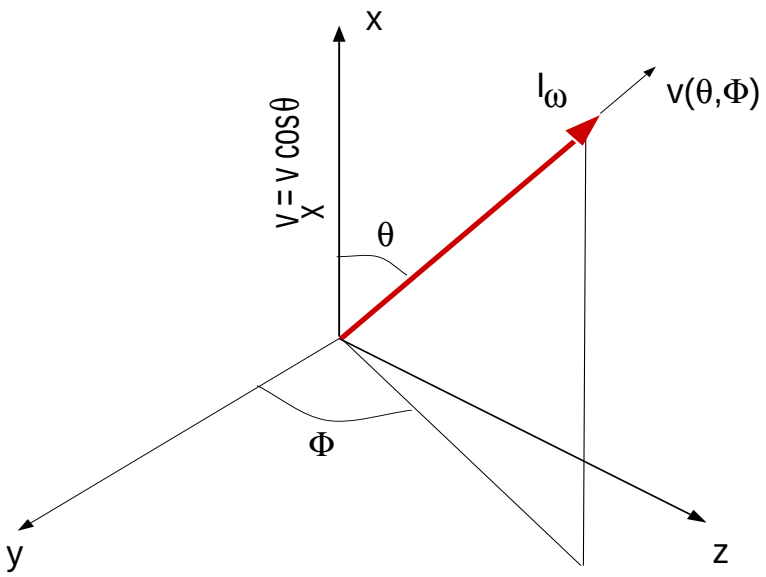

Figure 2.1 Phonon intensity I_ω and the azimuthal angles θ and ϕ defining the velocity vector

where, $\tau \boldsymbol{v}$ defines the mean free path in phonon collision, I_ω^o is the phonon intensity function at equilibrium state, and μ represents the cosine of the angle between the phonon velocity vector $\boldsymbol{v}$ and the x-axis. The right side of Eq. (2.24) represents disturbance of an equilibrium state by mutual interactions of phonons.

The heat flux vector $\boldsymbol{q}$ and the internal energy e at any point in space can be calculated as

$$\boldsymbol{q} = \int_{\omega=4\pi} \int_0^{\omega_D} \mu I_\omega d\omega d\Omega, \tag{2.25}$$

$$e = \int_{\omega=4\pi} \int_0^{\omega_D} \frac{I_\omega}{\nu} d\omega d\Omega, \qquad \text{with } d\Omega = sin\theta d\theta d\phi, \tag{2.26}$$

and ω_D being the Debye cut-off phonon frequency. Azimuthal symmetry in ϕ, $\boldsymbol{q}$ and e results in

$$\boldsymbol{q} = 2\pi \int_{-1}^{1} \int_0^{\omega_D} \mu I_\omega d\omega d\mu, \tag{2.27}$$

$$e = 2\pi \int_{-1}^{1} \int_0^{\omega_D} \frac{I_\omega}{\nu} d\omega d\mu. \tag{2.28}$$

Using Eqs. (2.27) and (2.28), multiplying Eq. (2.24) by 2π and integrating the resulting equation over μ and ω in the range $-1 < \mu < 1$ and $0 < \omega < \omega_D$ gives

$$\frac{\partial e}{\partial t} + \frac{\partial \boldsymbol{q}}{\partial x} = 2\pi \int_{-1}^{1} \int_{0}^{\omega_D} \left[\frac{I_\omega^0 - I_\omega}{\tau \boldsymbol{v}} d\omega d\mu \right]. \tag{2.29}$$

Eq. (2.29) yields a particular solution for $I_\omega^0(T(x))$:

$$I_\omega^0 = \frac{1}{2} \int_{-1}^{1} I_\omega d\mu. \tag{2.30}$$

Finally the PRT equation takes the form of an integro-differential equation to be solved for the phonon intensity function $I_\omega(x, t, \mu)$:

$$\frac{1}{\boldsymbol{v}} \frac{\partial I_\omega}{\partial t} + \mu \frac{\partial I_\omega}{\partial x} = \frac{\frac{1}{2}\int_{-1}^{1} I_\omega d\mu - I_\omega}{\tau \boldsymbol{v}}. \tag{2.31}$$

Once the phonon intensity is obtained from Eq. (2.31), the temperature distribution is obtained from the Bose-Einstein distribution function at an equilibrium state:

$$I_\omega^0(T) = \frac{1}{2} \int_{-1}^{1} I_\omega d\mu = \sum_p \boldsymbol{v}_p \frac{h\omega D(\omega)}{\exp\left[\frac{h\omega}{\kappa t(x)}\right] - 1}. \tag{2.32}$$

2.2.6 Dual Phase Lag (DPL) Model

Mathematically, the dual phase lag concept can be represented by

$$\boldsymbol{q}(\boldsymbol{r}, t + \tau_q) = -k \nabla T(\boldsymbol{r}, t + \tau_{_T}), \tag{2.33}$$

where $\tau_{_T}$ is the phase lag of the temperature gradient and $\tau_{_q}$ is the phase lag of the heat flux vector.

First order Taylor expansion of Eq. (2.33) gives

$$\boldsymbol{q}(\boldsymbol{r}, t) + \tau_q \frac{\partial \boldsymbol{q}(\boldsymbol{r}, t)}{\partial t} = -k \left(\nabla T(\boldsymbol{r}, t) + \tau_{_T} \frac{\partial (\nabla T(\boldsymbol{r}, t))}{\partial t} \right). \tag{2.34}$$

For the case of $\tau_T > \tau_q$, the temperature gradient established across a material volume is a result of the heat flow, implying that the heat flux vector is the cause and the temperature gradient is the effect. For $\tau_T < \tau_q$, on the other hand, heat flow is induced by the temperature gradient established at an earlier time, implying that the temperature gradient is the cause, while the heat flux vector is the effect.

Tzou [71] describes three important characteristics in the dual phase lag model:

1. The heat flux and temperature gradient shown in the Eq. (2.34) represent *local responses* within the solid medium and should not be confused with the *global* quantities specified in the boundary conditions. Application of heat flux at the boundary does not warrant the precedence of the heat flux vector to the temperature gradient at all; the temperature gradient established at a material point *within* the solid medium can still precede the heat flux vector. Whether heat flux vector precedes the temperature gradient or not depends on the combined effect of thermal loading, geometry of the specimen, and the thermal properties of the material.

2. There are *three* characteristic times involved in the dual phase lag model: the instant of time $(t + \tau_T)$ at which the temperature gradient is established across a material volume; the time $(t + \tau_q)$ for the onset of heat flow; and time t for the transient heat transport.

3. The two phase lags (τ_T) and (τ_q) are *intrinsic* thermal properties of the bulk material like the thermal conductivity and thermal diffusivity.

In order to understand the phase lags better, let us look into the internal mechanisms that take place during short-pulse laser heating of metals. Fig. 2.2 describes the delayed

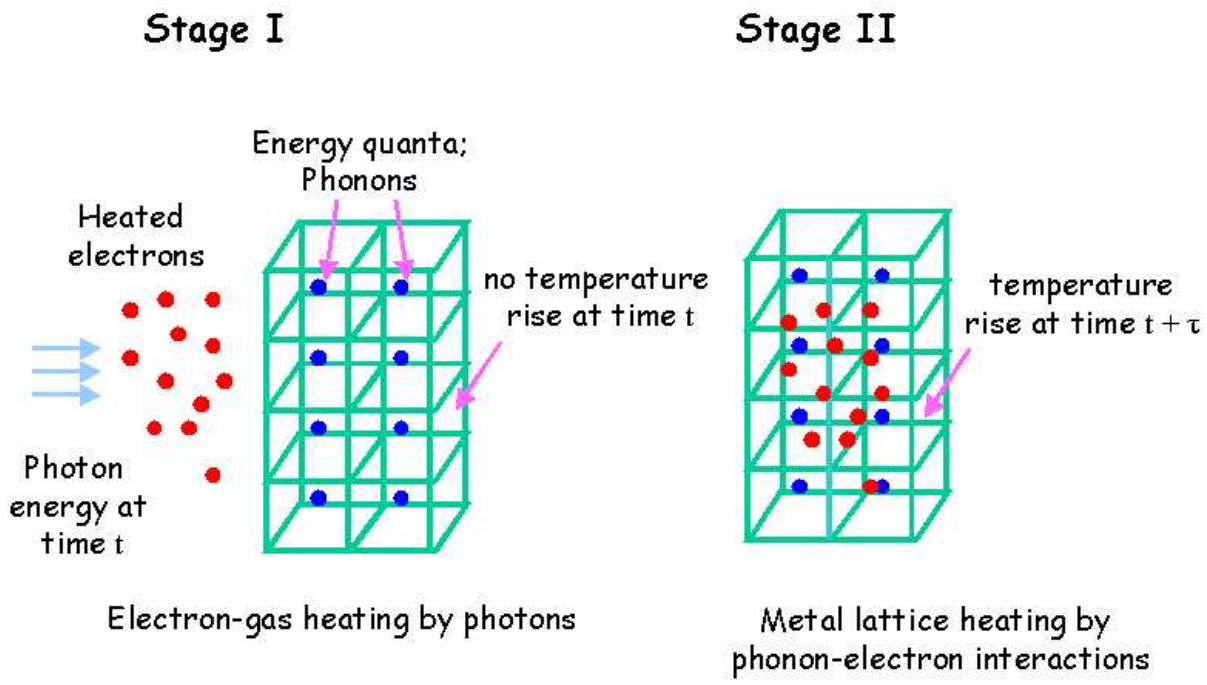

Figure 2.2 Internal mechanisms during short-pulse laser metal interaction (adapted from [71]).

response caused by the phonon-electron interactions in metallic structures. When a material is excited by a short-pulse laser, photons from the laser beam first heat the electron gas at a certain time t. At this moment, no appreciable temperature change can be detected in the metal lattice. Energy transport from the hot electron gas to phonons occurs through electron-phonon interactions, giving rise to appreciable rise of temperature in the metal lattice at a later time $t + \tau$. The phase lag τ corresponds to the finite time required for the electron-phonon interaction to take place. In general, when heat flow arrives at a compound system of phonons and electrons at time t, the temperature gradient across the same volume can only be established later, at $t + \tau_T$, because it requires a finite duration τ_T to raise

the temperature of the metal lattice by one degree. When heat flow leaves the compound system at time $t+\tau_q$ after another finite duration τ_q is required for effective collisions between phonons and electrons to take place for heat transport. The phase lag, τ_q refers to the finite time required to raise the temperature of the compound system by one degree. In short, τ_T indicates the delay behavior in establishing the temperature gradient, and τ_q indicates the delay behavior in heat-flow departure.

Eq. (2.34) coupled with the equation of energy conservation Eq. (2.2) gives the DPL heat conduction equation

$$\frac{\tau_q}{\alpha}\frac{\partial^2 T}{\partial t^2}+\frac{1}{\alpha}\frac{\partial T}{\partial t}-\tau_T\frac{\partial(\nabla^2 T)}{\partial t}=\nabla^2 T. \tag{2.35}$$

We can see that the DPL model Eq. (2.35) has exactly the same form as the two-step model Eqs. (2.17) and (2.18). By comparing the coefficients of Eq. (2.35) with those of Eqs. (2.17) and (2.18), we can represent the microscopic properties as

$$\alpha = \alpha_e \rightarrow \frac{k}{C_e C_l}, \tag{2.36a}$$

$$\tau_T = \frac{\alpha_e}{{C_E}^2} \rightarrow \frac{C_l}{G}, \tag{2.36b}$$

$$\tau_q = \frac{\alpha_e}{{C_E}^2} \rightarrow \frac{C_l C_e}{G(C_e+C_l)}. \tag{2.36c}$$

The microscopic effect vanishes when the phonon-electron coupling factor G approaches infinity, implying that τ_q and τ_T become zero, reducing Eq. (2.35) to the classical parabolic heat conduction equation. On the other hand, $\tau_T = 0$ results in a hyperbolic equation.

Also, Tzou has established perfect correlations between the dual phase lag model and macroscopic diffusion and thermal wave models, the heat flux equation of Jeffreys type [49, 50], the microscopic parabolic and hyperbolic two-step models and the pure phonon scattering model describing the momentum loss of phonon collisions in the Umklapp process

(see Table. 2.1, reproduced from Tzou [72]). Thus, the DPL model covers a wide range of physical responses from the microscopic to macroscopic scales in both space and time under special values of relaxation times associated, separately, with temperature gradient τ_T and heat flux τ_q. DPL model looks very promising for future research because it shows very good agreement with experiments across a wide range of length and time scales. Based on the experimental data for the heat capacities and the electron-phonon coupling factor Tzou further calculates the values of τ_T and τ_q for copper (Cu), silver (Ag), gold (Au), and lead (Pb). The results are shown in Table 2.2. as reproduced from Tzou [72].

DPL model [72]	Diffusion	CV-wave Classical [14, 76]	Heat-flux equation of Jeffreys type [49, 50]	Phonon-electron interactions (parabolic) [65, 66]	Phonon-electron interactions (hyperbolic) [65, 66]	Phonon scattering field [45]
τ_q	0	$\frac{\alpha}{C^2}$	τ	$\frac{1}{G}\left(\frac{1}{C_e}+\frac{1}{C_l}\right)^{-1}$	$\tau_F+\frac{1}{G}\left(\frac{1}{C_e}+\frac{1}{C_l}\right)^{-1}$	τ_R
τ_T	0	0	$k\tau$	$\frac{C_l}{G}$	$\frac{C_l}{G}$	$\frac{9}{5}\tau_N$
α	α	α	α	$\frac{K}{C_e+C_l}$	$\frac{K}{C_e+C_l}$	$\frac{c^2\tau_R}{3}$

Table 2.1 Correspondence of the dual phase lag model to diffusion, thermal wave, heat flux equation of Jeffreys-type, phonon electron interaction (parabolic and hyperbolic) and phonon scattering field theory in terms of τ_q and τ_T , $\tau_R \equiv$ the relaxation time in the Umklapp process; $\tau_N \equiv$ the relaxation time in the normal process; $\tau \equiv$ effective relaxation time in the Jeffreys-heat flux equation.

	K $(Wm^{-1}K^{-1})$	C_l $(Jm^{-3}K^{-1})$ $(\times 10^6)$	G $(Wm^{-3}K^{-1})$ $(\times 10^{16})$	α_E (m^2s^{-1}) $(\times 10^{-4})$	τ_F (ps)	τ_T (ps)	τ_q (ps)	C_E (ms^{-1})	$\sqrt{\alpha\tau_q}$ (ns)
Cu	386	3.4	4.8	1.1283	0.03	70.833	0.4648	2.7201	7.2418
Ag	419	2.5	2.8	1.6620	0.04	89.286	0.7838	2.1979	11.2135
Au	315	2.5	2.8	1.2495	0.04	89.286	0.7838	1.9058	9.8963
Pb	35	1.5	12.4	0.2301	0.005	12.097	0.1720	1.3718	1.9894

Table 2.2 Equivalent thermal diffusivity α_E, phase lags α_q and α_T and thermal wave speed C_E. $C_e = 2.1 \times 10^4 Jm^{-3}K^{-1}$ at room temperature

The heat transport equations used to describe the thermal behavior of microstructures can be expressed as [71]:

Energy equation:

$$-\nabla \cdot \boldsymbol{q} + S = \rho C_p \frac{\partial T}{\partial t}, \tag{2.37}$$

DPL model:

$$\boldsymbol{q}(\boldsymbol{r}, t) + \tau_q \frac{\partial \boldsymbol{q}}{\partial t} = -k \left[\nabla T + \tau_T \frac{\partial (\nabla T)}{\partial t} \right], \tag{2.38}$$

where S is the heat source. Over the years, analytic and numerical methods have been widely investigated [22, 30, 71] for the solving the above coupled Eqs. (2.37) and (2.38). Eliminating the heat flux $\boldsymbol{q}$ between the two Eqs. (2.37) and (2.38) we obtain the DPL equation in 1D as follows:

$$A \frac{\partial T}{\partial t} + B \frac{\partial^2 T}{\partial t^2} - C \frac{\partial^3 T}{\partial x^2 \partial t} - S = \frac{\partial^2 T}{\partial x^2}, \tag{2.39}$$

where A, B and C are constants. Tzou and Özisik [63, 71] studied the lagging behavior by solving the above heat transport equation (2.39) without body heating in a semi-inifinite slab subject to a sudden temperature rise on its boundaries. The solution was obtained using a Laplace transform method and the Riemann sum approximation for the inversion.

Tzou and Chiu [75] studied temperature-dependent thermal lagging in order to accurately describe the experimental data of femtosecond laser heating on gold films of various thickness in the sub-micron range. The thermal properties were determined by employing reverse analysis by adjusting the error between the numerical and experimental results.

Wang et al. [77, 78, 79] showed that the dual phase lag heat conduction equation possesses a unique solution for a finite region of dimension n ($n \geq 2$) under Dirichlet, Neumann or Robin boundary conditions and found the solution to be stable with respect to initial

conditions. Two solution structure theorems are developed for dual phase lag heat conduction equations under linear boundary conditions. These theorems express contributions (to the temperature field) of the initial temperature distribution and the source term by that of the initial time-rate of change of temperature revealing the structure of the temperature field and considerably simplifying the development of solutions to dual phase lag heat conduction equations.

Tang and Araki [70] derived an analytic solution in finite rigid slabs irradiated by short pulse lasers by using the Greens function method and a finite integral transform technique. By adjusting the relaxation parameters, various behaviors of conduction heat transfer, such as wave, wavelike, and diffusion, are exhibited by this model. The calculated temperature responses by this model showed good agreement with two experimental results measured under extremely low temperature and ultra-high speed heating, respectively.

Al-Nimr and Arpaci [3] proposed a simplified approach to describe the thermal behavior of a thin film exposed to a picosecond duration thermal pulse. The approach is based on the assumption that during ultra-fast laser heating the energy transfer through electron-phonon coupling is negligible and the energy transfer by diffusion becomes dominant. The proposed approach may be applied on metal films having modified Pėclet number (which is equal to the square root of GL^2/K_e) much larger than one. The modified Pėclet number describes the ratio of electron energy flow to electron energy diffusion. This model may be applied for thin films having very high coupling factor, very short thermal pulse duration and relatively low or moderate thermal conductivity.

Chen and Beraun [15] present a dual hyperbolic two-step radiation heating model to

investigate ultra-short laser pulse interactions with metal films, extending Qiu and Tien's (1993) theory by including the effect of heat conduction in the lattice. The effects of temperature dependence of the thermophysical properties also are examined. A mesh-free particle method is employed for solving the proposed model and results are compared with parabolic two-temperature model and Fourier's law. Numerical results from this model predicts more accurate thermal response comparable to experimental results than the existing theories considered.

Dai and Nassar [34] have developed a finite-difference scheme of the Crank-Nicolson type by introducing an intermediate function for solving Eq. (2.39) in a finite interval. The scheme is two-level in time. The DPL equation is split into a system of two equations. The individual equations are then discretized using the Crank-Nicolson scheme and solved simultaneously. It is shown by the discrete energy method [32, 33, 58] that the scheme is unconditionally stable, and the numerical scheme is nonoscillatory. The scheme has been generalized to a three-dimensional rectangular thin film case where the thickness is at the sub-microscale [29].

Further, Dai and Nassar [30, 31] developed high-order unconditionally stable two-level compact finite-difference schemes for solving Eq. (2.39) in one- and three-dimensional thin films, respectively. To solve the 3-D implicit finite-difference scheme, a preconditioned Richardson iteration technique is developed so that only a tridiagonal linear system is solved for each iteration. Dai et al. [22] have considered the heat transport equation in spherical cooordinates and have developed a three-level finite-difference scheme for solving the heat transport equation in a microsphere.

Zhang and Zhao [80, 81] have designed a computational procedure to solve the sparse linear systems arising from the discretized 3-D microscale heat transport equations. They examine a few iterative techniques and present comparisons in terms of average number of iterations per linear system solution (per time step) and CPU time in seconds for the entire simulation for the Gauss-Seidel, SOR (successive overrelaxation) with optimal overrelaxation parameters, CG (conjugate gradient), and PCG (preconditioned conjugate gradient). They indicate that both Gauss-Seidel and SOR methods are not very scalable with respect to the problem size, and the CPU timings are very large for large values of N (spatial discretization parameter). The average number of CG iterations increases faster than that of the PCG iterations, indicating that for very large size problems, PCG performs better than CG.

Chapter 3
HEAT CONDUCTION IN A SOLID BAR

In this chapter the classical problem involving heat conduction in a solid bar will be investigated. We will consider heat conduction in a semi-infinite solid slab starting from a stationary state subjected to a sudden temperature rise at the surface boundary. A finite-difference scheme employed for this problem, including one-dimensional stability criteria will be presented. The numerical results are compared with the available analytical results [16]. We will then consider heat conduction in a solid slab subject to temperature rise at both ends. The problem of violation of second law of thermodynamics by the conventional hyperbolic heat conduction (CHE) model will be revealed using this example. We will show that the DPL model accurately describes the heat conduction process compared to the parabolic and hyperbolic models.

3.1 Introduction

Baumeister and Hamill [7, 8] investigated heat conduction in a solid slab subject to sudden temperature rise on its boundaries to reveal the fundamental properties in thermal wave propagation. Taitel [69] and Barletta and Zanchini [6] used the conventional hyperbolic heat conduction equation to examine the same problem. Bai and Lavine [5] used a modified hyperbolic heat conduction equation (MHE) to examine heat conduction in a solid slab subjected to a sudden temperature drop at its boundaries. It has been shown that the DPL model can be reduced to the parabolic (diffusion) equation and the hyperbolic (CV wave) equation; therefore the finite-difference algorithm and the stability and convergent criterion

for the DPL model can be applied for both parabolic and hyperbolic equations.

3.2 Semi-Infinite Slab — Temperature raised at one end

In this section, heat conduction in a semi-infinte slab which undergoes a sudden temperature change on one of its boundaries is studied. The thermal conductivity k, thermal diffusivity α, specific heat at constant volume C_v and thermal relaxation time τ of the slab can be considered constant. Throughout the slab, at time $t = 0$ the heat flux density q is zero, and the temperature field T is uniform with the value T_0. As a consequence, $\partial T/\partial t$ is zero at time $t = 0$.

3.2.1 Mathematical Formulation

Without body heating the one-dimensional DPL equation is written as

$$\frac{\tau_q}{\alpha}\frac{\partial^2 T}{\partial t^2} + \frac{1}{\alpha}\frac{\partial T}{\partial t} - \tau_{_T}\frac{\partial^3 T}{\partial x^2 \partial t} = \frac{\partial^2 T}{\partial x^2}. \tag{3.1}$$

The suddenly raised boundary temperature at $x = 0$ is given by

$$T(0,t) = T_{_W} \qquad \text{for} \qquad t > 0, \tag{3.2}$$

where, $T_{_W}$ is the wall temperature.

Assuming an insulated boundary condition far from the heated boundary, we have

$$\frac{\partial T}{\partial x}(x,t) = 0 \qquad x \to \infty. \tag{3.3}$$

The initial conditions are

$$T(x,0) = T_0, \tag{3.4}$$

and

$$\frac{\partial T}{\partial t}(x,0) = 0 \qquad \text{for} \qquad x \in [0,\infty). \tag{3.5}$$

By introducing dimensionless quantities [16]

$$\theta(x,t) = \frac{T(x,t) - T_0}{T_W - T_0}, \qquad \beta = \frac{t}{\tau_q}, \qquad \delta = \frac{x}{\sqrt{\alpha \tau_q}}, \tag{3.6}$$

equations (3.1) to (3.5) become

$$\frac{\partial^2 \theta}{\partial \delta^2} + Z \frac{\partial^3 \theta}{\partial \delta^2 \partial \beta} = \frac{\partial^2 \theta}{\partial \beta^2} + \frac{\partial \theta}{\partial \beta}, \qquad \text{with} \qquad Z = \frac{\tau_T}{\tau_q} \tag{3.7}$$

$$\theta(0,\beta) = 1 \qquad \text{for} \qquad \beta > 0, \tag{3.8}$$

$$\frac{\partial \theta}{\partial \delta}(\delta,\beta) = 0 \qquad \delta \to \infty, \tag{3.9}$$

$$\theta(\delta,0) = 0, \tag{3.10}$$

$$\frac{\partial \theta}{\partial \beta}(\delta,0) = 0 \qquad \text{for} \qquad \delta \in [0,\infty). \tag{3.11}$$

In terms of the microscopic properties, the parameter Z can be expressed by [71]

$$Z = \frac{\tau_T}{2\tau_q} \begin{cases} \frac{18}{5}\frac{\tau_N}{\tau_R} & \text{(phonon scattering)} \\ \left[1 + \left(\frac{C_l}{C_e}\right)\right] & \text{(phonon-electron interaction).} \end{cases} \tag{3.12}$$

When the values for τ_T and τ_q are selected according to the perfect correlations shown in Table 2.1, the dual phase lag model captures the microstructural effects of phonon scattering and phonon-electron interactions. In the case of $\tau_T = 0$, implying $Z = 0$ according to Eq. (3.12), the DPL equation (3.7) reduces to the dimensionless form of the CV equation:

$$\frac{\partial^2 \theta}{\partial \delta^2} = \frac{\partial^2 \theta}{\partial \beta^2} + \frac{\partial \theta}{\partial \beta}. \tag{3.13}$$

The CV wave equation captures only the inertia effect in the fast-transient process (in time) while the spatial response remains macroscopic.

When $\tau_T = \tau_q = 0$ ($Z = 0$) the DPL equation (3.7) reduces to the classical diffusion equation. When $\tau_T = \tau_q$ ($Z = 1$), not necessarily equal to zero, Eq. (3.7) can be rearranged to

$$\left(\frac{\partial^2 T}{\partial x^2} - \frac{1}{\alpha}\frac{\partial T}{\partial t}\right) + \tau_q \frac{\partial}{\partial t}\left(\frac{\partial^2 T}{\partial x^2} - \frac{1}{\alpha}\frac{\partial T}{\partial t}\right) = 0. \tag{3.14}$$

For a homogeneous initial temperature, it has a general solution

$$\frac{\partial^2 T}{\partial x^2} - \frac{1}{\alpha}\frac{\partial T}{\partial t} = 0, \tag{3.15}$$

which is the classical diffusion equation. Thus, when $\tau_T = \tau_q$ the DPL equation reduces to the classical diffusion equation.

3.2.2 Explicit Finite-Difference Scheme

Re-writing Eq. (3.7) in terms of x, t and T, we have

$$\frac{\partial^2 T}{\partial t^2} + \frac{\partial T}{\partial t} - Z\frac{\partial^3 T}{\partial x^2 \partial t} = \frac{\partial^2 T}{\partial x^2} \qquad \text{with} \qquad Z = \frac{\tau_T}{\tau_q}. \tag{3.16}$$

The second-order derivativess in space and time in Eq. (3.16) are approximated using the centered differences

$$\frac{\partial^2 T}{\partial t^2} = \frac{1}{\Delta t^2}\left[T_i^{n+1} - 2T_i^n + T_i^{n-1}\right] \tag{3.17}$$

$$\frac{\partial^2 T}{\partial x^2} = \frac{1}{\Delta x^2}\left[T_{i+1}^n - 2T_i^n + T_{i-1}^n\right]. \tag{3.18}$$

The first-order derivative in time is approximated using a forward-difference method:

$$\frac{\partial T}{\partial t} = \frac{1}{\Delta t}\left[T_i^{n+1} - T_i^n\right]. \tag{3.19}$$

The mixed derivative is approximated by a centered difference in space and backward difference in time:

$$\frac{\partial^3 T}{\partial x^2 \partial t} = \frac{\left[T_{i+1}^n - 2T_i^n + T_{i-1}^n\right] - \left[T_{i+1}^{n-1} - 2T_i^{n-1} + T_{i-1}^{n-1}\right]}{\Delta x^2 \Delta t}, \tag{3.20}$$

where n and i are the indices of the locations in temporal and spatial grids, respectively; h and k are the space and time step, respectively. Substituting Eqs. (3.17) to (3.20) into Eq. (3.16) and rearranging we can represent the unknown T_i^{n+1} in terms of the known values on the right hand side:

$$T_i^{n+1} = C_1 * \left[C_2 * (T_{i+1}^n + T_{i-1}^n) + C_3 * T_i^n + C_4 * (T_{i+1}^{n-1} + T_{i-1}^{n-1}) + C5 * T_i^{n-1}\right], \qquad (3.21)$$

where,

$$C_1 = \frac{\Delta t^2}{\Delta t + 1}; \qquad (3.22a)$$

$$C_2 = \frac{1}{\Delta x^2} + \frac{Z}{\Delta x^2 \Delta t}; \qquad (3.22b)$$

$$C_3 = -\frac{2}{\Delta x^2} - \frac{2Z}{\Delta x^2 \Delta t} + \frac{1}{\Delta t} + \frac{2}{\Delta t^2}; \qquad (3.22c)$$

$$C_4 = -\frac{Z}{\Delta x^2 \Delta t}; \qquad (3.22d)$$

$$C_5 = \frac{2Z}{\Delta x^2 \Delta t} - \frac{1}{\Delta t^2}. \qquad (3.22e)$$

3.2.3 Stability Analysis

The stability and convergence criteria for the above finite-difference algorithm based on one-dimensional DPL model has been derived (see Chiu [16]) using von Neumann eigenmode analysis [2]. For simplicity let us take $\Delta x = h$ and $\Delta t = k$. Assuming the error propagation mode for the temperature in the following form:

$$T_j{}^n = \xi^n \exp[i\beta mh], \qquad \text{with} \qquad i = \sqrt{-1} \qquad (3.23)$$

the amplification factor ξ can be solved by substituting Eq. (3.23) into Eq. (3.21). To ensure stable and convergent solutions of $T_j{}^n$ it is required that

$$| \xi | < 1, \qquad (3.24)$$

which is the well-known von Neumann stability criterion.

Substituting Eq. (3.23) into Eq. (3.21) we have

$$\begin{aligned}
&\xi^2\left((h)^2\left(\cos(\beta h)+i\sin(\beta h)\right)+k(h)^2\left(\cos(\beta h)+i\sin(\beta h)\right)\right)+\\
&\xi\Big(-Zk\left(-1+\cos(\beta h)+i\sin(\beta h)\right)^2-k^2\left(-1+\cos(\beta h)+i\sin(\beta h)\right)^2-\\
&2h^2\left(\cos(\beta h)+i\sin(\beta h)\right)-kh^2\left(\cos(\beta h)+i\sin(\beta h)\right)\Big)+\\
&Zk\left(-1+\cos(\beta h)+i\sin(\beta h)\right)^2+h^2\left(\cos(\beta h)+i\sin(\beta h)\right)=0 \qquad (3.25)
\end{aligned}$$

Eq. (3.25) can be represented in terms of real and imaginary parts as follows:

$$\begin{aligned}
&\xi^2\left(h^2kh^2\right)+\\
&\xi\left(2Zk+2k^2-2h^2-kh^2-2Zk\cos(\beta h)-2k^2\cos(\beta h)\right)\\
&2Zk\cos(\beta h)-2Zk=0 \qquad (3.26)
\end{aligned}$$

$$\begin{aligned}
&\xi^2\left(h^2kh^2\right)+\\
&\xi\left(2Zk+2k^2-2h^2-kh^2-2Zk\cos(\beta h)-2k^2\cos(\beta h)\right)\\
&2Zk\cos(\beta h)-2Zk=0 \qquad (3.27)
\end{aligned}$$

Since the above equations are of the same mathematical form the solution for either one of the equations will satisfy Eq. (3.25). The solution for Eq. (3.25) is represented by the following equation

$$\xi=\frac{1}{2(1+k)h^2}\left(\begin{array}{l}-2Zk-2k^2+2h^2+kh^2+2Zk\cos(\beta h)+2k^2\cos(\beta h)\pm\\ \sqrt{\begin{array}{l}-4(1+k)h^2(-2Zk+h^2+2Zk\cos(\beta h))+\\ (2Zk+2k^2-2h^2-kh^2-2Zk\cos(\beta h)-2k^2\cos(\beta h))\end{array}}\end{array}\right). \qquad (3.28)$$

In order to satisfy the von Neumann stability condition Eq. (3.24), Eq. (3.28) has to satisfy

$$-1 \leq \xi \leq 1 \qquad \forall \beta h. \tag{3.29}$$

The right-hand side inequality implies

$$h^2 + 4Z + 4k \geq \sqrt{16Z^2 + 32Zk + 16k^2 - 16h^2 + 8Zk^2 - 8kh^2 + h^4}. \tag{3.30}$$

Assuming the total value inside the square root on the right-hand side of Eq. (3.30) is ≥ 0, Eq. (3.29) can be further simplified to

$$k \geq -1. \tag{3.31}$$

From the above equation we understand that for k to be valid, $h \geq 0$.

The left-hand side of Eq. (3.29) implies

$$4Z + 4k - \frac{4h^2}{k} - 3h^2 \leq \sqrt{16Z^2 + 32Zk + 16k^2 - 16h^2 + 8h^2 - 8kh^2 + h^4}. \tag{3.32}$$

Although k, k and Z are all real values, the total value on the left-hand side of Eq. (3.32) cannot be guaranteed greater than zero. In order to be able to further simplify the above equation, it is essential to assume the total value on the left-hand side of the Eq. (3.32) less than zero. In addition, assumed the total value inside the square root on the right-hand side of Eq. (3.32) is greater than or equal to zero. The result from assuring the above two assumptions yields

$$\frac{k(2k + 4Z)}{h^2(k + 2)} \leq 1. \tag{3.33}$$

Equation (3.33) represents the stability and convergence criterion for the finite-difference algorithm based on the one-dimensional DPL model. By employing the same analysis the

stability criteria for two and three-dimensional DPL models can be expressed by the following equations [16]

$$\frac{k(2k+4Z)}{{h_x}^2(k+2)}+\frac{k(2k+4Z)}{{h_y}^2(k+2)}\leq 1, \tag{3.34}$$

$$\frac{k(2k+4Z)}{{h_x}^2(k+2)}+\frac{k(2k+4Z)}{{h_y}^2(k+2)}+\frac{k(2k+4Z)}{{h_z}^2(k+2)}\leq 1. \tag{3.35}$$

Under a prescribed space increment, the maximum allowable time increment to achieve stable and convergent solutions is obtained by rearranging Eq. (3.33):

$$k\leq\frac{-(4Z-h^2)\pm\sqrt{(4Z-h^2)^2+16h^2}}{4}. \tag{3.36}$$

3.2.4 Results and Discussion

Temperature distribution corresponding to the analytical [16] and numerical results at non-dimensional time $\beta=1$ with different phase lag ratios Z are presented. $Z<1$ implies heat flux precedence; $Z=1$ gives the solution for the diffusion equation, $Z=0$ gives the solution for the CV wave equation and the temperature precedence is given by $Z>1$. At $\beta=1$, the disturbance caused by a suddenly raised temperature at the boundary propagates into the semi-infinite solid, and the penetration depth of the disturbance is found to be larger for the case of heat flux precedence ($Z>1$) than the temperature gradient precedence ($Z<1$).

Figure 3.1 shows comparisons between numerical and analytical non-dimensional temperature distributions for the case of heat flux precedence ($Z=5$ and $Z=10$), temperature gradient precedence ($Z=0.1$), diffusion ($Z=1$) and thermal wave ($Z=0$). For $Z=0$, the temperature distribution possesses a sharp thermal wave front (no significant dissipation and dispersion). For $Z=0.1$, corresponding to temperature gradient precedence, the

abrupt change in the temperature distribution has been changed into a rather smooth thermal wave front [74]. When the value of $Z = \tau_{_T}/\tau_{_q}$ further increases, the thermal penetration depth increases, and the temperature profile becomes smoother. Since $\tau_{_T}$ reflects the delayed response due to microstructural interaction effects, phonon scattering and phonon-electron interactions occurring in microscales seem to promote the temperature level [74].

3.3 Slab — Temperature Raised at Both Ends

In this section, heat conduction in a parallel and infinitely wide slab which undergoes a sudden temperature change at both ends of the slab is studied. The thermal conductivity k, the thermal diffusivity α, the specific heat at constant volume C_v and the thermal relaxation time τ of the slab can be considered constant. Throughout the slab, at time $t = 0$, the heat flux density q is zero and the temperature field T is uniform with the value T_0. As a consequence, $\partial T/\partial t$ is zero at time $t = 0$. For every $t > 0$, the temperature distribution on the two-sides of the slab is kept uniform with a value $T_{_W} \neq T_0$.

3.3.1 Mathematical Formulation

The governing equations can be expressed as

$$\frac{\partial^2 T}{\partial x^2} + \tau_{_T}\frac{\partial^3 T}{\partial x^2 \partial t} = \frac{\tau_q}{\alpha}\frac{\partial^2 T}{\partial t^2} + \frac{1}{\alpha}\frac{\partial T}{\partial t} \tag{3.37}$$

$$T(x,0) = T_0 \qquad \text{and} \qquad \frac{\partial T}{\partial t}(x,0) = 0 \qquad \text{for} \qquad x \in [0,\infty) \tag{3.38}$$

$$T(0,t) = T(l,t) = T_{_W} \qquad \text{for} \qquad t > 0, \tag{3.39}$$

where, $T_{_W}$ is the wall temperature.

By introducing dimensionless quantities

$$\theta(x,t) = \frac{T(x,t) - T_{_0}}{T_{_W} - T_{_0}}, \qquad \beta = \frac{t}{\tau_{_q}}, \qquad \delta = \frac{x}{\sqrt{\alpha\tau_{_q}}}, \tag{3.40}$$

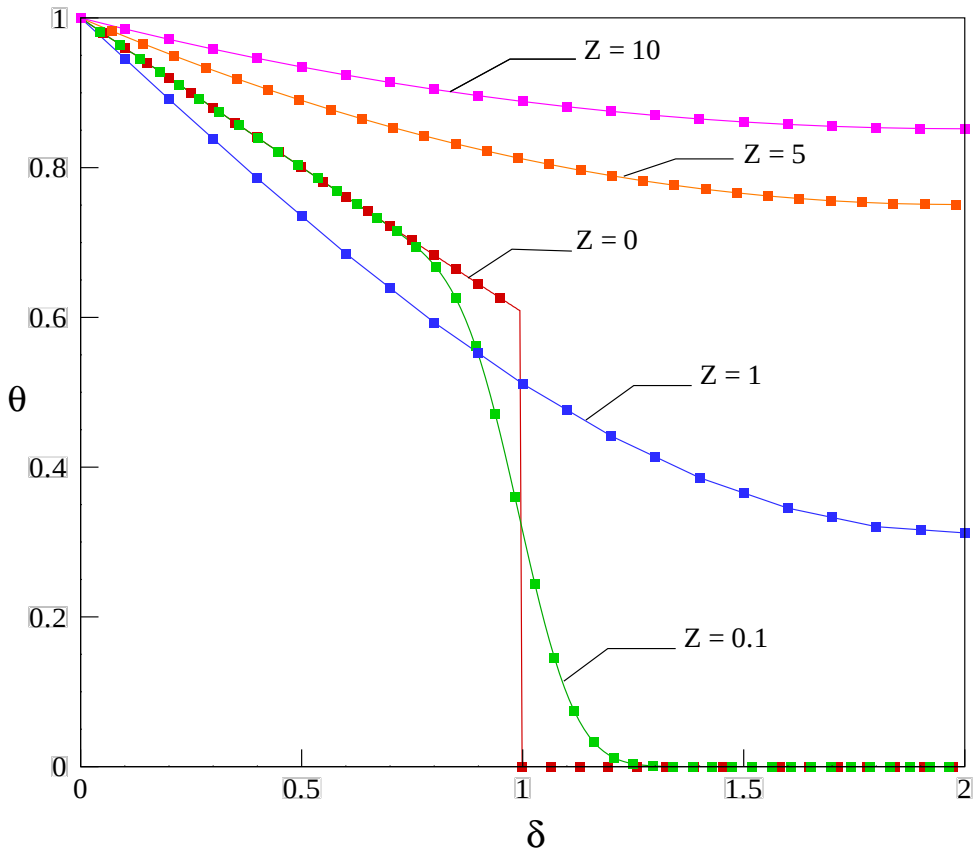

Figure 3.1 Comparison between numerical and analytical temperature distribution for various phase lag ratios ($Z = \tau_T/\tau_q$) at $\beta = 1$. – analytical and □ numerical. $Z = 0 \rightarrow$ hyperbolic solution, $Z = 1 \rightarrow$ parabolic solution, $Z < 1 \rightarrow$ temperature gradient precedence, $Z > 1 \rightarrow$ heat flux precedence.

equations (3.37) to (3.39) become

$$\frac{\partial^2\theta}{\partial\delta^2} + Z\frac{\partial^3\theta}{\partial\delta^2\partial\beta} = \frac{\partial^2\theta}{\partial\beta^2} + \frac{\partial\theta}{\partial\beta} \qquad \text{with} \qquad Z = \frac{\tau_T}{\tau_q} \tag{3.41}$$

$$\theta(\delta, 0) = 0, \qquad \text{and} \qquad \frac{\partial\theta}{\partial\beta}(\delta, 0) = 0 \qquad \text{for} \qquad \delta \in [0, \infty) \tag{3.42}$$

$$\theta(0, \beta) = \theta(\delta, \beta) = 1 \qquad \text{for} \qquad \beta > 0, \tag{3.43}$$

Eqs. (3.41) to (3.43) are solved using an explicit finite-difference method explained in the previous section.

3.3.2 Results and Discussion

Temperature distribution corresponding to the analytical [16] and numerical results at different non-dimensional times ($\beta = 0.1, 0.4, 0.7, 1.7$) with different phase lag ratios ($Z = 0, 1, \text{and} 10$) are presented. As explained in the previous section, $Z = 1$ gives solution for the diffusion equation, $Z = 0$ gives solution for the CV wave equation and the temperature precedence is given by $Z = 10$.

Figures 3.2–3.5 show comparisons between numerical and analytical non-dimensional temperature distributions at different non-dimensional times ($\beta = 0.1, 0.4, 0.7, 1.7$) with different phase lag ratios ($Z = 0, 1, \text{and } 10$). As the phase lag ratio Z is increased the thermal penetration depth increases. For $Z = 0$ the temperature disturbance propagates as a wave. From Figures 3.4 and 3.5, we can observe that the absolute value of the temperature change $T - T_0$ is greater than the $\mid T_W - T_0 \mid$. The transient temperature on the inside of the slab is greater than the temperature at the boundaries.

This temperature overshoot phenomenon clearly indicates violation of second law of thermodynamics because the temperature of the sink (interior of slab) cannot go higher than

the source (boundaries). The temperature rise will be accompanied by negative values of entropy. It has also been shown that the temperature rise at every point in the interior of the slab is accompanied by negative values of entropy [6]. Even though the solution is unrealistic there have been several arguments on whether or not the conventional hyperbolic heat conduction equation (CHE) is compatible with the second law of thermodynamics. This issue was discussed in Chapter II.

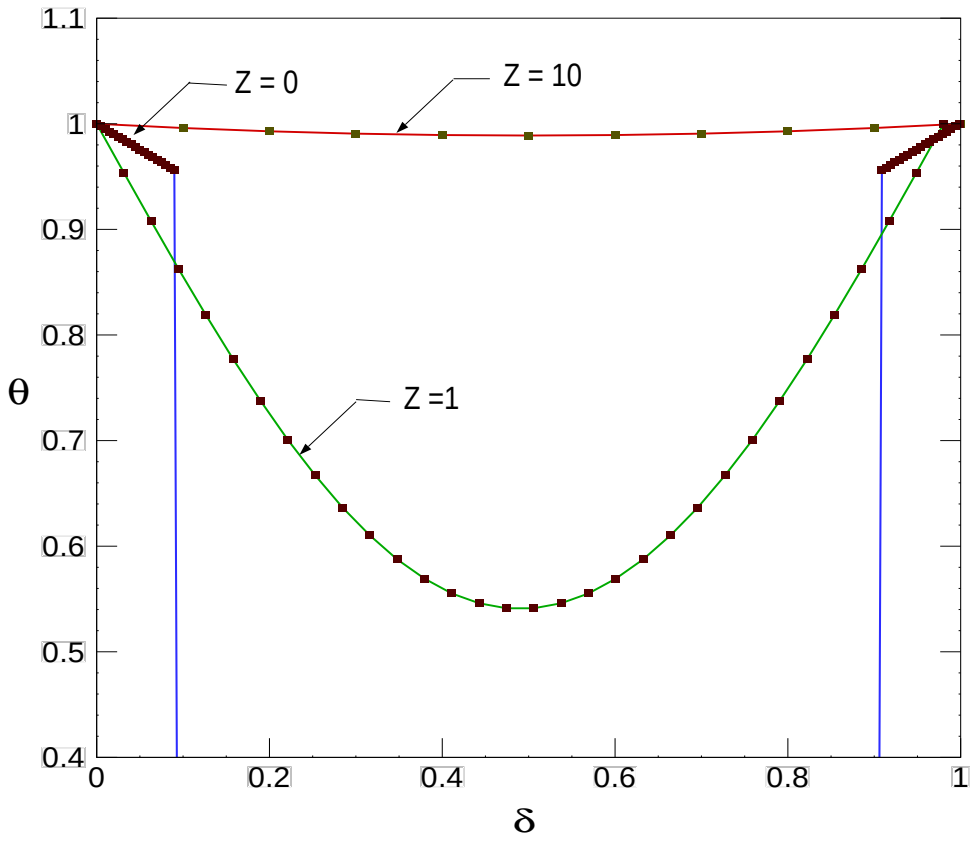

Figure 3.2 Comparison between numerical and analytical temperature distribution for various phase lag ratios ($Z = \tau_T/\tau_q$) at $\beta = 0.1$. – analytical and □ numerical. $Z = 0 \rightarrow$ hyperbolic solution, $Z = 1 \rightarrow$ parabolic solution, $Z < 1 \rightarrow$ temperature gradient precedence, $Z > 1 \rightarrow$ heat flux precedence.

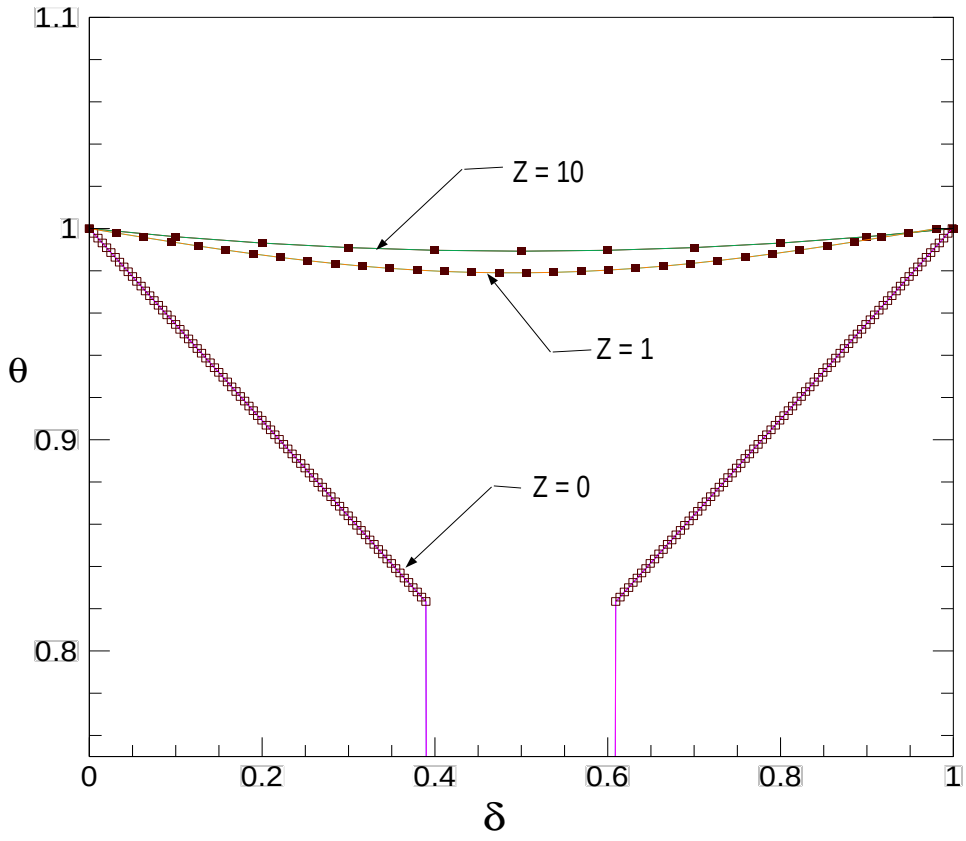

Figure 3.3 Comparison between numerical and analytical temperature distribution for various phase lag ratios ($Z = \tau_T/\tau_q$) at $\beta = 0.4$. – analytical and □ numerical. $Z = 0 \rightarrow$ hyperbolic solution, $Z = 1 \rightarrow$ parabolic solution, $Z < 1 \rightarrow$ temperature gradient precedence, $Z > 1 \rightarrow$ heat flux precedence.

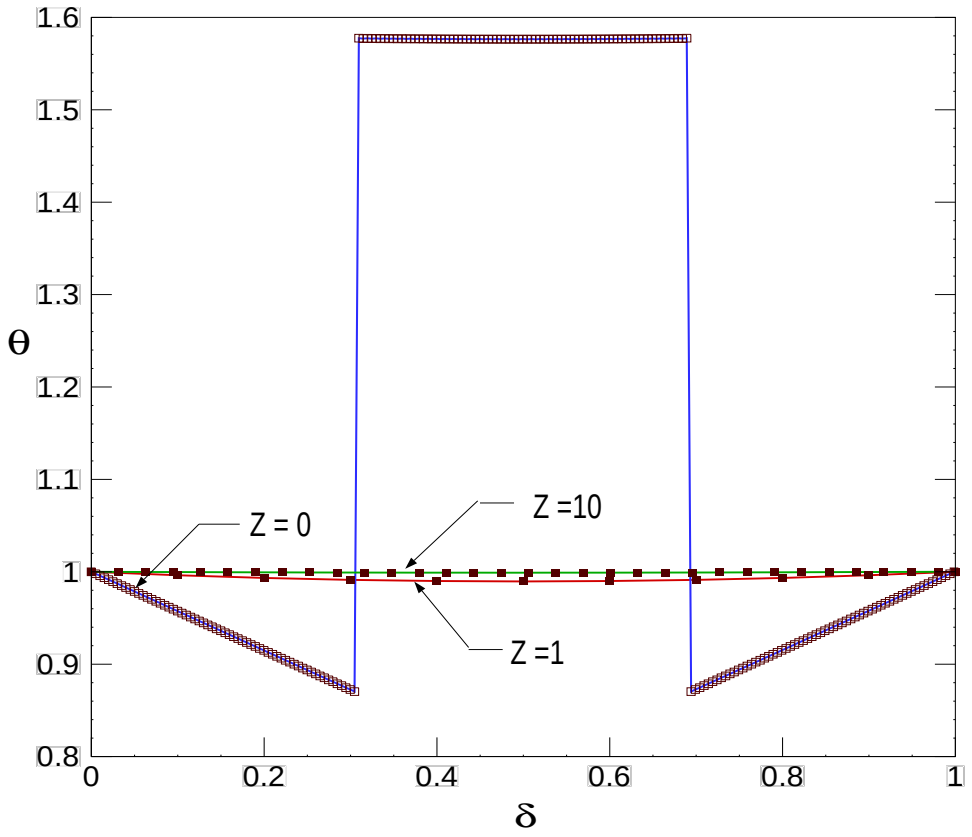

Figure 3.4 Comparison between numerical and analytical temperature distribution for various phase lag ratios ($Z = \tau_T/\tau_q$) at $\beta = 0.7$. – analytical and □ numerical. $Z = 0 \rightarrow$ hyperbolic solution, $Z = 1 \rightarrow$ parabolic solution, $Z < 1 \rightarrow$ temperature gradient precedence, $Z > 1 \rightarrow$ heat flux precedence.

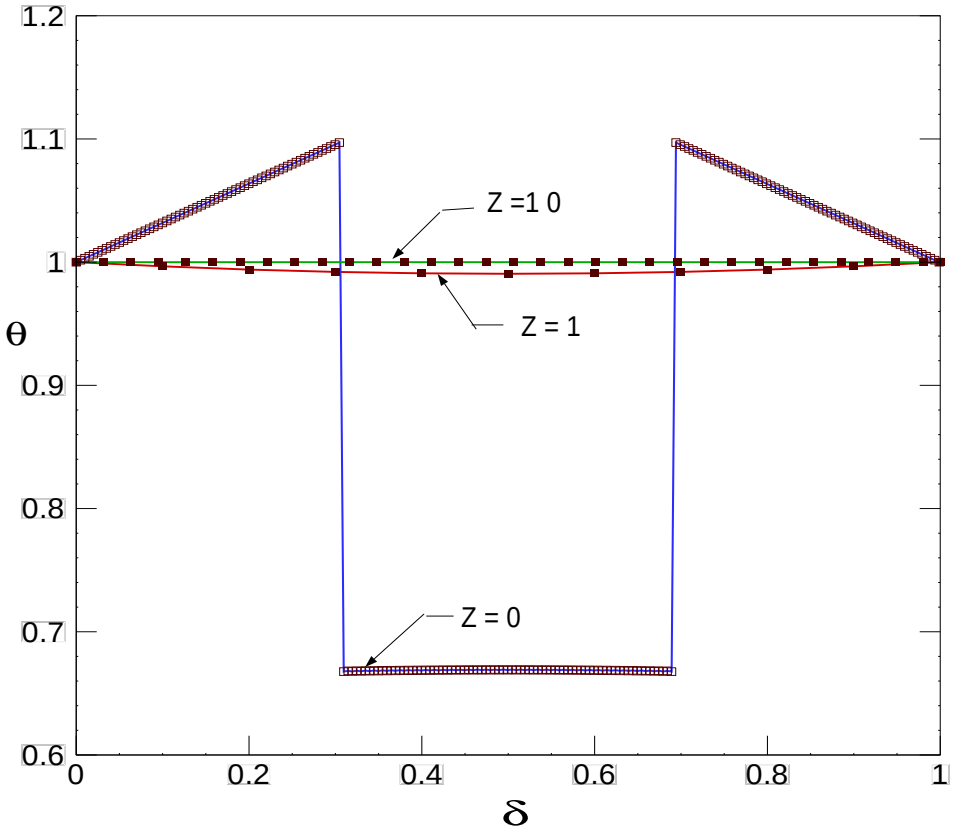

Figure 3.5 Comparison between numerical and analytical temperature distribution for various phase lag ratios ($Z = \tau_T/\tau_q$) at $\beta = 1.7$. – analytical and □ numerical. $Z = 0 \rightarrow$ hyperbolic solution, $Z = 1 \rightarrow$ parabolic solution, $Z < 1 \rightarrow$ temperature gradient precedence, $Z > 1 \rightarrow$ heat flux precedence.

Chapter 4
ONE-DIMENSIONAL SHORT PULSE LASER HEATING ON GOLD FILM

In this chapter, numerical simulation of femtosecond pulse laser heating of sub-micron sized gold film will be examined using the DPL model [71, 72, 73, 74] under different values of relaxation times, and the computed results will be compared with the experimental results by Brorson *et al.* [12], and Qiu and Tien [65, 66]. An explicit finite-difference scheme will be employed to solve the DPL equation.

4.1 Introduction

Short pulse lasers with pulse duration of the order of femtoseconds have been studied extensively over the past two decades. From a microscopic point of view, ultrafast laser heating of metals is composed of three processes: deposition of radiation energy on electrons, transport of energy by electrons and heating of the material lattice through phonon-electron interactions. Due to the high conducting nature of gold, the time frame of primary interest is only several picoseconds, and the penetration depth is of the order of submicrons. The classical diffusion equation and the CV wave equation neglect the energy exchange between phonons and electrons; their applicability to short pulse laser applications involving extremely small scales in both space and time becomes questionable. The heat transport phenomenon induced by ultra-fast laser pulse on a submicron sized gold film has been studied experimentally by Qiu and Tien [65, 66] and Brorson et al. [12]. The details of the experiment can be read elsewhere [71].

Gradient of the intensity of the laser beam, $I(t)$, appears as the volumetric heat source

term (the energy absorption rate in the sample) in the analytical modeling. The analytical form of the laser light intensity can be arbitrarily chosen, but the resulting autocorrelation of the laser pulse defined by

$$I_s(\tau) = C_0 \int_{-\infty}^{\infty} I(t)I(t+\tau)dt, \tag{4.1}$$

must be close to that measured experimentally. τ refers to the delay time of the probe beam (for measuring the reflectivity change of the sample) relative to the pump beam (see Qiu and Tien [67]). $I(t)$ is the intensity of the delayed beam, C_0 is a crystal constant and I_s is the measured light intensity obtained by summing $I_s(t,\tau)$ over the entire time domain. Based on the light intensity thus determined, the volumetric heating of the sample is given by

$$S(x,t) = S_0 e^{-\frac{x}{\delta}} I(t), \tag{4.2}$$

with δ denoting the penetration depth of laser radiation; $I(t)$ denotes the light intensity of laser (given by a traditional Gaussian profile):

$$I(t) = I_0 e^{-\psi\left(\frac{t}{t_p}\right)^2}, \qquad \psi = 4\ln(2) \cong 2.77, \tag{4.3}$$

with ψ being a constant. S_0 is the intensity of laser absorption [65, 66]:

$$S_0 = 0.94J\left(\frac{1-R}{t_p\delta}\right), \tag{4.4}$$

with J the laser fluence, δ the laser penetration depth, R the radiative reflectivity of the gold film and t_p the full width at half maximum (FWHM) of the duration of the laser pulse. t_p describes laser heating of the electron-phonon system from a thermalization state. Eq. (4.2) shows exponentially decaying heating intensity in the thickness direction of the sample. The light intensity function $I(t)$ can be arbitrarily chosed as long as it results in an autocorrelation

function comparable to experimental result. An alternate form of light intensity function $I(t)$ considered by Tzou [71]

$$I(t) = I_0 e^{-a|\frac{t}{t_p}|} \qquad \text{with} \qquad a \geq 0, \qquad t_p \geq 0 \tag{4.5}$$

gives an excellent autocorrelation of laser pulse with experimental results compared to the one used by Qiu and Tien [65, 66].

4.2 Heat Transport Mechanisms

Short pulse laser heating of thin metal films has been successfully modeled using the phonon-electron interaction model (two-step model) and the dual phase lag (DPL) model. In the following subsections we will look at how these two models are employed to investigate the heat transport phenomenon between the electrons and the metal lattices in the short transient period.

4.2.1 Phonon-Electron Interaction Model

In order to study the transient thermal response induced by femtosecond pulse laser, Qiu and Tien [65] employed the parabolic two-step model:

$$C_e \frac{\partial T_e}{\partial t} = \frac{\partial}{\partial x}\left(\frac{T_e}{T_l} k \frac{\partial T_e}{\partial x}\right) - G(T_e - T_l) + S \tag{4.6a}$$

$$C_l \frac{\partial T_l}{\partial t} = G(T_e - T_l). \tag{4.6b}$$

They accounted for the temperature dependent heat capacity of the electron gas and thermal conductivity to model the energy transport process between phonons and electrons. The phonon-electron coupling factor G dictates the refined mechanism of phonon-electron interaction in transporting heat. Employing the Gaussian profile Eq. (4.5), the laser heating

source in Eq. (4.6a) is obtained by substituting Eqs. (4.4) and (4.5) into Eq. (4.2).

$$S(x,t) = 0.94J\left[\frac{1-R}{t_p\delta}\right] e^{-\frac{x}{\delta}-2.77\left(\frac{t}{t_p}\right)^2}. \tag{4.7}$$

The front and back surfaces of the film are assumed to be thermally insulated due to the short period of laser heating:

$$\frac{\partial T_e}{\partial x}(0,t) = \frac{\partial T_e}{\partial x}(L,t) = \frac{\partial T_l}{\partial x}(0,t) = \frac{\partial T_l}{\partial x}(L,t) = 0, \tag{4.8}$$

where L is the film thickness. In order to describe laser heating of the electron-lattice system from a thermalization state, the initial conditions for both the electrons and metal lattice (room temperature, T_0) are shifted by $2t_p$

$$T_e(x,-2t_p) = T_l(x,-2t_p) = T_0. \tag{4.9}$$

Qui and Tien [65] employed Crank-Nicolson finite-difference scheme to solve the two-step system shown by Eqs. (4.6a) and (4.6b).

The reflectivity change result from the variations of electron distributions and the experimental results are in terms of reflectivity change. The experiment measures the transient reflectivity changes, ΔR. The probe laser excites electrons from the completely filled valence d band to the states near the Fermi level in the conduction band. The increase of the electron temperature changes the electron occupation probability, which in turn modulates the reflectivity. For example, the increase of the electron numbers in the final state of the transition decreases the radiation absorption and results in an increase of reflectivity. Therefore, the reflectivity change is a measure of the electron temperature. Brorson et al. [12] and Qiu and Tien [65] have shown that ΔR is proportional ΔT_e in the laser-intensity range of their

experiments. Therefore, the normalized electron temperature changes can be deduced from the measured normalized reflectivity change as

$$\frac{\Delta T_e}{(\Delta T_e)_{max}} \cong \frac{\Delta R}{(\Delta R)_{max}}. \tag{4.10}$$

4.2.2 Dual Phase Lag Model

It has been previously shown that the DPL model produces the same results as the parabolic two-step model. Using the autocorrelation for the light intensity of laser pulse Eq. (4.5) given by Tzou [71], the laser heating source S becomes

$$S(x,t) = 0.94J\left[\frac{1-R}{t_p\delta}\right] e^{-\frac{x}{\delta}-\frac{a|t-2t_p|}{t_p}}. \tag{4.11}$$

The factor $t-2t_p$ results from the shift of initial time from zero to $(2t_p)$. The temperature formulation for the linearized DPL model is given by

$$\frac{\tau_q}{\alpha}\frac{\partial^2 T}{\partial t^2} + \frac{1}{\alpha}\frac{\partial T}{\partial t} = \frac{\partial^2 T}{\partial x^2} + \tau_T \frac{\partial^3 T}{\partial x^2 \partial t} + \frac{1}{k}\left(S + \tau_q \frac{\partial S}{\partial t}\right). \tag{4.12}$$

with initial conditions:

$$T(x,0) = T_0, \qquad \text{and} \qquad \frac{\partial T}{\partial t}(x,0) = 0 \tag{4.13}$$

Insulated boundary conditions are assumed at the front and back surfaces, because the heat losses are negligible during the short period of laser heating

$$\frac{\partial T}{\partial x}(0,t) = \frac{\partial T}{\partial x}(L,t) = 0. \tag{4.14}$$

Tzou obtained an analytical solution for Eq. (4.12) subject to the initial and boundary conditions given by Eqs. (4.13) and (4.14) by applying Laplace transformation. The transformed

solution is given by

$$\overline{T}(x,p) = A_1 \exp(Bx) + A_2 \exp(-Bx) + A_3 \exp(-x/\delta), \tag{4.15}$$

where

$$A_1 = \frac{(A_3/\delta)(\exp(-L/\delta) - \exp(-BL))}{B(\exp(BL) - \exp(-BL))}; \qquad A_2 = A_1 - \frac{A_3}{B\delta}; \tag{4.16}$$

$$A_3 = \frac{S_0(C_2 \exp(-2a) - C_1 S_b)}{(1/\delta)^2 - B^2}; \qquad B = \sqrt{\frac{p(1+p\tau_q}{\alpha(1+p\tau_T)}}; \qquad C_1 = \frac{1+p\tau_q}{k(1+p\tau_{T)}}; \tag{4.17}$$

$$C_2 = \frac{\tau_q}{k(1+p\tau_{T)}}; \qquad S_b = t_p \left[\frac{\exp(-2a) - \exp(-2p\tau_q)}{pt_p - a} + \frac{\exp(-2p\tau_q)}{pt_p + a} \right]. \tag{4.18}$$

By using Eqs. (4.15) to (4.18) Tzou [71] has successfully simulated the transient thermal response on the front surface of 100 nm and 200 nm thick gold films with $\tau_T = 90\ ps$ and $\tau_q = 8.5\ ps$

4.3 Numerical Solution of the DPL Equation

The heat transport equations used to describe the thermal behavior of microstructures in 1D can be expressed as [71]:

$$-\nabla \cdot q + S = \rho C_p \frac{\partial T}{\partial t}, \tag{4.19}$$

$$q + \tau_q \frac{\partial q}{\partial t} = -k \left[\frac{\partial T}{\partial x} + \tau_T \frac{\partial}{\partial t} \left(\frac{\partial T}{\partial x} \right) \right], \tag{4.20}$$

where S is the heat source. Eliminating the heat flux q between the two Eqs. (4.19) and (4.20) we obtain the DPL equation in 1D as follows:

$$\frac{\tau_q}{\alpha} \frac{\partial^2 T}{\partial t^2} + \frac{1}{\alpha} \frac{\partial T}{\partial t} = \frac{\partial^2 T}{\partial x^2} + \tau_T \frac{\partial^3 T}{\partial x^2 \partial t} + \frac{1}{k} \left(S + \tau_q \frac{\partial S}{\partial t} \right). \tag{4.21}$$

An explicit finite-difference scheme will be employed to solve equation (4.21) subject to the initial and boundary conditions

$$T(x,0) = T_0, \qquad \text{and} \qquad \frac{\partial T}{\partial t}(x,0) = 0, \tag{4.22}$$

$$\frac{\partial T}{\partial x}(0,t) = \frac{\partial T}{\partial x}(L,t) = 0. \tag{4.23}$$

Centered differencing approximates the second-order derivatives in space:

$$\frac{\partial^2 T}{\partial x^2} = \frac{1}{\Delta x^2}[T_{i+1}^n - 2T_i^n + T_{i-1}^n]. \tag{4.24}$$

The mixed derivative is approximated using centered difference in space and backward difference in time:

$$\frac{\partial^3 T}{\partial t \partial x^2} = \frac{1}{\Delta t \Delta x^2}[T_{i+1}^n - 2T_i^n + T_{i-1}^n - T_{i+1}^{n-1} + 2T_i^{n-1} - T_{i-1}^{n-1}]. \tag{4.25}$$

Forward differencing approximates the first-order derivative in time:

$$\frac{\partial T}{\partial t} = \frac{1}{\Delta t}[T_i^{n+1} - T_i^n]. \tag{4.26}$$

Centered differencing is employed for the time derivative in the source term:

$$\frac{\partial S}{\partial t} = \frac{1}{2\Delta t}[S_i^{n+1} - S_i^{n-1}]. \tag{4.27}$$

Substituting Eqs. (4.24)–(4.27) into Eq. (4.21) renders an explicit finite-difference equation to be solved for the unknown T_i^{n+1}.

4.4 Stability Analysis

The stability and convergence criteria for this finite-difference algorithm subject to initial and boundary conditions (4.22)–(4.23) can be obtained by performing the von Neumann

eigen mode analysis [16]. For a prescribed space increment, the maximum allowed time increment to achieve a stable solution is given by

$$\Delta t = \frac{-(4\alpha\tau_{_T} - \Delta x^2) + \sqrt{(4\alpha\tau_{_T} - \Delta x^2)^2 + 16\alpha\tau_{_q}\Delta x^2}}{4\alpha}. \tag{4.28}$$

For $\tau_{_T} = \tau_{_q} = 0$ Eq. (4.21) reduces to Fourier diffusion and for $\tau_{_T} = 0$ Eq. (4.21) reduces to CV wave equation.

4.5 Results and Discussion

Figure 4.1 shows the comparison between the numerical, analytical [16] and the experimental results of Brorson et al. [12] and Qiu and Tien [65, 66] corresponding to the front surface transient response for a $0.1\mu m$ thick gold film. The thermal properties ($\alpha = 1.2 \times 10^{-4} m^2 s^{-1},\ k = 315 W m^{-1} K^{-1},\ \tau_{_T} = 90ps,\ \tau_q = 8.5ps$) are assumed to be constant. The temperature change is normalized by the maximum value that occurs during the short-time transient:

$$\frac{\Delta T(0,t)}{[\Delta T(0,t)]_{max}} \equiv \frac{T(0,t) - T_0}{[T(0,t) - T_0]_{max}}. \tag{4.29}$$

The resulting normalized temperature change is proportional to the normalized surface reflectivity measured directly in experiments.

The numerical result with $\tau_T = 90ps$ and $\tau_q = 8.5ps$ [75] and the analytical result agree with experimental results very well, supporting the lagging behavior in the short-pulse laser heating process on metals. But the numerical results corresponding to $\tau_T = 0$ and $\tau_q = 0$ (diffusion) and $\tau_T = 0$ (CV wave) do not agree with the experimental results. This suggests that the parabolic and the hyperbolic heat conduction equations fail to capture the microscale responses during short pulse laser metal interaction. The classical diffusion and

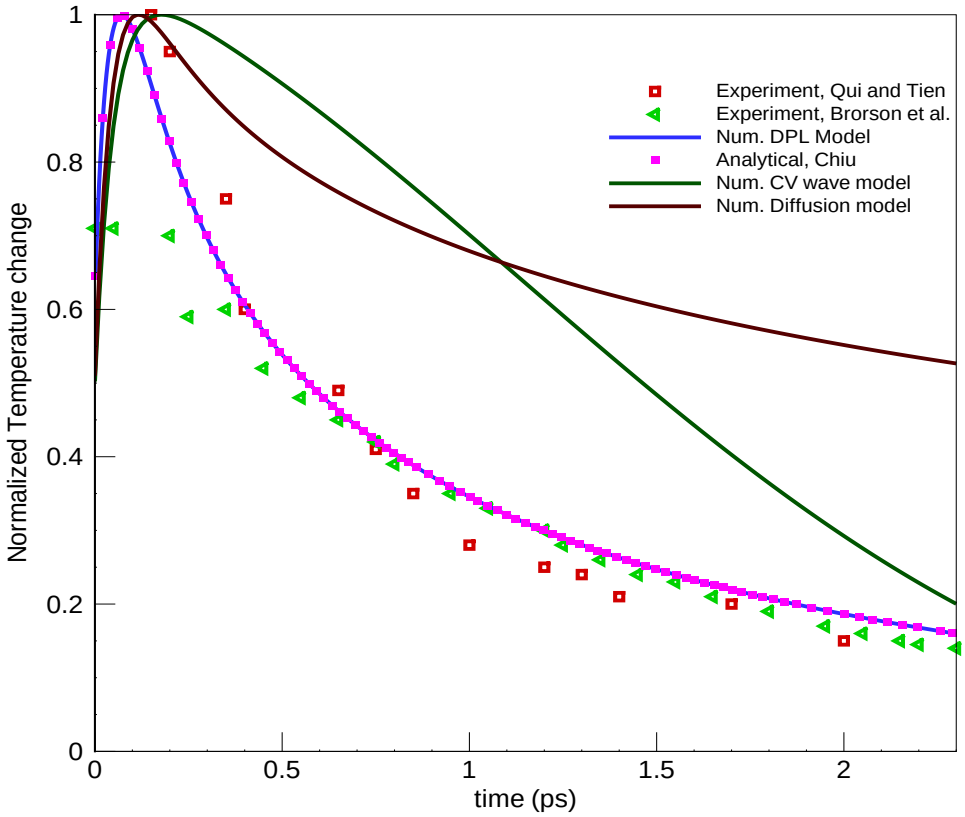

Figure 4.1 Front surface transient response for a $0.1\mu m$ gold film. Comparison between numerical, analytical [16] and experimental results [12, 65]. $\alpha = 1.2 \times 10^{-4} m^2 s^{-1}$, $k = 315 W m^{-1} K^{-1}$, $\tau_T = 90 ps$, $\tau_q = 8.5 ps$.

CV wave models cannot describe the slow thermalization process shown by the DPL equation. From a physical point of view, the macroscopic approach employed in these models neglects the microstructural interaction effect in the short-time transient, rendering an overestimated temperature in the transient response. This is shown in the Figure 4.1. In the thermalization process, the diffusion model predicts the highest temperature among all three (DPL, CV wave and parabolic models). Compared to the experimental result, the large difference arises from neglect of both the microstructural interaction effect in space and the fast-transient effect in time. The CV wave model accounting for the fast-transient effect in the short-time response, reduces the difference between the diffusion model and the experimental result. Since the CV wave model neglects the microstructural interaction in space, still it overestimates the transient temperature. Since the dual phase lag model incorporates the delay time caused by the phonon-electron interaction in microscale, the transient temperature is found to be closer to the experimental observation. For $\Delta x = 5nm$ the maximum allowed time step to obtain stable solutions is $3.27fs$, obtained using Eq. (4.28). The finite-difference analysis provided in this section can be extended to study multi-dimensional effects in thin-film heating. This will be the subject of study in the next Chapter.

Chapter 5
THREE-DIMENSIONAL SHORT PULSE LASER HEATING ON GOLD FILM

In this chapter, the transient temperature distribution in a sub-micron sized gold film exposed to a femtosecond laser beam will be examined numerically in three dimensions. The laser source term is modified to accomodate the three-dimensional laser heating at different locations of the gold film. We will also consider laser heating at different locations of the gold film. The finite-difference method for this problem will be presented along with three-dimensional stability criteria derived using von Neumann stability analysis. Significant differences seen in the transient temperature among DPL, parabolic and hyperbolic models will be explained.

5.1 Introduction

In continuing the investigation of the transient response on a sub-micron sized gold film, we will now try to capture the three-dimensional effect in thin film heating. We will investigate femtosecond laser heating of gold film in three dimensions using the dual phase lag (DPL) model and consider laser heating at different locations on the metal film, as shown in Figure 5.1. The thickness of the gold film is $100nm$, while the length and width are $500nm$. A numerical solution based on an explicit finite-difference method will be employed to solve the DPL heat conduction equation. The stability and convergence criteria for this finite-difference algorithm is obtained using von Neumann eigenmode analysis [16], and grid function convergence tests will be performed. The energy absorption rate, which is used to model femtosecond laser heating, will be modified to accommodate this three-dimensional

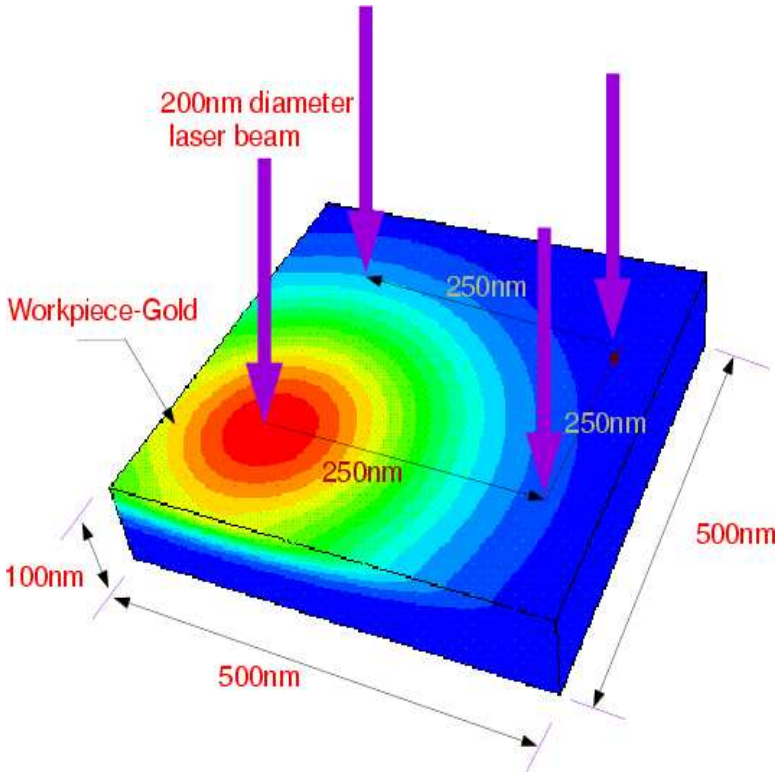

Figure 5.1 3-D schematic of laser heating at different locations

case. The DPL model reduces to parabolic and hyperbolic models under different values of relaxation times; the diffusion model results when $\tau_T = 0$ and $\tau_q = 0$, while the CV wave model is obtaining by setting $\tau_T = 0$. We will compare the transient temperature distribution produced by these three models and demonstrate significant differences between them.

5.2 Mathematical Formulation

The heat transport equations used to describe the thermal behavior of microstructures are expressed in [71] as

Energy equation:

$$-\nabla \cdot \boldsymbol{q}(\boldsymbol{r}, t) + S = \rho C_p \frac{\partial T(\boldsymbol{r}, t)}{\partial t}, \tag{5.1}$$

Heat Flux equation (DPL model):

$$\boldsymbol{q}(\boldsymbol{r}, t + \tau_q) = -k\nabla T(\boldsymbol{r}, t + \tau_{_T}), \tag{5.2}$$

where $\boldsymbol{q}$ is the heat flux vector, T is temperature, k is thermal conductivity, C_v is specific heat, ρ is density, S is a heat source; τ_T (relaxation time corresponding to temperature gradient), τ_q (relaxation time corresponding to the heat flux) and $\tau_{_T}$ (relaxation time corresponding to the temperature gradient) are positive constants.

Using Taylor series expansion, the first order approximation of Eq. (5.2) gives

$$\boldsymbol{q}(\boldsymbol{r}, t) + \tau_q \frac{\partial \boldsymbol{q}(\boldsymbol{r}, t)}{\partial t} = -k\left(\nabla T(\boldsymbol{r}, t) + \tau_{_T} \frac{\partial(\nabla T(\boldsymbol{r}, t))}{\partial t}\right). \tag{5.3}$$

In one dimension the heat source is given by

$$S(x, t) = 0.94J\left[\frac{1 - R}{t_p \delta}\right] \exp\left(-\frac{x}{\delta} - \frac{1.992 \mid t - 2t_p \mid}{t_p}\right) \tag{5.4}$$

where laser fluence $J = 13.7J/m^2$, $t_p = 96fs\,(1fs = 10^{-15}s)$, penetration depth $\delta = 15.3nm\,(1nm = 10^{-9}m)$, and $R = 0.93$ [75]. In three dimensions we can extend this heat source term to

$$S(\boldsymbol{r}, t) = 0.94J\left[\frac{1 - R}{t_p \delta}\right] \exp\left(-\frac{(x - \frac{L_x}{2})^2 + (y - \frac{L_y}{2})^2}{2r_o^2} - \frac{z}{\delta} - \frac{1.992 \mid t - 2t_p \mid}{t_p}\right) \tag{5.5}$$

5.3 Numerical Analysis

To develop a finite-difference scheme, we first rewrite the heat transport equation (5.3) as follows:

$$q_1 + \tau_q \frac{\partial q_1}{\partial t} = -k\left[\frac{\partial T}{\partial x} + \tau_{_T} \frac{\partial}{\partial t}\left(\frac{\partial T}{\partial x}\right)\right], \tag{5.6a}$$

$$q_2 + \tau_q \frac{\partial q_2}{\partial t} = -k\left[\frac{\partial T}{\partial y} + \tau_{_T} \frac{\partial}{\partial t}\left(\frac{\partial T}{\partial y}\right)\right], \tag{5.6b}$$

$$q_3 + \tau_q \frac{\partial q_3}{\partial t} = -k\left[\frac{\partial T}{\partial z} + \tau_{_T} \frac{\partial}{\partial t}\left(\frac{\partial T}{\partial z}\right)\right], \tag{5.6c}$$

Differentiating Eqs. (5.6a)–(5.6c) with respect to x, y, z, respectively, and substituting the results into Eq. (5.1) leads to

$$\frac{\tau_q}{\alpha}\frac{\partial^2 T}{\partial t^2}+\frac{1}{\alpha}\frac{\partial T}{\partial t}-\tau_{_T}\frac{\partial(\nabla^2 T)}{\partial t}=\nabla^2 T+\frac{1}{k}\left(S+\tau_q\frac{\partial S}{\partial t}\right), \tag{5.7}$$

where ∇^2 is the Laplace operator and α the thermal diffusivity. The initial conditions were chosen as follows:

$$T(x,y,z,0)=T_0, \qquad \frac{\partial T}{\partial t}(x,y,z,0)=0, \tag{5.8}$$

with $T_0=300K$. Insulated boundary conditions are imposed on all sides of the film because heat loss from the film surface is nearly negligible during the picosecond heating period:

$$\frac{\partial T}{\partial n}=0 \qquad \text{where,} \qquad n=x,y,z. \tag{5.9}$$

An explicit finite-difference scheme has been employed to solve Eq. (5.7) subject to the initial and boundary conditions given by Eqs. (5.8) and (5.9). Centered differencing approximates second-order derivatives in space, second-order derivative in time and first-order derivative in the laser heat source term:

$$\frac{\partial^2 T}{\partial x^2} = \frac{1}{\Delta x^2}[T^n_{i+1,j,l}-2T^n_{i,j,l}+T^n_{i-1,j,l}] \tag{5.10a}$$

$$\frac{\partial^2 T}{\partial y^2} = \frac{1}{\Delta y^2}[T^n_{i,j+1,l}-2T^n_{i,j,l}+T^n_{i,j-1,l}] \tag{5.10b}$$

$$\frac{\partial^2 T}{\partial z^2} = \frac{1}{\Delta z^2}[T^n_{i,j,l+1}-2T^n_{i,j,l}+T^n_{i,j,l-1}]. \tag{5.10c}$$

$$\frac{\partial^2 T}{\partial t^2} = \frac{1}{(\Delta t)^2}[T^{n+1}_{i,j,l}-2T^n_{i,j,l}+T^{n-1}_{i,j,l}]. \tag{5.10d}$$

$$\frac{\partial S}{\partial t} = \frac{1}{2\Delta t}[S^{n+1}_{i,j,l}-S^{n-1}_{i,j,l}], \tag{5.10e}$$

The mixed derivative is approximated using a centered difference in space and backward difference in time [75]:

$$\frac{\partial^3 T}{\partial t \partial x^2} = \frac{1}{\Delta t \Delta x^2}[T^n_{i+1,j,l} - 2T^n_{i,j,l} + T^n_{i-1,j,l} - T^{n-1}_{i+1,j,l} + 2T^{n-1}_{i,j,l} - T^{n-1}_{i-1,j,l}] \quad (5.11a)$$

$$\frac{\partial^3 T}{\partial t \partial y^2} = \frac{1}{\Delta t \Delta y^2}[T^n_{i,j+1,l} - 2T^n_{i,j,l} + T^n_{i,j-1,l} - T^{n-1}_{i,j+1,l} + 2T^{n-1}_{i,j,l} - T^{n-1}_{i,j-1,l}] \quad (5.11b)$$

$$\frac{\partial^3 T}{\partial t \partial z^2} = \frac{1}{\Delta t \Delta z^2}[T^n_{i,j,l+1} - 2T^n_{i,j,l} + T^n_{i,j,l-1} - T^{n-1}_{i,j,l+1} + 2T^{n-1}_{i,j,l} - T^{n-1}_{i,j,l-1}]. \quad (5.11c)$$

Forward differencing approximates the first-order derivative in time:

$$\frac{\partial T}{\partial t} = \frac{1}{\Delta t}[T^{n+1}_{i,j,l} - T^n_{i,j,l}], \quad (5.12)$$

where n is the index of location in time and i, j and k are the indices of the locations in x, y and, z directions respectively. By substituting Eqs. (5.10a) to (5.12) into Eq. (5.7) and rearranging we can represent the unknown $T^{n+1}_{i,j,k}$ in terms of the known values on the right hand side:

$$\begin{aligned} T^{n+1}_{i,j,l} = {} & C_1 * [C_2 * [T^n_{i+1,j,l} + T^n_{i-1,j,l}] + C_4 * [T^n_{i,j+1,l} + T^n_{i,j-1,l}] \\ & + C_5 * [T^n_{i,j,l+1} + T^n_{i,j,l-1}] + C_3 * T^n_{(i,j,l)} + C_7 * [T^{n-1}_{i+1,j,l} + T^{n-1}_{i-1,j,l}] \\ & + C_8 * [T^{n-1}_{i,j+1,l} + T^{n-1}_{i,j-1,l}] + C_9 * [T^{n-1}_{i,j,l+1} + T^{n-1}_{i,j,l-1}] + C_6 * T^{n-1}_{(i,j,l)} \\ & + \frac{1}{k}\left[S^n_{i,j,l} + \tau_q\left(\frac{1}{2\Delta t}[S^{n+1}_{i,j,l} - S^{n-1}_{i,j,l}]\right)\right]], \end{aligned} \quad (5.13)$$

where

$$C_1 = \frac{\Delta t^2}{\Delta t + 1}; \quad (5.14a)$$

$$C_2 = \frac{1}{\Delta x^2} + \frac{\tau_T}{\Delta x^2 \Delta t}; \quad (5.14b)$$

$$C_3 = -\frac{2}{\Delta x^2} - \frac{2}{\Delta y^2} - \frac{2}{\Delta z^2} - \frac{2\tau_T}{\Delta x^2 \Delta t} - \frac{2\tau_T}{\Delta y^2 \Delta t} - \frac{2\tau_T}{\Delta z^2 \Delta t} + \frac{1}{\alpha \Delta t} + \frac{2\tau_q}{\alpha \Delta t^2}; \quad (5.14c)$$

$$C_4 = \frac{1}{\Delta y^2} + \frac{\tau_T}{\Delta y^2 \Delta t}; \quad (5.14d)$$

$$C_5 = \frac{1}{\Delta z^2} + \frac{\tau_{_T}}{\Delta z^2 \Delta t}; \tag{5.15a}$$

$$C_6 = \frac{2\tau_{_T}}{\Delta x^2 \Delta t} + \frac{2\tau_{_T}}{\Delta y^2 \Delta t} + \frac{2\tau_{_T}}{\Delta z^2 \Delta t} + \frac{\tau_{_q}}{\alpha \Delta t^2}; \tag{5.15b}$$

$$C_7 = -\frac{\tau_{_T}}{\Delta x^2 \Delta t}; \tag{5.15c}$$

$$C_8 = -\frac{\tau_{_T}}{\Delta y^2 \Delta t}; \tag{5.15d}$$

$$C_9 = -\frac{\tau_{_T}}{\Delta z^2 \Delta t}. \tag{5.15e}$$

The 3-D explicit finite-difference FORTRAN 90 code written for this problem can be found in Appendix A.

5.4 Stability Analysis

The stability criterion for this finite-difference algorithm subject to the initial and boundary conditions (5.8)-(5.9) is obtained using Von Neumann eigenmode analysis [16] :

$$\frac{\Delta t(2\Delta t + 4\tau_{_T})}{\Delta x^2(\Delta t + 2\tau_q)} + \frac{\Delta t(2\Delta t + 4\tau_{_T})}{\Delta y^2(\Delta t + 2\tau_q)} + \frac{\Delta t(2\Delta t + 4\tau_{_T})}{\Delta z^2(\Delta t + 2\tau_q)} \leq 1 \tag{5.16}$$

The maximum allowed time increment to achieve stable and convergent solutions under a prescribed space increment is obtained by rearranging Eq. (5.16):

$$\Delta t = \frac{-b \pm \sqrt{b^2 - 4ac}}{2a} \tag{5.17}$$

where

$$a = -2\alpha(\Delta y^2 \Delta z^2 + \Delta x^2 \Delta z^2 + \Delta x^2 \Delta y^2) \tag{5.18a}$$

$$b = \Delta x^2 \Delta y^2 \Delta z^2 - 4\alpha \Delta y^2 \Delta z^2 \tau_{_T} - 4\alpha \Delta x^2 \Delta z^2 \tau_{_T} - 4\alpha \Delta y^2 \Delta y^2 \tau_{_T} \tag{5.18b}$$

$$c = \Delta x^2 \Delta y^2 \Delta z^2 \tau_q. \tag{5.18c}$$

5.5 Results and Discussion

Fig. 5.1 shows schematic of pulsating laser beam of $200nm$ diameter, heating the top surface of the gold film at various locations of the film every $0.3ps$. The energy absorption rate given by Eq. (5.5) is used to model three-dimensional laser heating. We assume insulated boundary walls and constant thermal properties ($\alpha = 1.2 \times 10^{-4} m^2 s^{-1}$, $k = 315 W m^{-1} K^{-1}$, $\tau_T = 90ps$, $\tau_q = 8.5ps$).

To start with, a uniform grid $101 \times 101 \times 21$ was used. The simulation was performed for a duration of $2.5ps$. For $\Delta x = \Delta y = \Delta z = 5nm$, Δt which satisfies the stability criterion was found to be $3.27fs$. Furthermore, different grids $51 \times 51 \times 11$ and $201 \times 201 \times 41$ were used to check the consistency of the numerical solution in the form of grid function convergence tests. Fig. 5.2 shows the temperature plots obtained on the top surface of the gold film at $t = 0.3ps$ using grids $51 \times 51 \times 11$, $101 \times 101 \times 21$, $201 \times 201 \times 41$. We can see from Fig. 5.2 that reducing the step size by a factor of two and time step by a factor of four results in reduction of error by a factor of four, implying that the numerical solution is consistent.

Figures 5.3–5.6 show the comparison of transient temperature distribution of the gold at different time, predicted by DPL, hyperbolic and parabolic heat conduction models. As explained earlier, $\tau_T = 90ps$, $\tau_q = 8.5ps \rightarrow$ DPL model; $\tau_T = 0$, $\tau_q = 0 \rightarrow$ parabolic model and $\tau_q = 8.5ps$, $\tau_T = 0 \rightarrow$ hyperbolic model. The finite-difference code is thus capable of capturing parabolic and hyperbolic models and the stability and convergence criterion can be applied to parabolic and hyperbolic models.

From Figures 5.3–5.6 we can see that the hyperbolic and parabolic models predict a higher temperature compared to the DPL model on the top surface of the gold film. We

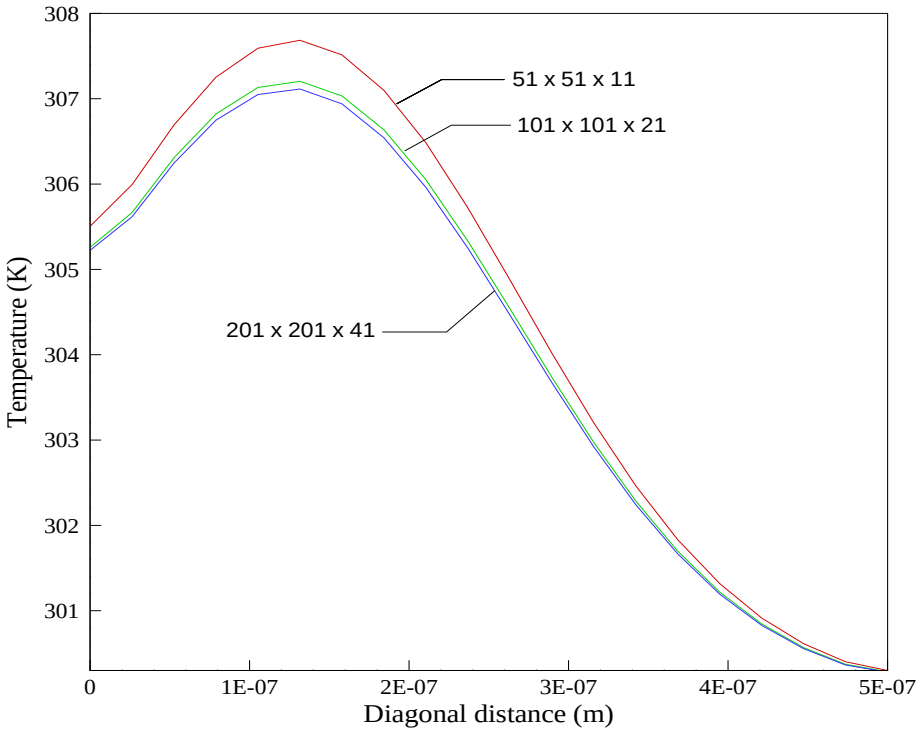

Figure 5.2 Temperature plots obtained on the top surface of the gold film at $t = 0.3ps$ using grids $51 \times 51 \times 11$, $101 \times 101 \times 21$ and, $201 \times 201 \times 41$.

can also observe that the heat affected zone is significantly larger for the DPL model than the other models. Thermally undisturbed zones can be observed for the diffusion and the CV wave models. The microstructural interaction effect incorporated in the DPL model, reflected by the delayed time for establishing the temperature gradient across a material volume (τ_T) significantly extends the physical domain of the thermal penetration depth. In fact, Qiu and Tien [65] indicated that a larger heat-affected zone and the higher temperature level within the heat-affected zone are the main reasons that the parabolic two-step model agrees well with the experimental results of the short-pulse laser heating on metals [12]. The CV wave model and the diffusion model predict a higher temperature level in the heat affected zone than the DPL model, but the penetration depth is much shorter owing to the formation of the thermally undisturbed zone. One more phenomenon which can be observed in the results is that the hyperbolic model shows more diffusion than the parabolic model until $t \sim 1.56$ (see Figures 5.3 and 5.4). This might sound contradictory, but the one-dimensional results (see Fig. 4.1) seem to show the same behavior until $t \sim 1.56$. After $t \sim 1.56$ the parabolic model shows more diffusion than the hyperbolic model (see Figures 5.5 and 5.6) as observed in the one-dimensional results (see Fig. 4.1). Since the DPL results in 3D exhibit behavior similar to the 1-D results, we believe it should be physically realizable in three dimensions. Also, since the dual phase lag model incorporates a delay time associated with the effects of phonon-electron interaction at microscale level, we must expect that the transient temperature will be close to the experimental observation. The large difference between the DPL and the parabolic model can be attributed to the fact that the latter neglects both the microstructural interaction effect in space and the fast-transient effect

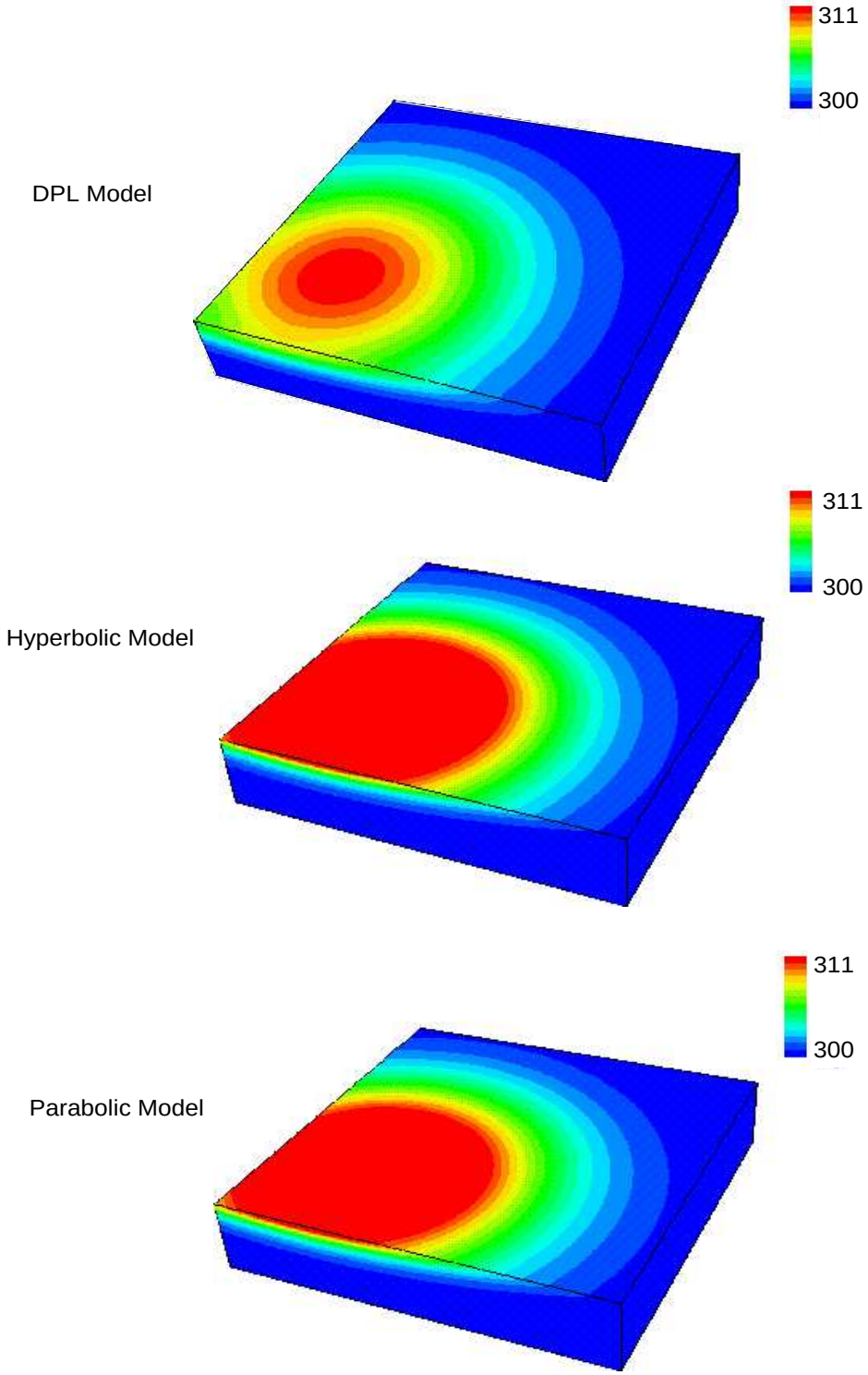

Figure 5.3 Temperature distribution of gold film at $0.31ps$ predicted by DPL, hyperbolic and parabolic models

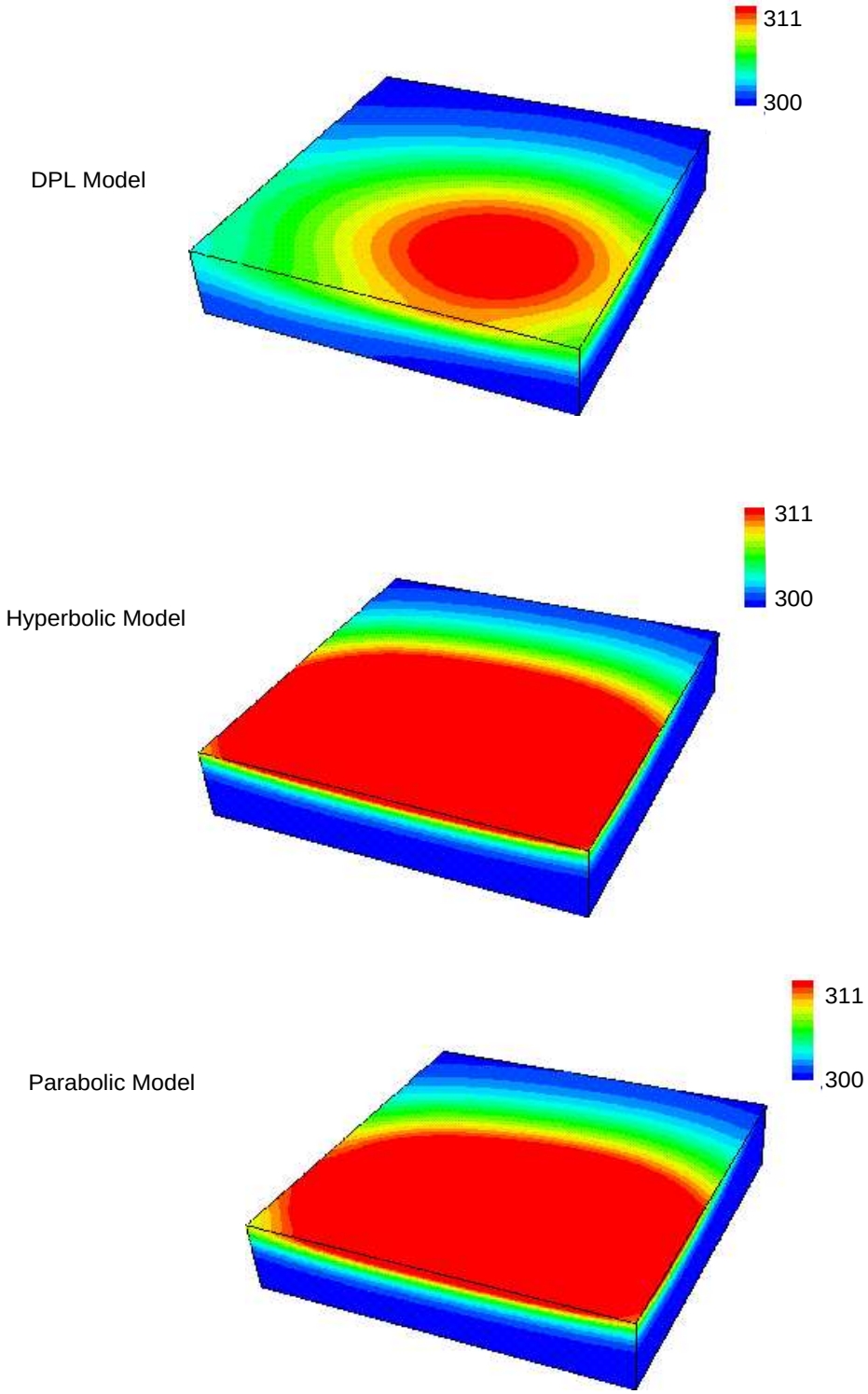

Figure 5.4 Temperature distribution of gold film at 0.93ps predicted by DPL, hyperbolic and parabolic models

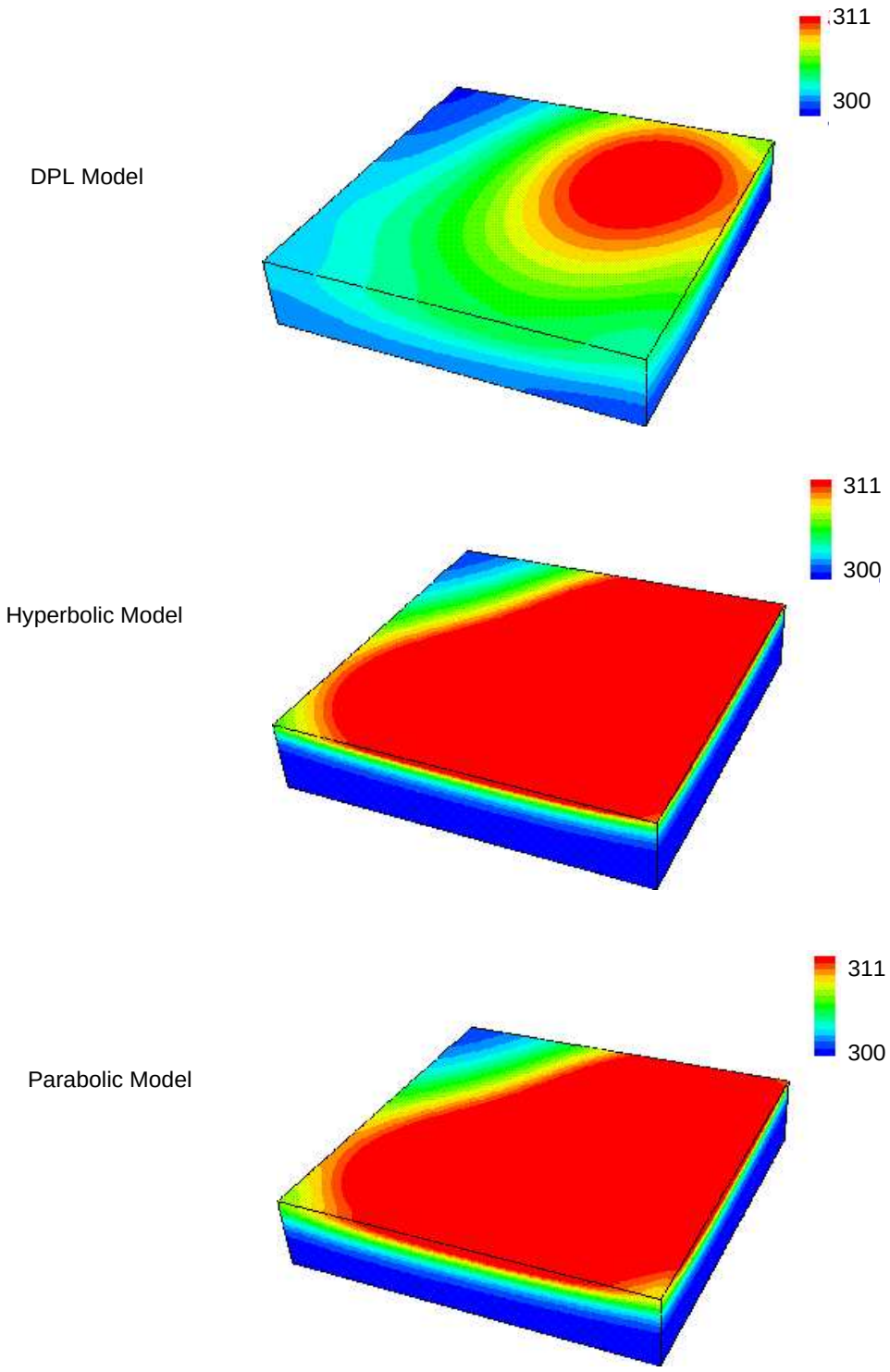

Figure 5.5 Temperature distribution of gold film at 1.56ps predicted by DPL, hyperbolic and parabolic models

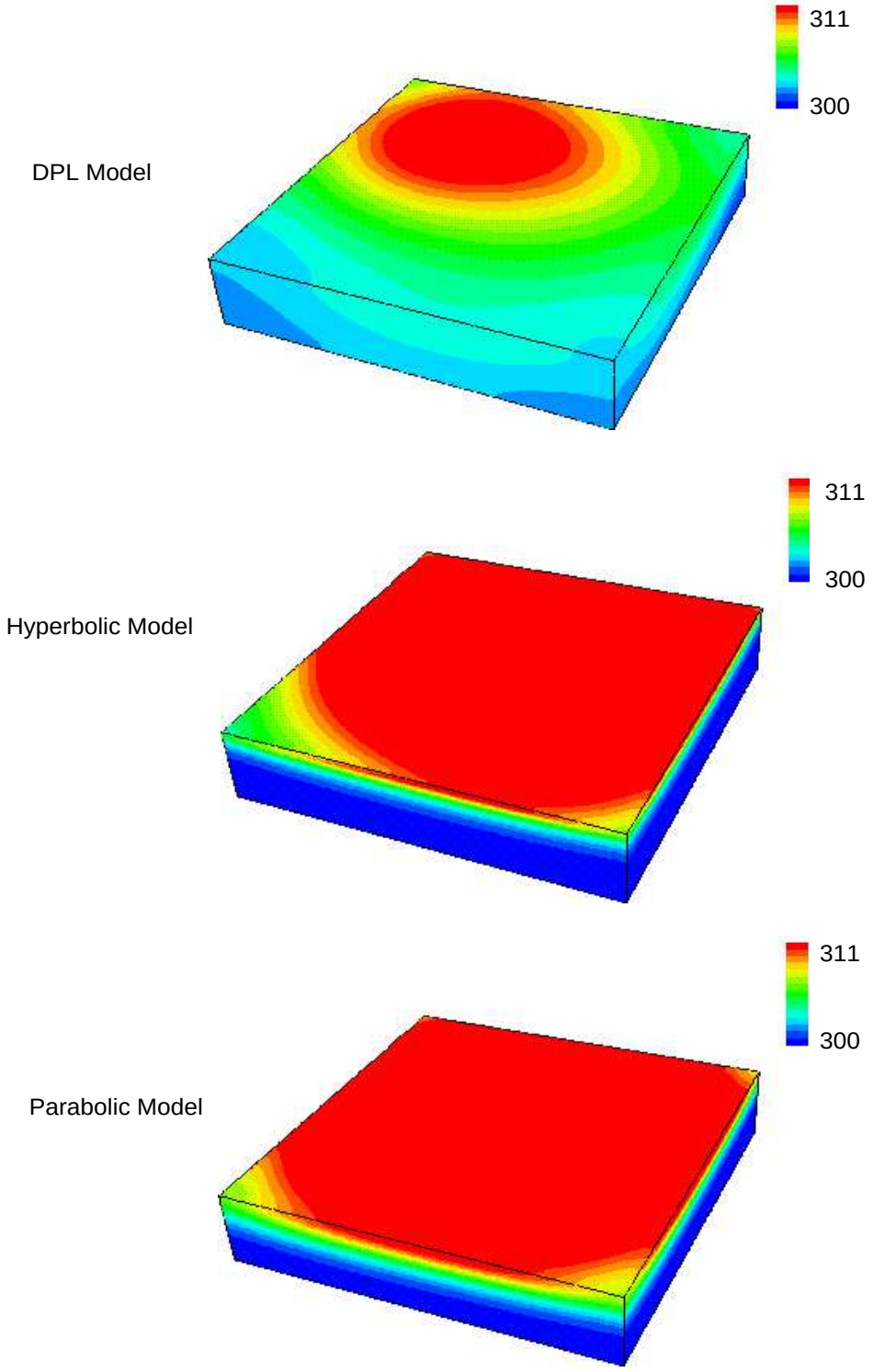

Figure 5.6 Temperature distribution of gold film at 2.18*ps* predicted by DPL, hyperbolic and parabolic models

in time. The CV model differs from the DPL model due to the fact that it neglects the microstructural interaction effect in space and considers only the fast-transient effect in the short-time response.

The finite-difference algorithm used here is based on an explicit finite-difference scheme which is only conditionally stable. The important consequence of the stability criterion is that as the spatial grid is refined to achieve accuracy, the time steps must be decreased as the square of the spatial grid size to maintain stability. This is often too restrictive, and it has led to the development of implicit methods. In the next chapter we will develop an implicit finite-difference scheme of the Crank–Nicolson type for solving the DPL equation.

Chapter 6
A NEW NUMERICAL TECHNIQUE TO SOLVE 1-D and 3-D DPL EQUATIONS

In this chapter, we will develop an implicit finite-difference scheme of the Crank–Nicolson type for solving the one-dimensional DPL equation. Grid function convergence tests will be performed to test the convergence of the numerical solution. Stability analysis will be performed using a von Neumann stability analysis. We will show that the proposed numerical technique is unconditionally stable. For the sake of comparison we will develop a numerical procedure for the semi-infinite slab problem considered in Chapter III. We will also develop a different numerical formulation to solve the DPL equation implicitly. The numerical technique will be extended to three-dimensions and a numerical procedure for computing the transient temperature distribution during short pulse laser heating of thin films will be presented. The discretized 3-D microscale DPL equation will be solved using a Douglas–Gunn time-splitting method and δ-*form* Douglas–Gunn time-splitting method. The performance of the proposed numerical scheme will be compared with the numerical techniques available in the literature and shown to be superior to all other methods known to this author.

6.1 Introduction

The finite-difference algorithm used in the previous sections is based on an explicit finite-difference scheme that is only conditionally stable. If we recall that

$$k \leq \frac{-(4Z - h^2) \pm \sqrt{(4Z - h^2)^2 + 16h^2}}{4}, \tag{6.1}$$

In order to achieve accuracy the spatial grid has to be reduced, and consequently the time step must be decreased as the square of the spatial grid size to maintain stability. This is often too restrictive, and it has led to the development of implicit methods such as those we next consider.

Dai and Nassar [34] have developed an implicit finite-difference scheme of the Crank–Nicolson type by introducing an intermediate function for solving the DPL Eq. (2.39) in a finite interval. The scheme is two-level in time. The DPL equation is split into a system of two equations. The individual equations are then discretized using Crank–Nicolson scheme and solved sequentially. It is shown by the discrete energy method [32, 33, 58] that the scheme is unconditionally stable, and the numerical scheme is non-oscillatory. The scheme has been generalized to a three-dimensional rectangular thin film case where the thickness is at the sub-microscale [29].

Further, Dai and Nassar [30, 31] developed high-order unconditionally stable two-level compact finite-difference schemes for solving Eq. (2.39) in one- and three-dimensional thin films, respectively. To solve the 3-D implicit finite-difference scheme, a preconditioned Richardson iteration technique is developed so that only a tridiagonal linear system is solved for each iteration. Dai et al., [22] have considered the heat transport equation in spherical co-ordinates and have developed a three-level finite-difference scheme for solving the heat transport equation in a microsphere.

Zhang and Zhao [80, 81] have designed a computational procedure to solve the sparse linear systems arising from the discretized 3-D microscale heat transport equations. They examine a few iterative techniques (see Table 6.1) and present comparisons in terms of aver-

Iterative methods	average number of iterations				total CPU time in seconds			
	N=11	N=21	N=31	N=41	N=11	N=21	N=31	N=41
Gauss–Seidel	196	719	1568	2744	12.85	554.92	9422.70	38752.46
SOR	33	66	95	123	2.44	53.91	584.70	1171.84
CG	1.91	3.40	4.28	5.98	0.28	2.73	19.42	67.73
PCG	2	2	2	3	0.38	3.76	19.87	68.05

Table 6.1 Performance comparison of different iteration methods without scaling the linear systems ($\Delta t = 0.01$) (reproduced from [81]).

age number of iterations per linear system solution (per time step) and CPU time in seconds for the entire simulation for the Gauss–Seidel, SOR (successive overrelaxation) with optimal overrelaxation parameters, CG (conjugate gradient), and PCG (preconditioned conjugate gradient). The data in Table 6.1 indicate that both Gauss–Seidel and SOR methods are not very scalable with respect to the problem size and the CPU timings are very large for large values of N. The average number of CG iterations increases faster than that of the PCG iterations, indicating that for very large size problems PCG performs better than CG. Zhang and Zhao [80, 81] have used Dirichlet boundary conditions in their formulation. Applying Neumann boundary conditions results in *non-symmetric* seven banded positive semi-definite matrices that are not suitable for iterative methods like CG and PCG. Given this, we have to seek a different numerical technique.

In this chapter we will develop an implicit finite-difference scheme of Crank–Nicolson type for solving the one-dimensional DPL equation. Unlike other techniques available in the literature which split the DPL equation into a system of two equations and then apply discretization the proposed numerical technique solves the governing equations directly. This approach considerably reduces the number of arithmetic operations involved, and consequently, the computational time is reduced. The method can be easily generalized to solve

the heat transport equation with variable thermal properties. We will also develop a different numerical formulation to solve the DPL equation implicitly.

The numerical technique will be extended to three-dimensions and a numerical procedure for computing the transient temperature distribution during short pulse laser heating of thin films will be presented. The discretized 3-D microscale DPL equation is then solved using the *δ-form* Douglas–Gunn time splitting technique. Performance of the proposed numerical technique will be compared with that of numerical techniques available in the literature.

6.2 Unconditionally stable numerical scheme for solving 1-D DPL equation

For the sake of comparison we will again consider heat conduction in a semi-infinite slab subject to a sudden temperature rise on one of its boundaries. First mathematical formulation will be presented followed by numerical scheme, von Neumann stability analysis and results.

6.2.1 Mathematical Formulation

Recalling the formulation for the non-dimensional form of the one-dimensional DPL model from Chapter III we can represent the governing equations as

$$\frac{\partial T}{\partial t} + \frac{\partial^2 T}{\partial t^2} - Z\frac{\partial}{\partial t}\left(\frac{\partial^2 T}{\partial x^2}\right) = \frac{\partial^2 T}{\partial x^2}. \tag{6.2}$$

Initial Conditions:

$$T(x,0) = 0, \tag{6.3}$$

$$\frac{\partial T}{\partial t}(x,0) = 0 \qquad \text{for} \qquad x \in [0,\infty). \tag{6.4}$$

Boundary Conditions:

$$T(0,t) = 1 \qquad \text{for} \qquad t > 0, \tag{6.5}$$

$$\frac{\partial T}{\partial x}(x,t) = 0 \qquad x \to \infty, \tag{6.6}$$

6.2.2 Finite-difference Scheme

Applying trapezoidal integration to Eq. (6.2) results in

$$T_m^{n+1} - T_m^n + \left(\frac{\partial T}{\partial t}\right)_m^{n+1} - \left(\frac{\partial T}{\partial t}\right)_m^n - Z\left[\left(\frac{\partial^2 T}{\partial x^2}\right)_m^{n+1} - \left(\frac{\partial^2 T}{\partial x^2}\right)_m^n\right] = \frac{\Delta t}{2}\left[\left(\frac{\partial^2 T}{\partial x^2}\right)_m^{n+1} + \left(\frac{\partial^2 T}{\partial x^2}\right)_m^n\right]. \tag{6.7}$$

We apply a second-order backward difference for the time derivative at $n+1$ and a centered difference for the time derivative at n. The second-order derivatives in space are approximated using a centered-difference scheme:

$$\left(\frac{\partial T}{\partial t}\right)_m^{n+1} = \frac{1}{2\Delta t}\left[3T_m^{n+1} - 4T_m^n + T_m^{n-1}\right], \tag{6.8a}$$

$$\left(\frac{\partial T}{\partial t}\right)_m^{n} = \frac{1}{2\Delta t}\left[T_m^{n+1} - T_m^{n-1}\right], \tag{6.8b}$$

$$\frac{\partial^2 T}{\partial x^2} = \frac{1}{\Delta x^2}\left[T_{m+1} - 2T_m + T_{m-1}\right]. \tag{6.8c}$$

The discretization shown in Eqs. (6.8a)–(6.8c) is second order accurate locally which makes the entire numerical scheme only first order accurate globally.

After plugging Eqs. (6.8a)-(6.8c) into Eq. (6.7) we obtain

$$T_m^{n+1} - T_m^n + \left(\frac{1}{2\Delta t}\left[3T_m^{n+1} - 4T_m^n + T_m^{n-1}\right]\right) - \left(\frac{1}{2\Delta t}\left[T_m^{n+1} - T_m^{n-1}\right]\right) - \frac{Z}{\Delta x^2}\left(\left[T_{m+1}^{n+1} - 2T_m^{n+1} + T_{m-1}^{n+1}\right] - \left[T_{m+1}^n - 2T_m^n + T_{m-1}^n\right]\right) = \frac{\Delta t}{2\Delta x^2}\left(\left[T_{m+1}^{n+1} - 2T_m^{n+1} + T_{m-1}^{n+1}\right] + \left[T_{m+1}^n - 2T_m^n + T_{m-1}^n\right]\right) \tag{6.9}$$

After simplifications and rearrangement we obtain

$$C_4\left(T_{m-1}^{n+1}+T_{m+1}^{n+1}\right)+C_5T_m^{n+1}=C_6\left(T_{m-1}^{n}+T_{m+1}^{n}\right)+C_7T_m^{n}-\frac{1}{\Delta t}T_m^{n-1}, \tag{6.10}$$

where,

$$C_4 = -\left(Z+\frac{\Delta t}{2}\right)\frac{1}{\Delta x^2}, \tag{6.11a}$$

$$C_5 = \left(Z+\frac{\Delta t}{2}\right)\frac{2}{\Delta x^2}+\left(1+\frac{1}{\Delta t}\right), \tag{6.11b}$$

$$C_6 = \left(-Z+\frac{\Delta t}{2}\right)\frac{1}{\Delta x^2}, \tag{6.11c}$$

$$C_7 = \left(-Z+\frac{\Delta t}{2}\right)\frac{-2}{\Delta x^2}+\left(1+\frac{2}{\Delta t}\right). \tag{6.11d}$$

Notice that Eq. (6.10) is three-level in time. The right hand side of Eq. (6.10) consists of known values. The implicit part of Eq. (6.10) is tridiagonal and can be easily solved using the familiar LU decomposition method. The 1-D implicit finite-difference FORTRAN 90 code written for this problem can be found in Appendix B.

6.2.3 Stability Analysis

We analyze the stability of the above scheme via a von Neumann analysis. Because the Eq. (6.10) is a three-level difference scheme, the von Neumann condition supplies only a necessary (and not sufficient) stability requirement in general. For the present problem we define

$$v_m^{n+1}=T_m^n, \tag{6.12}$$

and replace Eq. (6.10) by the system

$$C_4\left(T_{m-1}^{n+1}+T_{m+1}^{n+1}\right)+C_5T_m^{n+1}=C_6\left(T_{m-1}^{n}+T_{m+1}^{n}\right)+C_7T_m^{n}-\frac{1}{\Delta t}v_m^{n} \tag{6.13}$$

$$v_m^{n+1}=T_m^n. \tag{6.14}$$

For $\beta \in \mathbb{R}$ we can write

$$T_{m+1}^n = e^{i\beta h} T_m^n, \qquad \text{and} \qquad T_{m-1}^n = e^{-i\beta h} T_m^n. \tag{6.15}$$

Then

$$C_4 \left(e^{i\beta h} + e^{-i\beta h}\right) T_m^{n+1} + C_5 T_m^{n+1} = C_6 \left(e^{i\beta h} + e^{-i\beta h}\right) T_m^n + C_7 T_m^n - \frac{1}{\Delta t} v_m^n \tag{6.16}$$

$$v_m^{n+1} = T_m^n. \tag{6.17}$$

After simplifications we have

$$T_m^{n+1} = \frac{C_6(2\cos\beta h) + C_7}{C_4(2\cos\beta h) + C_5} T_m^n - \frac{1}{\left[C_4(2\cos\beta h) + C_5\right]\Delta t} v_m^n \tag{6.18}$$

$$v_m^{n+1} = T_m^n, \tag{6.19}$$

which, in matrix form can be written as

$$\begin{bmatrix} T_m^{n+1} \\ v_m^{n+1} \end{bmatrix} = \begin{bmatrix} \frac{C_6(2\cos\beta h)+C_7}{C_4(2\cos\beta h)+C_5} & \frac{-1}{[C_4(2\cos\beta h)+C_5]\Delta t} \\ 1 & 0 \end{bmatrix} \begin{bmatrix} T_m^n \\ v_m^n \end{bmatrix}. \tag{6.20}$$

We know that the error vector must satisfy this same equation. Denoting this by $z_m^n \in (\mathbb{C})^2$, we see that

$$z_m^{n+1} = C z_m^n, \tag{6.21}$$

where

$$C = \begin{bmatrix} \frac{C_6(2\cos\beta h)+C_7}{C_4(2\cos\beta h)+C_5} & \frac{-1}{[C_4(2\cos\beta h)+C_5]\Delta t} \\ 1 & 0 \end{bmatrix} \tag{6.22}$$

is the amplification matrix for the present scheme. The von Neumann necessary condition for stability is

$$\|C\| \leq 1, \tag{6.23}$$

where $\|\cdot\|$ denotes the spectral norm. Hence, we need to calculate the eigenvalues of C. The characteristic polynomial is

$$\lambda^2 - \left[\frac{C_6(2\cos\beta h) + C_7}{C_4(2\cos\beta h) + C_5}\right]\lambda + \frac{1}{[C_4(2\cos\beta h) + C_5]\,\Delta t} = 0 \tag{6.24}$$

which has the roots

$$\lambda_\pm = \frac{\frac{C_6(2\cos\beta h)+C_7}{C_4(2\cos\beta h)+C_5} \pm \sqrt{\left(\frac{C_6(2\cos\beta h)+C_7}{C_4(2\cos\beta h)+C_5}\right)^2 - 4\frac{1}{[C_4(2\cos\beta h)+C_5]\Delta t}}}{2}. \tag{6.25}$$

We must determine the larger of these, and from the requirement

$$\max(|\lambda_+|, |\lambda_-|) \leq 1, \tag{6.26}$$

establish permissible bounds on Δt and Δx. Since it is very tedious to solve Eq.(6.25), we solve Eq.(6.25) numerically by changing the values of Δt and Δx for different wave numbers β. Figure 6.1 shows the distribution of λ for different values of Δt and Δx at wave numbers $\beta = 1, 4, 7$ and $Z = 10$. From the figure we can see that $\max(|\lambda_+|) \leq 1$. It is also found that $\max(|\lambda_-|) \leq 1$ even though we have not shown it here. Tests were conducted for different values of Z and it was found that the stability requirement Eq. (6.26) is satisfied for all the values of Z. This suggests that the proposed numerical scheme is unconditionally stable. The stability requirement is also met for $Z = 0$ (hyperbolic case) and $Z = 1$ (parabolic case) implying that the numerical scheme is unconditionally stable and the stability analysis can be applied for both parabolic and hyperbolic models.

6.2.4 Results and Discussion

Temperature distribution corresponding to the analytical [16] and numerical results at non-dimensional time $\beta = 1$ with different phase lag ratios Z are presented. Figures 6.2-6.5

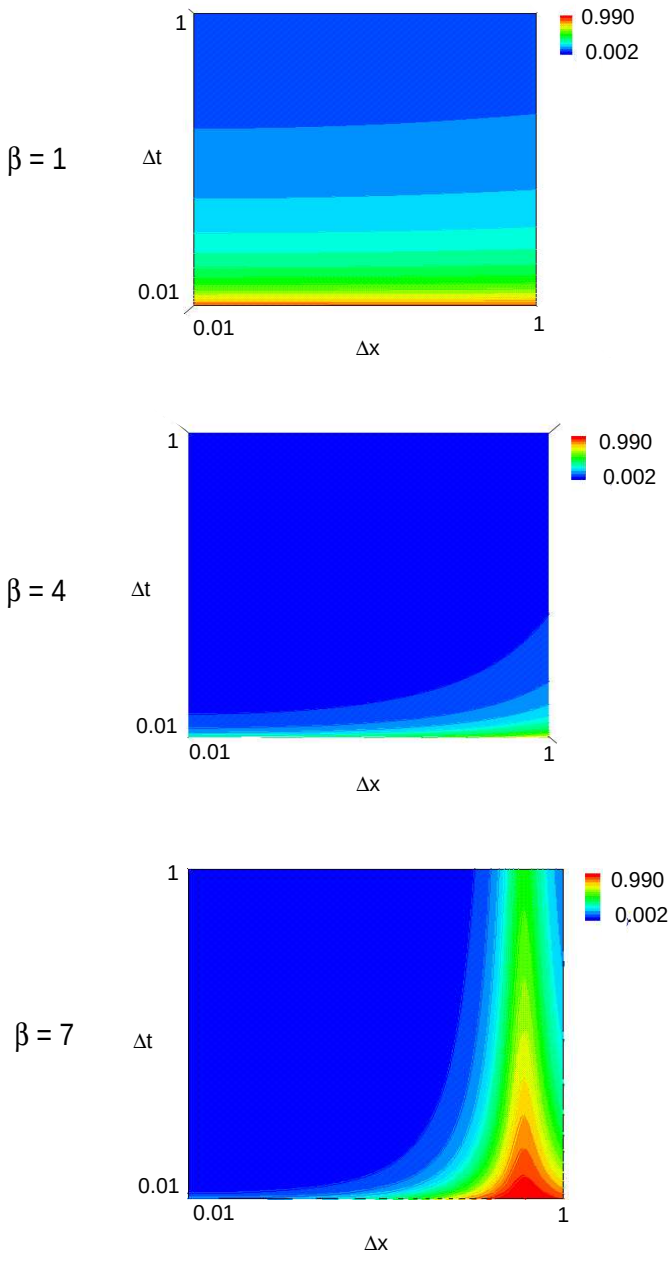

Figure 6.1 Distribution of λ_+ for different values of Δt and Δx at wave numbers $\beta = 1, 4, 7$ and $Z = 10$

shows comparisons between numerical (explicit and implicit) and analytical non-dimensional temperature distributions for the case of heat flux precedence ($Z = 100$), temperature gradient precedence ($Z = 0.01$), diffusion ($Z = 1$) and thermal wave ($Z = 0$).

The stability analysis has been carried out using von Neumann analysis and shown that the proposed numerical scheme is unconditionally stable. We see that the results from the present implicit numerical scheme and explicit scheme compares well with the analytical results for phase lag ratios $Z > 0$. The numerical results from the implicit scheme do not match the analytical results at $Z = 0$, but the numerical results from the explicit scheme compares well with the analytical results. The present numerical scheme is not able to capture the sharp thermal wave front caused by setting $Z = 0$ (mixed derivative term = 0 in the DPL equation). This is due to the fact that for $Z = 0$ the stability analysis yields complex eigenvalues leading to oscillatory numerical solution. Grid function convergence tests were performed. Reduction in the step size by a factor of two leads to the reduction in error by a factor of four. Estimated order of the present numerical scheme is found to be $q_1 \sim 1$, which is calculated by employing the following formula

$$q_1 = \frac{\ln\left[\frac{f_i^h - f_i^{h/2}}{f_i^{h/2} - f_i^{h/4}}\right]}{\ln 2}, \tag{6.27}$$

in agreement with theory.

6.3 Different numerical formulation to solve 1-D DPL equation implicitly

In this section we will develop a different formulation to solve the DPL equation implicitly. For the sake of comparison we will again consider the problem of short pulse laser heating of thin metal film considered in Chapter V.

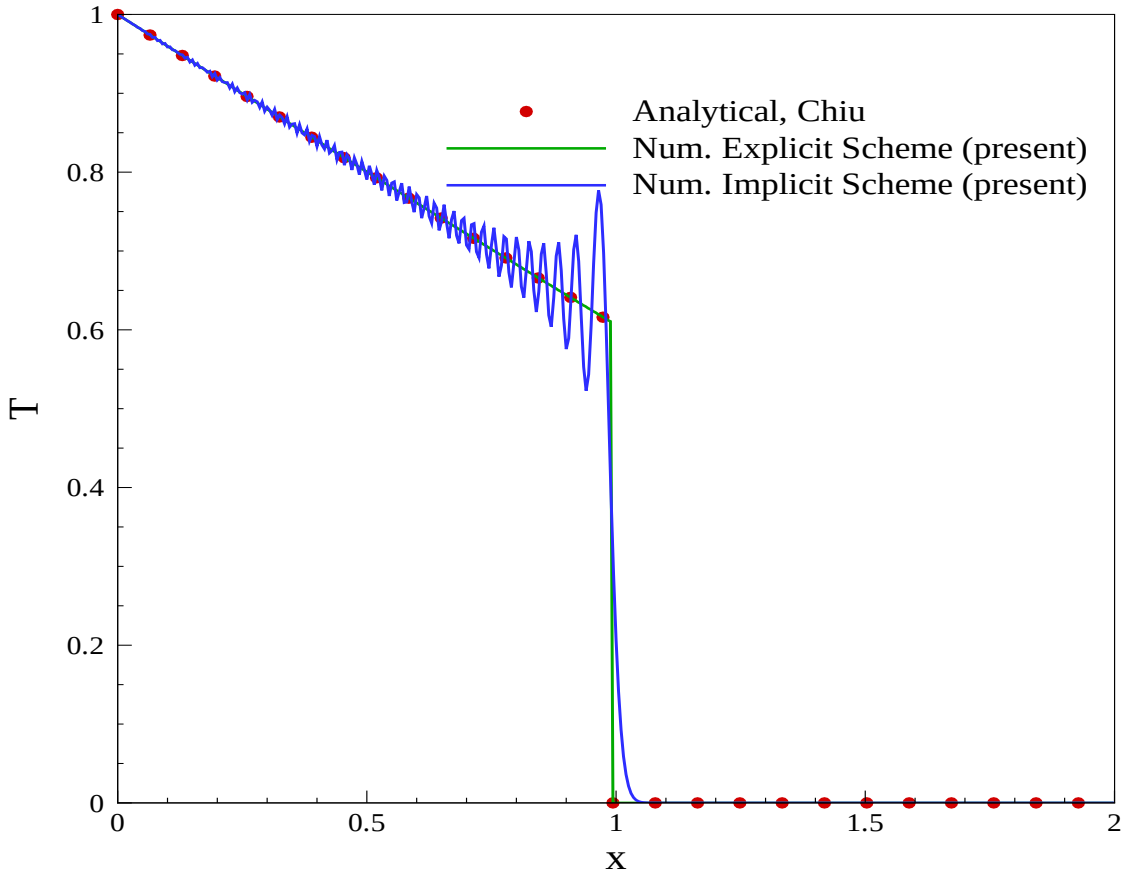

Figure 6.2 Comparison between numerical (explicit and implicit schemes) and analytical temperature distribution for phase lag ratio $Z = 0$ at $\beta = 0.1$.

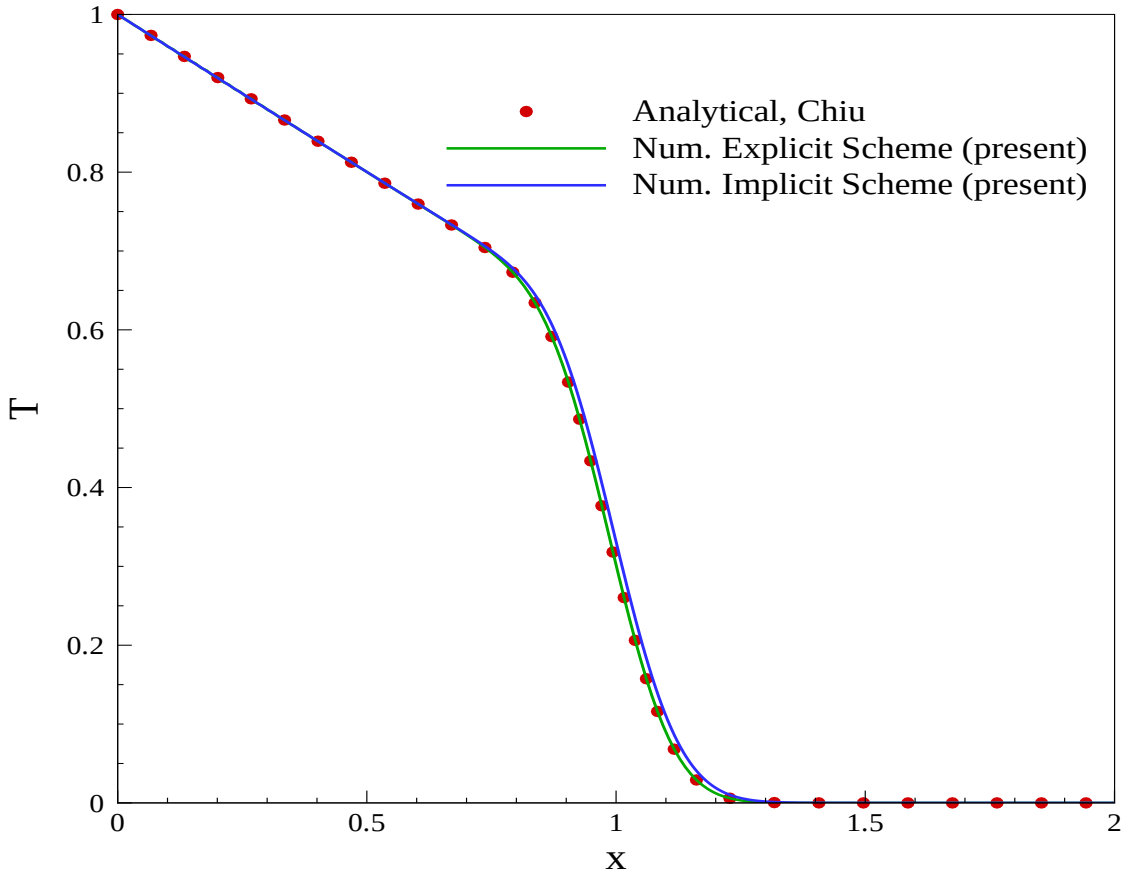

Figure 6.3 Comparison between numerical (explicit and implicit schemes) and analytical temperature distribution for phase lag ratio $Z = 0.01$ at $\beta = 0.1$.

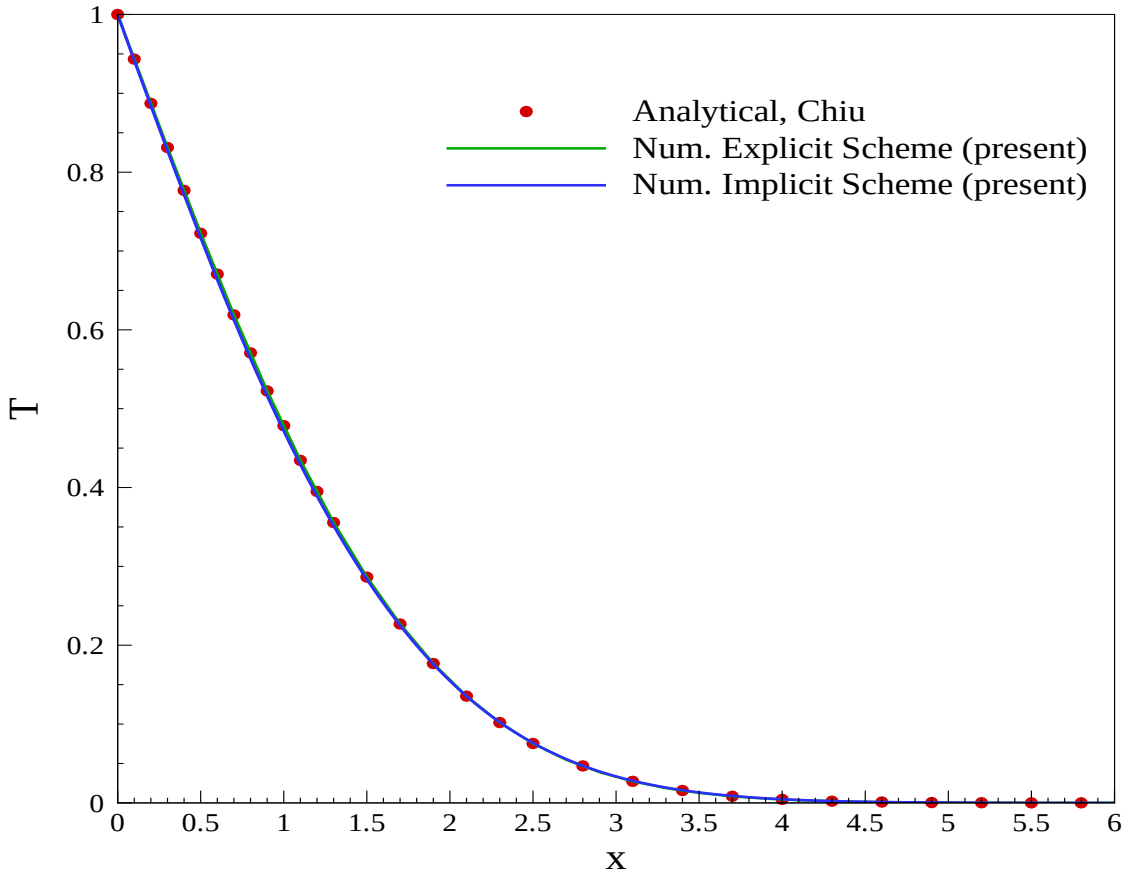

Figure 6.4 Comparison between numerical (explicit and implicit schemes) and analytical temperature distribution for phase lag ratio $Z = 1$ at $\beta = 0.1$.

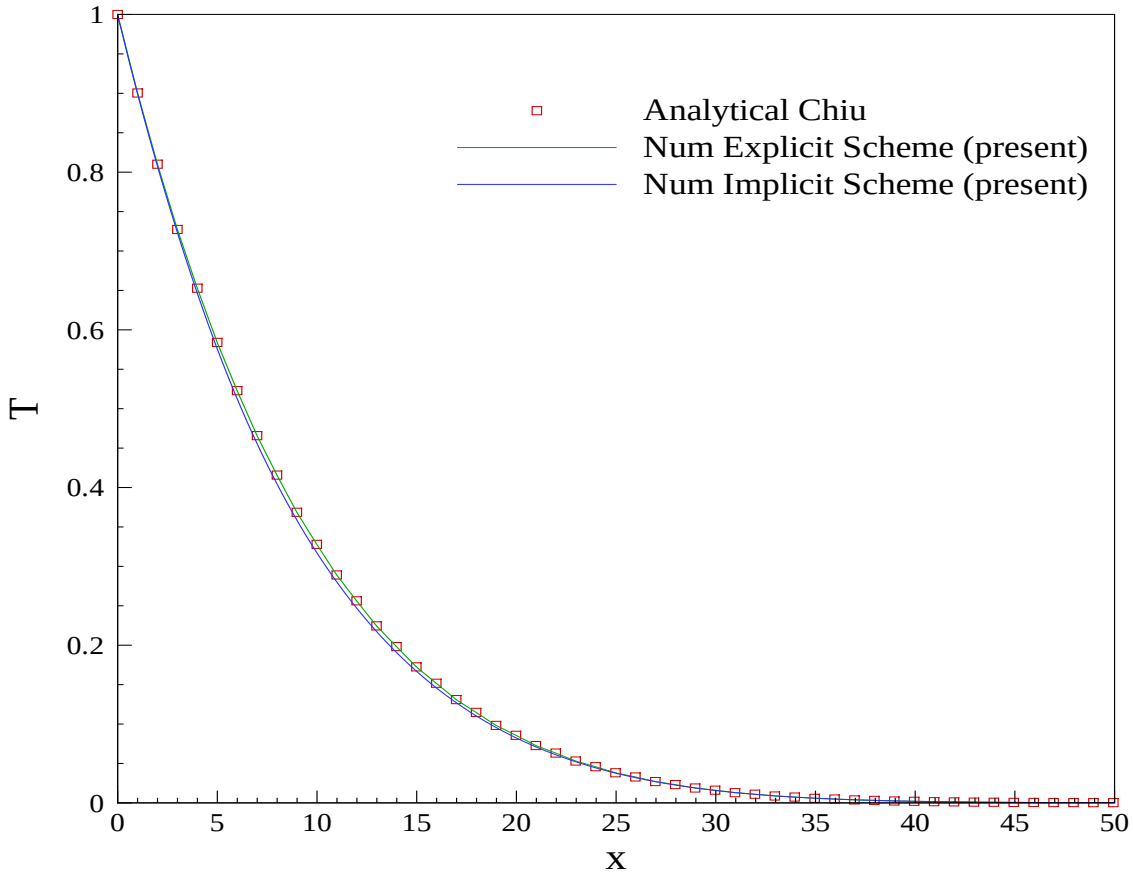

Figure 6.5 Comparison between numerical (explicit and implicit schemes) and analytical temperature distribution for phase lag ratio $Z = 100$ at $\beta = 0.1$.

6.3.1 Numerical Formulation

The heat transport equation used to describe the thermal behavior of microstructures in 1D can be expressed as

$$\frac{\tau_q}{\alpha}\frac{\partial^2 T}{\partial t^2}+\frac{1}{\alpha}\frac{\partial T}{\partial t}=\frac{\partial^2 T}{\partial x^2}+\tau_{_T}\frac{\partial^3 T}{\partial x^2\partial t}+\frac{1}{k}\left(S+\tau_{_q}\frac{\partial S}{\partial t}\right). \tag{6.28}$$

We will develop a different formulation to solve the above DPL equation Eq. (6.28) implicitly subject to the initial and boundary conditions

$$T(x,0)=T_0 \qquad \text{and} \qquad \frac{\partial t}{\partial t}(x,0)=0, \tag{6.29}$$

$$\frac{\partial T}{\partial x}(0,t)=\frac{\partial T}{\partial x}(L,t)=0. \tag{6.30}$$

We can write Eq. (6.28) as

$$\frac{\partial^2 T}{\partial x^2}-\frac{1}{\alpha}\frac{\partial T}{\partial t}+\frac{1}{k}\left(S+\tau_{_q}\frac{\partial S}{\partial t}\right)=\frac{\partial}{\partial t}\left[-\tau_{_T}\frac{\partial^2 T}{\partial x^2}+\frac{\tau_q}{\alpha}\frac{\partial T}{\partial t}\right]. \tag{6.31}$$

Let

$$U=-\tau_{_T}\frac{\partial^2 T}{\partial x^2}+\frac{\tau_q}{\alpha}\frac{\partial T}{\partial t}. \tag{6.32}$$

Eq. (6.31) can be written as

$$\frac{1}{\alpha}\frac{\partial T}{\partial t}+\frac{\partial U}{\partial t}-\frac{\tau_{_q}}{k}\left(\frac{\partial S}{\partial t}\right)=\frac{\partial^2 T}{\partial x^2}+\frac{S}{k}. \tag{6.33}$$

Applying trapezoidal integration to the above equation we have

$$\frac{1}{\alpha}\left(T_m^{n+1}-T_m^n\right)+\left(U_m^{n+1}-U_m^n\right)-\frac{\tau_{_q}}{k}\left(S_m^{n+1}-S_m^n\right)=\frac{\Delta t}{2}\left[\begin{array}{c}\frac{T_{m-1}^{n+1}-2T_m^{n+1}+T_{m-1}^{n+1}}{h^2}\\ \\ \frac{T_{m-1}^{n}-2T_m^{n}+T_{m-1}^{n}}{h^2}\end{array}\right]+\frac{\Delta t}{k}\left(\frac{S_m^{n+1}+S_m^n}{2}\right). \tag{6.34}$$

Now applying trapezoidal integration to Eq. (6.32) and rearranging we have

$$U_m^{n+1} = -C_1\left(T_{m-1}^{n+1} + T_{m+1}^{n+1}\right) + C_2 T_m^{n+1} - C_1\left(T_{m-1}^{n} + T_{m+1}^{n}\right) + C_3 T_m^{n} - U_m^{n}. \tag{6.35}$$

Substituting the above equation into Eq. (6.34) and after simplifications and re-arrangement we obtain

$$\begin{aligned} C_4\left(T_{m-1}^{n+1} + T_{m+1}^{n+1}\right) + C_5 T_m^{n+1} = C_4\left(T_{m-1}^{n} + T_{m+1}^{n}\right) + C_6 T_m^{n} - \frac{2U_m^n}{2} \\ -S^{n+1}\left(\frac{h^2}{k} + \frac{\tau_q}{rk}\right) - S^{n}\left(\frac{h^2}{k} - \frac{\tau_q}{rk}\right), \end{aligned} \tag{6.36}$$

where,

$$r = \frac{\Delta t}{2h^2} \tag{6.37a}$$

$$C_1 = \frac{\tau_T}{h^2} \tag{6.37b}$$

$$C_2 = 2\left(\frac{\tau_T}{h^2} + \frac{\tau_q}{\alpha \Delta t}\right) \tag{6.37c}$$

$$C_3 = 2\left(\frac{\tau_T}{h^2} - \frac{\tau_q}{\alpha \Delta t}\right) \tag{6.37d}$$

$$C_4 = 1 + \frac{\tau_T}{rh^2} \tag{6.37e}$$

$$C_5 = \frac{C_2}{r} + 2 + \frac{1}{\alpha r} \tag{6.37f}$$

$$C_6 = \frac{C_3}{r} + 2 - \frac{1}{\alpha r}. \tag{6.37g}$$

The implicit part of Eq. (6.36) is tridiagonal and can be easily solved using LU decomposition. According to the initial condition $U_m^0 = 0$ at $t = 0$. For $t > 0$ U_m^n can be found from Eq. (6.35). Eqs. (6.35) and (6.36) are solved simultaneously subject to the initially and boundary conditions given by Eqs. (6.29) and (6.30). The 1-D implicit finite-difference FORTRAN 90 code written for this problem can be found in Appendix C

6.3.2 Results and Discussion

Figure 6.6 shows the comparison between explicit numerical scheme, new formulation of implicit finite difference scheme, analytical [16] and experimental results [12, 65] corresponding to the front surface transient response for a $0.1\mu m$ thick gold film. The thermal properties ($\alpha = 1.2 \times 10^{-4} m^2 s^{-1},\ k = 315 W m^{-1} K^{-1},\ \tau_{_T} = 90ps,\ \tau_q = 8.5ps$) are assumed to be constant. The temperature change is normalized by the maximum value that occurs during the short-time transient:

$$\frac{\Delta T(0,t)}{[\Delta T(0,t)]_{max}} \equiv \frac{T(0,t) - T_0}{[T(0,t) - T_0]_{max}}. \tag{6.38}$$

The resulting normalized temperature change is proportional to the normalized surface reflectivity measured directly in experiments. We can see that the results from the new formulation of solving the DPL implicitly agrees well with the analytical and experimental results. However, the stability of this new numerical scheme is still under investigation. In the next section, we extend the numerical scheme developed in Section 6.2 to three dimensions and develop a numerical procedure to predict the transient temperature response during short pulse laser heating of gold film.

6.4 Numerical scheme for solving 3-D microscale DPL equation

In the following sections, we will present the numerical formulation in 3D for computing the transient temperature distribution during short pulse laser heating of thin films considered in Chapter V. The discretized 3-D microscale DPL equation will be solved using Douglas–Gunn time-splitting method and *δ-form* Douglas–Gunn time-splitting method. The performance of the proposed numerical scheme will be compared with the numerical

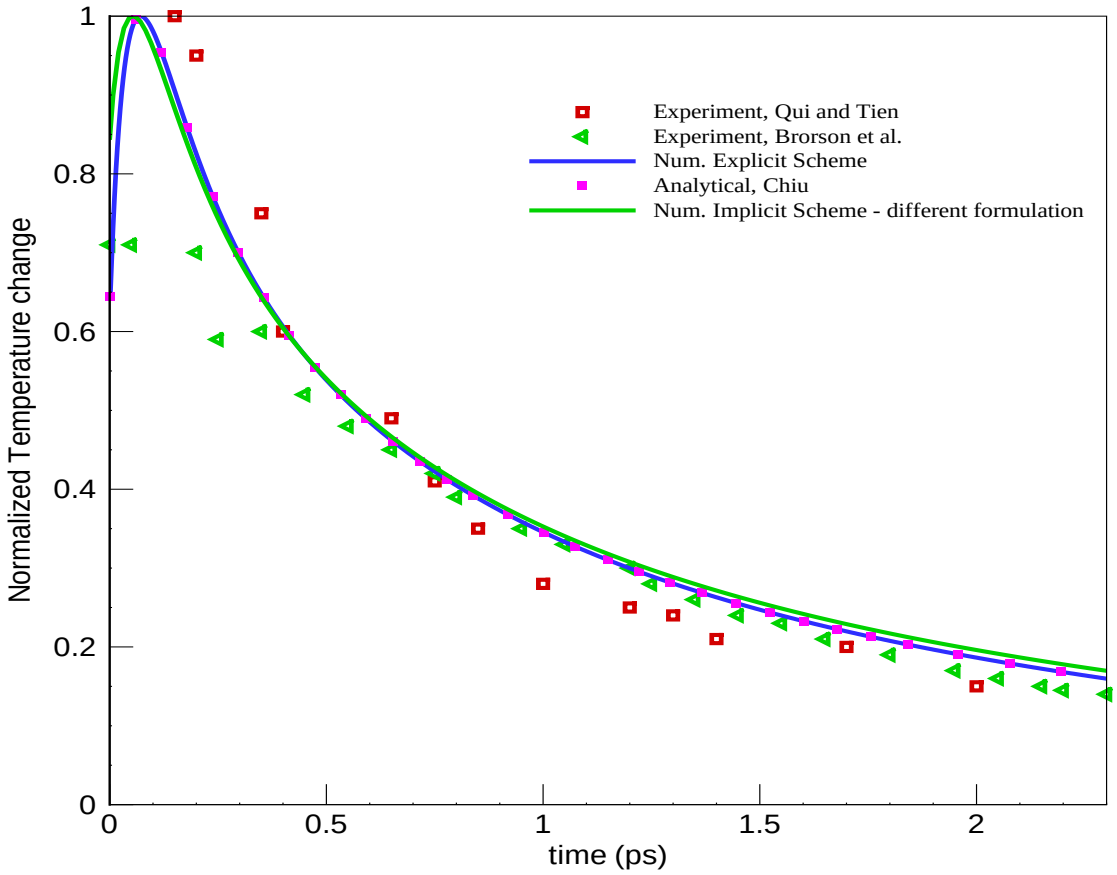

Figure 6.6 Front surface transient response for a $0.1\mu m$ gold film. Comparison between explicit numerical scheme, new formulation of implicit finite difference scheme, analytical [16] and experimental results [12, 65]. $\alpha = 1.2 \times 10^{-4} m^2 s^{-1}$, $k = 315 W m^{-1} K^{-1}$, $\tau_T = 90ps$, $\tau_q = 8.5ps$.

techniques available in the literature.

6.4.1 Mathematical Formulation

The governing equation used to describe the thermal behavior of microstructures in 3D is expressed as [71]

$$\frac{\tau_q}{\alpha}\frac{\partial^2 T}{\partial t^2} + \frac{1}{\alpha}\frac{\partial T}{\partial t} - \tau_{_T}\frac{\partial(\nabla^2 T)}{\partial t} = \nabla^2 T + \frac{1}{k}\left(S + \tau_q \frac{\partial S}{\partial t}\right), \tag{6.39}$$

where,

$$S(x,t) = 0.94J\left[\frac{1-R}{t_p\delta}\right]\exp\left(-\frac{x}{\delta} - \frac{1.992 \mid t - 2t_p \mid}{t_p}\right) \tag{6.40}$$

Initial conditions:

$$T(x,y,z,0) = T_0, \qquad \frac{\partial T}{\partial t}(x,y,z,0) = 0 \tag{6.41}$$

Boundary conditions:

$$\frac{\partial T}{\partial n} = 0, \qquad \text{where,} \qquad n = x, y, z. \tag{6.42}$$

6.4.2 Finite-difference Scheme

Applying trapezoidal integration to Eq. (6.39) we obtain

$$\begin{aligned}\frac{\tau_q}{\alpha}\left[T^{n+1}_{i,j,k} - T^{n}_{i,j,k}\right] + \frac{1}{\alpha}\left[\left(\frac{\partial T}{\partial t}\right)^{n+1}_{i,j,k} - \left(\frac{\partial T}{\partial t}\right)^{n}_{i,j,k}\right] - \tau_T\left[\ (\nabla^2 T)^{n+1} - (\nabla^2 T)^{n}\ \right] \\ = \frac{\Delta t}{2}\left[\ (\nabla^2 T)^{n+1} + (\nabla^2 T)^{n}\ \right] + \frac{\Delta t}{k}\left[\frac{S^{n+1}_{i,j,k} + S^{n}_{i,j,k}}{2} + \tau_q \frac{S^{n+1}_{i,j,k} - S^{n}_{i,j,k}}{2}\right]\end{aligned} \tag{6.43}$$

We apply second-order backward difference for the time derivative at $n+1$ and a centered difference for the time derivative at n. Second-order derivatives in space are approximated

using the usual centered-difference scheme. Thus we have

$$\left(\frac{\partial T}{\partial t}\right)^{n+1}_{i,j,k} = \frac{1}{2\Delta t}\left[3T^{n+1}_{i,j,k} - 4T^{n}_{i,j,k} + T^{n-1}_{i,j,k}\right] \tag{6.44a}$$

$$\left(\frac{\partial T}{\partial t}\right)^{n}_{i,j,k} = \frac{1}{2\Delta t}\left[T^{n+1}_{i,j,k} - T^{n-1}_{i,j,k}\right] \tag{6.44b}$$

$$\frac{\partial^2 T}{\partial x^2} = \frac{1}{\Delta x^2}\left[T_{i+1,j,k} - 2T_{i,j,k} + T_{i-1,j,k}\right] \tag{6.44c}$$

$$\frac{\partial^2 T}{\partial y^2} = \frac{1}{\Delta y^2}\left[T_{i,j+1,k} - 2T_{i,j,k} + T_{i,j+1,k}\right] \tag{6.44d}$$

$$\frac{\partial^2 T}{\partial z^2} = \frac{1}{\Delta z^2}\left[T_{i,j,k+1} - 2T_{i,j,k} + T_{i,j,k-1}\right] \tag{6.44e}$$

After plugging Eqs. (6.44a)–(6.44e) into Eq. (6.43), and further simplifications, we obtain

$$C_4 T^{n+1}_{i,j,k} + C_5\left(T^{n+1}_{i+1,j,k} + T^{n+1}_{i-1,j,k}\right) + C_6\left(T^{n+1}_{i,j+1,k} + T^{n+1}_{i,j-1,k}\right) + C_7\left(T^{n+1}_{i,j,k+1} + T^{n+1}_{i,j,k-1}\right) = F^n, \tag{6.45}$$

where,

$$F^n = C_8 T^{n}_{i,j,k} + C_9\left(T^{n}_{i+1,j,k} + T^{n}_{i-1,j,k}\right) + C_{10}\left(T^{n}_{i,j+1,k} + T^{n}_{i,j-1,k}\right) + C_{11}\left(T^{n}_{i,j,k+1} + T^{n}_{i,j,k-1}\right) - \frac{\tau_q}{\alpha\Delta t} T^{n-1}_{i,j,k} + \Delta t G^* \tag{6.46}$$

$$C_5 = -\left(\tau_T + \frac{\Delta t}{2}\right)\frac{1}{\Delta x^2}, \tag{6.47a}$$

$$C_6 = -\left(\tau_T + \frac{\Delta t}{2}\right)\frac{1}{\Delta y^2}, \tag{6.47b}$$

$$C_7 = -\left(\tau_T + \frac{\Delta t}{2}\right)\frac{1}{\Delta z^2}, \tag{6.47c}$$

$$C_4 = \left(\frac{1}{\alpha} + \frac{\tau_q}{\alpha\Delta t}\right) - 2(C_5 + C_6 + C_7) \tag{6.47d}$$

$$C_8 = -2\left(-\tau_T + \frac{\Delta t}{2}\right)\left[\frac{1}{\Delta x^2} + \frac{1}{\Delta y^2} + \frac{1}{\Delta z^2}\right] + \left(\frac{1}{\alpha} + \frac{2\tau_q}{\alpha \Delta t}\right), \tag{6.48a}$$

$$C_9 = \left(-\tau_T + \frac{\Delta t}{2}\right)\frac{1}{\Delta x^2}, \tag{6.48b}$$

$$C_{10} = \left(-\tau_T + \frac{\Delta t}{2}\right)\frac{1}{\Delta y^2}, \tag{6.48c}$$

$$C_{11} = \left(-\tau_T + \frac{\Delta t}{2}\right)\frac{1}{\Delta z^2}. \tag{6.48d}$$

$$G^* = \left[\frac{S^{n+1}_{i,j,k} + S^n_{i,j,k}}{2} + \tau_q \frac{S^{n+1}_{i,j,k} - S^n_{i,j,k}}{2}\right] \tag{6.48e}$$

Equation (6.45) is three-level in time, and it can be efficiently solved using *δ-form* Douglas–Gunn time splitting. This form is now widely used in computational algorithms and is the most efficient of the forms found in the literature. Divide both sides of Eq. (6.45) by

$$\frac{1}{\alpha} + \frac{\tau_q}{\alpha \Delta t} \tag{6.49}$$

to obtain

$$\left[1 - 2C'_5 - 2C'_6 - 2C'_7\right] T^{n+1}_{i,j,k} + C'_5\left(T^{n+1}_{i+1,j,k} + T^{n+1}_{i-1,j,k}\right) + C'_6\left(T^{n+1}_{i,j+1,k} + T^{n+1}_{i,j-1,k}\right) + C'_7\left(T^{n+1}_{i,j,k+1} + T^{n+1}_{i,j,k-1}\right) = S^n \tag{6.50}$$

where,

$$S^n = \frac{F^n}{\left(\frac{1}{\alpha} + \frac{\tau_q}{\alpha \Delta t}\right)}, \tag{6.51a}$$

$$C'_5 = \frac{C_5}{\left(\frac{1}{\alpha} + \frac{\tau_q}{\alpha \Delta t}\right)}, \tag{6.51b}$$

$$C'_6 = \frac{C_6}{\left(\frac{1}{\alpha} + \frac{\tau_q}{\alpha \Delta t}\right)}, \tag{6.51c}$$

$$C'_7 = \frac{C_7}{\left(\frac{1}{\alpha} + \frac{\tau_q}{\alpha \Delta t}\right)}, \tag{6.51d}$$

$$C'_4 = 1 - 2(C'_5 + C'_6 + C'_7). \tag{6.51e}$$

Observe that this is now in the general form required for construction of a multilevel Douglas and Gunn time splitting [36]. We now split Eq. (6.50) into three equations corresponding to

x, y and z directions:

$$(1-2C_5')\,T_{i,j,k}^{n+1} + C_5'\left(T_{i+1,j,k}^{n+1} + T_{i-1,j,k}^{n+1}\right) = S^n \tag{6.52a}$$

$$(-2C_6')\,T_{i,j,k}^{n+1} + C_6'\left(T_{i,j+1,k}^{n+1} + T_{i,j-1,k}^{n+1}\right) = 0 \tag{6.52b}$$

$$(-2C_7')\,T_{i,j,k}^{n+1} + C_7'\left(T_{i,j,k+1}^{n+1} + T_{i,j,k-1}^{n+1}\right) = 0. \tag{6.52c}$$

Applying Douglas–Gunn time-splitting technique to Eqs. (6.52a)–(6.52c) we have

$$(I + A_x)T^{(1)} = S^n - A_yT^n - A_zT^n \tag{6.53a}$$

$$(I + A_y)T^{(2)} = T^{(1)} - A_yT^n \tag{6.53b}$$

$$(I + A_z)T^{(3)} = T^{(2)} - A_zT^n, \tag{6.53c}$$

where,

$$I + A_x = (1-2C_5')\,T_{i,j,k}^{n+1} + C_5'\left(T_{i+1,j,k}^{n+1} + T_{i-1,j,k}^{n+1}\right) \tag{6.54a}$$

$$I + A_y = (1-2C_6')\,T_{i,j,k}^{n+1} + C_6'\left(T_{i,j+1,k}^{n+1} + T_{i,j-1,k}^{n+1}\right) \tag{6.54b}$$

$$I + A_z = (1-2C_7')\,T_{i,j,k}^{n+1} + C_7'\left(T_{i,j,k+1}^{n+1} + T_{i,j,k-1}^{n+1}\right) \tag{6.54c}$$

$T^{(1)}$, $T^{(2)}$ and $T^{(3)}$ denote intermediate estimates of T^{n+1} with $T^{n+1} = T^{(3)}$. The implicit part (T^{n+1}) of the above equations (6.53a)–(6.53c) is tridiagonal, and is thus easily solved using LU decomposition.

Now applying δ-*form* the Douglas–Gunn time-splitting [36] we can represent Eqs. (6.52a)–

(6.52c) into the following

$$(I + A_x)T^{(1)} = S^n - (I + A)T^n \tag{6.55a}$$

$$(I + A_y)T^{(2)} = T^{(1)} \tag{6.55b}$$

$$(I + A_z)T^{(3)} = T^{(2)} \tag{6.55c}$$

$$T^{n+1} = T^{(3)} + T^n \tag{6.55d}$$

where, $A = I + A_x + A_y + A_z$. We remark that this form is the most efficient of the forms we have considered. Again, the implicit part of the above equations (6.55a)–(6.55d) is tridiagonal, and is thus easily solved using LU decomposition.

6.4.3 Results and Discussion

Figure 6.7 shows the comparison between the numerical (explicit and implicit scheme), analytical [16] and the experimental results of Brorson et al. [12] and Qiu and Tien [65, 66] corresponding to the front surface transient response for a $0.1\mu m$ thick gold film. The thermal properties ($\alpha = 1.2 \times 10^{-4} m^2 s^{-1},\ k = 315 W m^{-1} K^{-1},\ \tau_T = 90ps,\ \tau_q = 8.5ps$) are assumed to be constant. The temperature change is normalized by the maximum value that occurs during the short-time transient as was done earlier in the 1-D case. The normalized temperature distribution does not change with respect to change in k or J but the magnitude of the temperature distribution changes. The results from the implicit numerical scheme compare well with the experimental and analytical results at later time $\sim 0.5ps$. At earlier time $0 \sim 0.5$ the numerical results to not compare well with the experimental results. This may be due to experimental inconsistency or theoretical incompatibility at such duration of time.

Stability properties of the Douglas–Gunn splitting method are not completely known. It is clear that von Neumann analysis will provide only necessary conditions for stability in this case. The research work on stability for the numerical scheme in 3D has not yet been done. However, by following the same procedure for 1-D case we can easily determine the stability of the 3D numerical scheme.

Tables 6.2 and 6.3 show the CPU time in seconds taken for the entire simulation for the explicit, Gauss–Seidel, conjugate gradient, Douglas–Gunn time-splitting and δ-form Douglas–Gunn time-splitting methods using different values of the spatial discretization parameter N [68]. The implicit methods namely Gauss–Seidel, conjugate gradient, Douglas–Gunn time-splitting and δ-form Douglas–Gunn time-splitting methods in Table 6.2 are obtained using Dai's numerical technique [25] while the implicit methods from Table 6.2 are obtained from the present numerical technique.

Numerical techniques	Total CPU time taken in seconds			
	N=21	N=41	N=51	N=101
Explicit Scheme	4.88	147.62	450.26	7920.00
Gauss–Seidel	13.46	175.1	415.86	7800
Conjugate gradient	12.12	110.5	233.96	2733.4
D-G time-splitting	9.75	82.29	166.90	1792.4
δ-form D-G	9.15	75.22	153.3	1638

Table 6.2 Performance comparison of different numerical methods for solving the discretized 3-D DPL equation [68].

We can make several observations from Tables 6.2 and 6.3. The present numerical scheme outperforms Dai's [25] numerical technique in terms of computational time taken to complete the simulation. Also, the δ-form Douglas-Gunn time-splitting consumes the least CPU time compared to all other numerical techniques available in the literature for large values of N.

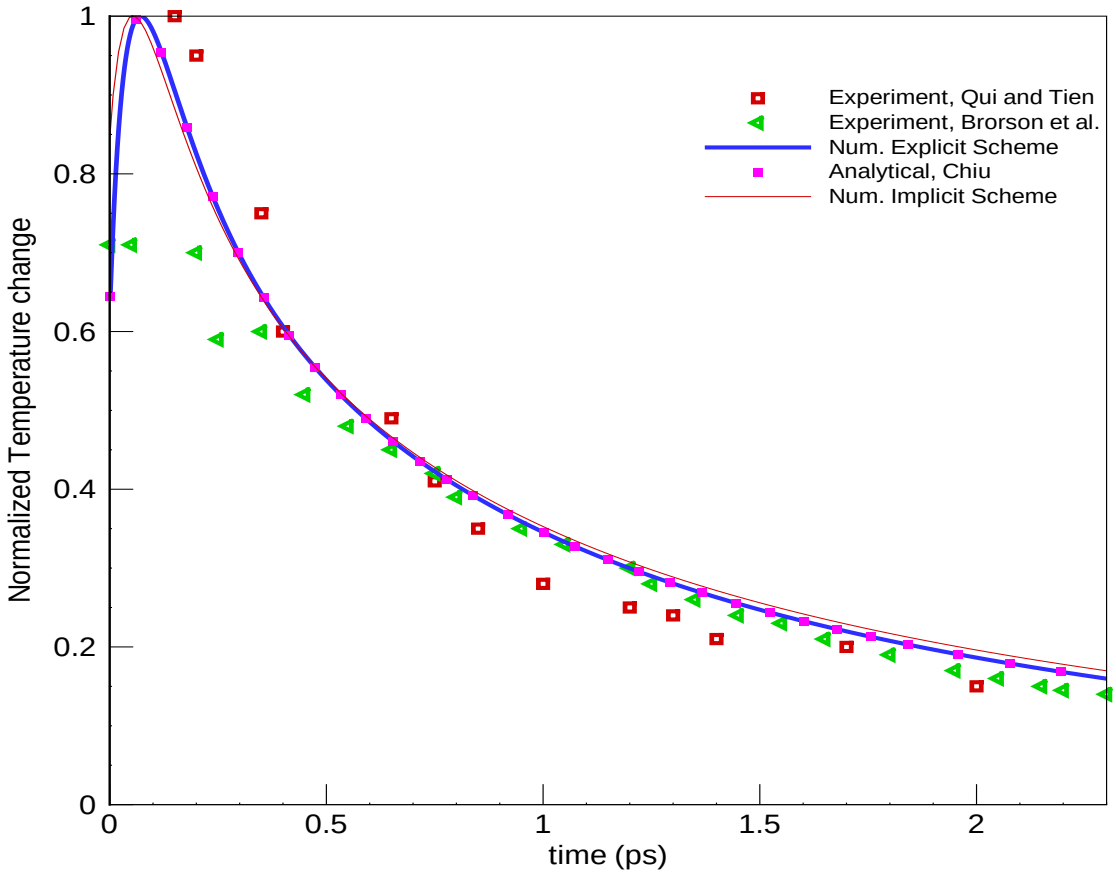

Figure 6.7 Front surface transient response for a $0.1\mu m$ gold film. Comparison between numerical (explicit and implicit schemes), analytical [16] and experimental results [12, 66]. $\alpha = 1.2 \times 10^{-4} m^2 s^{-1}$, $k = 315 W m^{-1} K^{-1}$, $\tau_T = 90 ps$, $\tau_q = 8.5 ps$.

When $N = 21$ the explicit method consumes less CPU time than the rest of the numerical techniques but for the spatial discretization parameter $N > 21$, all implicit methods except the Gauss–Seidel method perform better than the explicit method employed in this research. We are still investigating the reason for the poor performance of the Gauss–Seidel method compared to the explicit method.

Numerical techniques	Total CPU time taken in seconds			
	N=21	N=41	N=51	N=101
Explicit Scheme	4.88	147.62	450.26	7920.00
Gauss–Seidel	14.14	253.42	627.03	11343.06
Conjugate Gradient	12.33	124.83	270.3	3614.69
D-G time-splitting	9.24	82.44	165.76	1506.38
δ-form D-G	8.54	70.5	140.92	1344.4

Table 6.3 Performance comparison of different numerical methods for solving the discretized 3-D DPL equation [68].

Chapter 7
SUMMARY AND CONCLUSIONS

In this chapter, a summary of the present research will be given. We will then present a list of conclusions drawn from the research. Finally, a brief note on future work that can be done as a consequence of this research will be presented.

7.1 Summary

1. Chapter II summarized the various heat transfer models including macroscopic models (parabolic heat conduction model, hyperbolic heat conduction model or thermal wave model), microscale heat transfer models (microscopic two-step model or phonon-electron interaction model, phonon-scattering model and phonon radiative transfer model), and universal model (dual phase lag model).

2. The classical problem of heat conduction in a solid slab starting from a stationary state subjected to a sudden temperature change at the surface boundary has been investigated in Chapter III. The violation of second law of thermodynamics by the hyperbolic heat conduction equation has been investigated. The effect of heat flux precedence and temperature gradient precedence has been shown.

3. Numerical simulation of femtosecond pulse laser heating of sub-micron sized gold film has been carried out using the 1-D DPL model under different values of relaxation times, and the results compared with the experimental results by Brorson *et al.* [12], and Qiu and Tien [65, 66]. The significance of dual phase lagging and the disagreement of the parabolic and hyperbolic models with the experimental results has been

explained.

4. Energy absorption rate used to model femtosecond laser heating in 1D has been modified to accommodate for 3-D laser heating. Simulation of 3-D laser heating at various locations of a thin film has been carried out using a pulsating laser beam ($\sim 0.3ps$ pulse duration) and the transient temperature distribution compared with parabolic, hyperbolic and DPL models. The difference seen in the transient temperature distribution among the three models has been explained with help of the lagging concept. Furthermore, different grids $51 \times 51 \times 11$, $101 \times 101 \times 21$ and $201 \times 201 \times 41$ were used to check the consistency of the numerical solution in the form of grid function convergence tests.

5. In Chapter VI, we have developed an unconditionally stable implicit finite-difference scheme of the Crank–Nicolson type for solving the one-dimensional DPL equation. Grid function convergence tests have performed to test the convergence of the numerical solution. Stability analysis has been performed using a von Neumann stability analysis. A numerical procedure has been presented for the semi-infinite slab problem considered in Chapter III.

6. The numerical technique is then extended to three dimensional geometry, and a numerical procedure for computing the transient temperature distribution during short pulse laser heating of thin films has been presented. The discretized 3-D microscale DPL equation has been solved using Douglas–Gunn time-splitting method and δ-*form* Douglas–Gunn time-splitting method. The performance of the proposed numerical scheme has been compared with the numerical techniques available in the literature in

terms of CPU time in seconds taken for the entire simulation.

7.2 Conclusions

1. The dual phase lag model proposed by Tzou [72, 73, 74] reduces to diffusion, thermal wave, the phonon-electron interaction, and the pure phonon scattering models under special values of τ_q and τ_T, covering a wide range of physical responses from microscopic to macroscopic scales in both space and time. There is no need to switch from one model to another when the response time becomes smaller (femtosecond laser applications) and the microscale effect becomes predominant.

2. The effect of τ_q is mainly responsible for the presence of a sharp wavefront in heat propagation seen in classical hyperbolic heat conduction. τ_T diminishes the sharp wavefront and extends the heat-affected zone deeper into the solid medium. Since τ_T reflects the delayed response due to microstructural interaction effects, phonon scattering and phonon-electron interactions occurring in microscales promote the temperature level [74].

3. The agreement of the numerical result with $\tau_T = 90ps$ and $\tau_q = 8.5ps$ (DPL model) agree with experimental results very well, supporting the lagging behavior in the short-pulse laser heating process on metals. Within the framework of the dual phase lag model, the time delay due to the fast-transient effect of thermal inertia is absorbed in the phase-lag τ_q of the heat flux vector and the time delay due to the finite time required for the phonon-electron interaction to take place is absorbed in the phase-lag τ_T of the temperature gradient. The agreements also suggest that the heat flux vector

precedes the temperature gradient, i.e., $\tau_q < \tau_T$, when the lagging behavior is caused by the phonon-electron interaction.

4. The parabolic (classical diffusion) and the CV wave equations fail to capture the microscale responses during short pulse laser metal interaction. The classical diffusion and CV wave models cannot describe the slow thermalization process shown by the DPL equation. From a physical point of view, the macroscopic approach employed in these models neglects the microstructural interaction effect in the short-time transient, rendering an overestimated temperature in the transient response.

5. In the thermalization process, the diffusion model predicts the highest temperature among all three (DPL, CV wave and parabolic models). Compared to the experimental result, the large difference arises from negligence of both the microstructural interaction effect in space and the fast-transient effect in time.

6. The CV wave model accounting for the fast-transient effect in the short-time response, reduces the difference between the diffusion model and the experimental result. Since the CV wave model neglects the microstructural interaction in space, still it overestimates the transient temperature.

7. In 3-D laser heating the CV wave model and the diffusion model predict a higher temperature level in the heat affected zone than the DPL model, but the penetration depth is much shorter owing to the formation of the thermally undisturbed zone. The heat affected zone is significantly larger for the DPL model than the other models because the microstructural interaction effect incorporated in the DPL model, reflected

by the delayed time for establishing the temperature gradient across a material volume (τ_T) significantly extends the physical domain of the thermal penetration depth.

8. The DPL results in 3D exhibit similar behavior as the one-dimensional results; so the transient temperature distribution should be physically realizable in three dimensions.

9. In the stability analysis, for $\Delta x = \Delta y = \Delta z = 5nm$, Δt which satisfies the stability criterion was found to be $3.27fs$. Results from the grid function convergence tests show that reducing the step size by a factor of two and time step by a factor of four results in reduction of error by a factor of four, implying the validity of the numerical solution.

10. The proposed implicit finite-difference scheme solves one equation unlike other techniques available in the literature which split the DPL equation into a system of two equations and then apply discretization. This approach considerably reduces the number of arithmetic operations involved, and consequently, the computational time is reduced.

11. It is found from the von Neumann stability analysis that the new proposed numerical scheme is unconditionally stable. The results from the present implicit numerical scheme and explicit scheme compares well with the analytical results for phase lag ratios $Z > 0$. The present numerical scheme is not able to capture the sharp thermal wave front caused by setting $Z = 0$ (mixed derivative term = 0 in the DPL equation). The different formulation to solve the the DPL equation implicitly agrees with the the analytical results quite well. However, stability analysis has not been carried out for

this new formulation.

12. The results from the 3-D implicit numerical scheme compares well with the experimental and analytical results during short pulse laser heating of thin films. The proposed numerical scheme outperforms Dai's [25] numerical technique in terms of computational time taken to complete the simulation. Also, the δ-form Douglas-Gunn time-splitting method consumes the least CPU time compared to all other numerical techniques available in the literature for large values of N.

13. When $N = 21$ the explicit method consumes less CPU time than the rest of the numerical techniques, but for the spatial discretization parameter $N > 21$ all implicit methods except the Gauss–Seidel method perform better than the explicit method employed in this research. We are still investigating the reason for the poor performance of the Gauss–Seidel method compared to the explicit method.

7.3 Future work

Further work needs to be done with the 3-D implicit finite-difference algorithm. Stability properties of the Douglas–Gunn time-splitting method are not completely known. It is clear that von Neumann stability analysis will provide only necessary conditions for stability. We have shown that the 1-D implicit numerical scheme is unconditionally stable using von Neumann stability analysis. Dai and Nassar have [34] employed a discrete energy method [32, 33, 58] to show that their numerical scheme is unconditionally stable. We will investigate both von Neumann analysis and discrete energy method to show stability of the numerical technique. We are also investigating a different numerical formulation to the solve the 3-

D DPL equation implicitly. Further the 3-D implicit finite-difference algorithm has to be modified to accommodate temperature dependent thermal properties. We will then be able to simulate micro-machining process using ultra-fast lasers describing the microscale thermal mechanisms more accurately.

Appendix A
3–D EXPLICIT FINITE–DIFFERENCE FORTRAN 90 CODE

```
!This is a 3-D explicit finite-difference program for modeling temperature
!distribution in a gold film by using the dual phase lag model with the laser
!heat source term S

program ilay
  implicit double precision (a-h,o-z)

  PARAMETER(NMX=202,NMY=202,NMZ=42)
  DIMENSION T(0:NMX,0:NMY,0:NMZ),T1(0:NMX,0:NMY,0:NMZ),To(0:NMX,0:NMY,0:NMZ)
  DIMENSION distx(0:NMX),disty(0:NMY),distz(0:NMZ),time(0:33556)
  DIMENSION FR(0:1220),RE(0:1220),FRONT(0:1220),REAR(0:1220)
  DIMENSION X(0:NMX,0:NMY,0:NMZ),Y(0:NMX,0:NMY,0:NMZ),Z(0:NMX,0:NMY,0:NMZ)
  DIMENSION SUM1(0:NMY,0:NMZ),SUM2(0:NMY,0:NMZ),SUM3(0:NMY,0:NMZ)
  DIMENSION SUM4(0:NMZ),SUM5(0:NMZ)
  CHARACTER*13   SNPSHTFL   !---> Snapshots file
  CHARACTER*3   SSN   !---> Snapshots file

  KSSN = 0
  Temp=300.D0

!-------PROPERTIES-------------------------!
  tt=90.D-12
  tq=8.5D-12
!  tt=0.D0
!  tq=0.D0
  alpha=1.2D-4
  zj=13.4D0
  zR=0.93D0
  tp=96.D-15
  a=1.992D0
  ak=315.D0
  delta=15.3D-9
  So=0.94D0*zj*(1.D0-zr)/(delta*tp)

!------dk=dimensional increment of time----------------!
!------dh,di,dz=dimensional increment of space---------!

  dh=5.D-9!*2.D0
```

```
  di=dh
  dz=dh

  aa=-2.D0*alpha*((di**2)*(dz**2)+&
       &(dh**2)*(dz**2)+(dh**2)*(di**2))
  bb=((dh**2)*(di**2)*(dz**2))&
       &-(4.D0*alpha*(di**2)*(dz**2)*tt)&
       &-(4.D0*alpha*(dh**2)*(dz**2)*tt)&
       &-(4.D0*alpha*(dh**2)*(di**2)*tt)
  cc=2.D0*(dh**2)*(di**2)*(dz**2)*tq

  dkk1=sqrt((bb**2)-4.D0*aa*cc)
  dk=(-bb-dkk1)/(2.D0*aa)

!------ENTER SPACE STEPS-----------------!

Nx=(5.D0*0.1D-6)/(dh)+1
Ny=(5.D0*0.1D-6)/(dh)+1
Nz=(1.D0*0.1D-6)/(dh)+1
Nt=2.5D-12/(dk)+1

  time(1)=0.D0
  distx(1)=0.D0
  disty(1)=0.D0
  distz(1)=0.D0

  do  k=1,Nt
     time(k+1)=time(k)+dk
  end do

  do  i=1,Nx
     distx(i+1)=distx(i)+dh
  end do


  do  j=1,Ny
     disty(j+1)=disty(j)+di
  end do

  do  L=1,Nz
     distz(L+1)=distz(L)+dz
  end do

!-----------  Constants  ----------------------------!
```

```
  c1=(alpha*dk**2)/(dk+tq)
  c2=1.D0/(dh**2)+tt/(dk*(dh**2))
  c3=-2.D0/(dh**2)-2.D0/(di**2)-2.D0/(dz**2)&
       &-2.D0*tt/(dk*(dh**2))-2.D0*tt/(dk*(di**2))&
       &-2.D0*tt/(dk*(dz**2))&
       &+1.D0/(alpha*dk)+&
       &2*tq/(alpha*dk**2)
  c4=1.D0/(di**2)+tt/(dk*(di**2))
  c5=1.D0/(dz**2)+tt/(dk*(dz**2))
  c6=2.D0*tt/(dk*(dh**2))+ 2.D0*tt/(dk*(di**2))+&
       &2.D0*tt/(dk*(dz**2))-tq/(alpha*dk**2)
  c7=-tt/(dk*(dh**2))
  c8=-tt/(dk*(di**2))
  c9=-tt/(dk*(dz**2))

!--------------initial condition----------------------- ----!
  do i=0,Nx+1
     do j=0,Ny+1
        do l=0,Nz+1
           To(i,j,l)=Temp
        end do
     end do
  end do

  do i=0,Nx+1
     do j=0,Ny+1
        do  l=0,Nz+1
           T1(i,j,l)=To(i,j,l)
        end do
     end do
  end do


   do k=1,Nt
     FR(k)=Temp
     RE(k)=Temp
  end do


!--------------BOUNDARY CONDITION --------------------------!
do L=1,Nz
   do j=1,Ny
      To(0,j,L)=To(2,j,L)
```

```
      T1(0,j,L)=T1(2,j,L)
      T1(Nx+1,j,L)=T1(Nx-1,j,L)
      To(Nx+1,j,L)=To(Nx-1,j,L)
   end do
end do

do L=1,Nz
   do i=1,Nx
      To(i,0,L)=To(i,2,L)
     T1(i,0,L)=T1(i,2,L)
      T1(i,Ny+1,L)=T1(i,Ny-1,L)
      To(i,Ny+1,L)=To(i,Ny-1,L)
   end do
end do


do j=1,Ny
   do i=1,Nx
      To(i,j,0)=To(i,j,2)
      T1(i,j,0)=T1(i,j,2)

      T1(i,j,Nz+1)=T1(i,j,Nz-1)
     To(i,j,Nz+1)=To(i,j,Nz-1)

   end do
end do

!-------------     GRID  GENERATION    -------------------------!

           do l=1,Nz+1
              do j=1,Ny+1
                 do i=1,Nx+1
                    X(i,j,l)=DH*(i-1)
                 end do
              end do
           end do

           do l=1,Nz+1
              do i=1,Nx+1
                 do j=1,Ny+1
                    Y(i,j,l)=DI*(j-1)
                 end do
              end do
           end do
```

```
            do j=1,Ny+1
               do i=1,Nx+1
                  do l=1,Nz+1
                     Z(i,j,l)=Dz*(l-1)
                  end do
               end do
            end do


                  OPEN(22,FILE='grid3D.xyz',STATUS='unknown')
                  WRITE(22,*)NX,NY,NZ
                  WRITE(22,'(5(E14.6))') &
                      &((((SNGL(X(I,J,L))),I=1,NX),J=1,NY),L=1,NZ),&
                      &((((SNGL(Y(I,J,L))),I=1,NX),J=1,NY),L=1,NZ),&
                      &((((SNGL(Z(I,J,L))),I=1,NX),J=1,NY),L=1,NZ)
                 CLOSE(22)

!----------------Begin Time stepping-----------------------------------!
do k=3,Nt
   do L=1,Nz
      do j=1,Ny
         To(0,j,L)=To(2,j,L)
         T1(0,j,L)=T1(2,j,L)
         T1(Nx+1,j,L)=T1(Nx-1,j,L)
         To(Nx+1,j,L)=To(Nx-1,j,L)
      end do
   end do

   do L=1,Nz
      do i=1,Nx
         To(i,0,L)=To(i,2,L)
         T1(i,0,L)=T1(i,2,L)
         T1(i,Ny+1,L)=T1(i,Ny-1,L)
         To(i,Ny+1,L)=To(i,Ny-1,L)
      end do
   end do

    do j=1,Ny
      do i=1,Nx
         To(i,j,0)=To(i,j,2)
         T1(i,j,0)=T1(i,j,2)

         T1(i,j,Nz+1)=T1(i,j,Nz-1)
```

```
         To(i,j,Nz+1)=To(i,j,Nz-1)

      end do
   end do


   do L=1,Nz
      do j=1,Ny
         do i=1,Nx

!------------   1D  SOURCE TERM  -------------------------------------!

               s=so*exp(-(distz(l)/delta)-a*&
                    &abs((time(k-1)-2*tp)/tp))


                ss=(so*tq/(2.D0*dk))*(exp(-(distz(l)/delta)-&
                    &a*abs((time(k)-2*tp)/tp))-&
                    &exp(-(distz(l)/delta)-&
                    &a*abs((time(k-2)-2*tp)/tp)))


!------------   3D  SOURCE TERM  -------------------------------------!
!               s=so*exp(-(((distx(i)-(Nx*dh)/2)**2+(disty(j)-&
!                    &1.D0*(Ny*di)/8)**2))&
!                    &/(200.D-9)**2-(distz(l)/delta)-a*&
!                    &abs((time(k-1)-2*tp)/tp))


!                ss=(so*tq/(2.D0*dk))*(exp(-(((distx(i)-(Nx*dh)/2)**2+&
!                    &(disty(j)-&
!                    &1.D0*(Ny*di)/8)**2))&
!                    &/(200.D-9)**2-(distz(l)/delta)-&
!                    &a*abs((time(k)-2*tp)/tp))-&
!                    &exp(-(((distx(i)-(Nx*dh)/2)**2+(disty(j)-&
!                    &1.D0*(Ny*di)/8)**2))&
!                    &/(200.D-9)**2-(distz(l)/delta)-&
!                    &a*abs((time(k-2)-2*tp)/tp)))

!------------   3D  SOURCE TERM  WITH MOVING LASER BEAM  ------------!
!            if(k.lt.Nt/4)then
!               s=so*exp(-(((distx(i)-(Nx*dh)/4)**2+(disty(j)-&
!                    &(Ny*di)/4)**2))&
!                    &/(200.D-9)**2-(distz(l)/delta)-a*&
```

```
!                    &abs((time(k-1)-2*tp)/tp))


!                ss=(so*tq/(2.D0*dk))*(exp(-(((distx(i)-(Nx*dh)/4)**2+&
!                    &(disty(j)-(Ny*di)/4)**2))&
!                    &/(200.D-9)**2-(distz(l)/delta)-&
!                    &a*abs((time(k)-2*tp)/tp))-&
!                    &exp(-(((distx(i)-(Nx*dh)/4)**2+(disty(j)-&
!                    &(Ny*di)/4)**2))&
!                    &/(200.D-9)**2-(distz(l)/delta)-&
!                    &a*abs((time(k-2)-2*tp)/tp)))

!            else if((k.lt.Nt/2).and.(k.gt.Nt/4))then
!               s=so*exp(-(((distx(i)-(Nx*dh)/4)**2+(disty(j)-&
!                    &3.D0*(Ny*di)/4)**2))&
!                    &/(200.D-9)**2-(distz(l)/delta)-a*&
!                    &abs((time(k-(Nt/4)-1)-2*tp)/tp))

!               ss=(so*tq/(2.D0*dk))*(exp(-(((distx(i)-(Nx*dh)/4)**2+&
!                    &(disty(j)-3.D0*(Ny*di)/4)**2))&
!                    &/(200.D-9)**2-(distz(l)/delta)-&
!                    &a*abs((time(k-(Nt/4))-2*tp)/tp))-&
!                    &exp(-(((distx(i)-(Nx*dh)/4)**2+(disty(j)-&
!                    &3.D0*(Ny*di)/4)**2))&
!                    &/(200.D-9)**2-(distz(l)/delta)-&
!                    &a*abs((time(k-(Nt/4)-2)-2*tp)/tp)))


!            else if((k.lt.3*Nt/4).and.(k.gt.Nt/2)) then
!               s=so*exp(-(((distx(i)-3.D0*(Nx*dh)/4)**2+(disty(j)-&
!                    &3.D0*(Ny*di)/4)**2))&
!                    &/(200.D-9)**2-(distz(l)/delta)-a*&
!                    &abs((time(k-(Nt/2)-1)-2*tp)/tp))

!               ss=(so*tq/(2.D0*dk))*(exp(-(((distx(i)-3.D0*(Nx*dh)/4)**2+&
!                    &(disty(j)-3.D0*(Ny*di)/4)**2))&
!                    &/(200.D-9)**2-(distz(l)/delta)-&
!                    &a*abs((time(k-(Nt/2))-2*tp)/tp))-&
!                    &exp(-(((distx(i)-3.D0*(Nx*dh)/4)**2+(disty(j)-&
!                    &3.D0*(Ny*di)/4)**2))&
!                    &/(200.D-9)**2-(distz(l)/delta)-&
!                    &a*abs((time(k-(Nt/2)-2)-2*tp)/tp)))

!            else if((k.lt.Nt).and.(k.gt.3.D0*Nt/4))then
```

```
!               s=so*exp(-(((distx(i)-3.D0*(Nx*dh)/4)**2+(disty(j)-&
!                    &(Ny*di)/4)**2))&
!                    &/(200.D-9)**2-(distz(l)/delta)-a*&
!                    &abs((time(k-(3.D0*Nt/4)-1)-2*tp)/tp))


!               ss=(so*tq/(2.D0*dk))*(exp(-(((distx(i)-3.D0*(Nx*dh)/4)**2+&
!                    &(disty(j)-(Ny*di)/4)**2))&
!                    &/(200.D-9)**2-(distz(l)/delta)-&
!                    &a*abs((time(k-(3.D0*Nt/4))-2*tp)/tp))-&
!                    &exp(-(((distx(i)-3.D0*(Nx*dh)/4)**2+(disty(j)-&
!                    &(Ny*di)/4)**2))&
!                    &/(200.D-9)**2-(distz(l)/delta)-&
!                    &a*abs((time(k-(3.D0*Nt/4)-2)-2*tp)/tp)))
! end if

                         T(i,j,L)=c1*(c2*(T1(i+1,j,L)+T1(i-1,j,L))+&
                              &C4*(T1(i,j+1,L)+T1(i,j-1,L))+&
                              &C5*(T1(i,j,L+1)+T1(i,j,L-1))+&
                              &c3*T1(i,j,L)+&
                              &c7*(To(i+1,j,L)+To(i-1,j,L))+&
                              &C8*(To(i,j+1,L)+To(i,j-1,L))+&
                              &C9*(To(i,j,L+1)+To(i,j,L-1))+&
                              &c6*To(i,j,L)+&
                              & (s+ss)/ak)


                           end do
                        end do
                     end do

                     do L=0,Nz+1
                        do j=0,Ny+1
                           do i=0,Nx+1
                              To(i,j,l)=T1(i,j,L)
                              T1(i,j,L)=T(i,j,L)
                           end do
                        end do
                     end do

!--------------   3D OUTPUT  -------------------------           ---------!

                     IF(MOD(K,NT/8).EQ.0)THEN
```

```
                    KSSN = KSSN + 1
                    NVARS = 5
                    SSN=CHAR(48+KSSN/100)//CHAR(48+MOD(KSSN,100)/10)//&
                         &CHAR(48+MOD(KSSN,10))
                    SNPSHTFL = 'output'//SSN//'.c1q'
                    OPEN(23,FILE=SNPSHTFL,STATUS='unknown')
               WRITE(23,*)NX,NY,NZ,NVARS
               WRITE(23,'(5(E14.6))') ((((SNGL(T(I,J,L))),I=1,NX),&
                         &J=1,NY),L=1,NZ), ((((SNGL(T(I,J,L))),I=1,NX),&
                         &J=1,NY),L=1,NZ), ((((SNGL(T(I,J,L))),I=1,NX),&
                         &J=1,NY),L=1,NZ), ((((SNGL(T(I,J,L))),I=1,NX),&
                         &J=1,NY),L=1,NZ), ((((SNGL(T(I,J,L))),I=1,NX),&
                         &J=1,NY),L=1,NZ)

                    CLOSE(23)
                 END IF
      FR(k)=T(Nx/2,Ny/2,1)
      RE(k)=T(Nx/2,Ny/2,Nz/2)
           end do

!---------------End of time stepping -------------------------------------!
!-------------- NORMALIZED TEMPERATURE-------------------!

      T1max=FR(1)
              T2max=RE(1)

      open (25,file='FRONT',status='unknown')
      open (26,file='REAR',status='unknown')

              do k=1,Nt
                 if (FR(k).GE.T1max) T1max=FR(k)
                 if (RE(k).GE.T2max) T2max=RE(k)
              end do

              print*,'T1max',T1max,'T2max',T2max

              do k=1,Nt
                 if(FR(k).LE.TEMP) then
                    FR(k)=TEMP

  ELSE
                    FRONT(k)=(FR(k)-TEMP)/(T1max-TEMP)
                 endif
               WRITE(25,*)(((k-1)*dk)-2*tp)*1.D12,FRONT(k)
```

```
               end do

               do k=1,Nt
                  if(RE(k).LE.TEMP) then
                     RE(k)=TEMP

  ELSE
                     REAR(k)=(RE(k)-TEMP)/(T2max-TEMP)
                  endif
                 WRITE(26,*)(((k-1)*dk)-2*tp)*1.D12,REAR(k)
               end do

close(25)
close(26)
!---------------  END NORMALIZED TEMPERATURE CHANGE  -----!----

!---------------GRID FUNCTION CONVERGENCE TEST-------!

               DO L=1,NZ
                  DO J=1,NY
                     SUM1(J,L)=0.D0
                     SUM2(J,L)=0.D0
                  END DO
               END DO

               DO L=1,NZ
                  DO J=1,NY
                     DO I=2,NX-1
                        SUM1(J,l)=SUM1(J,L)+T(I,J,L)
                     END DO
                  END DO
               END DO

               DO L=1,NZ
                  DO J=1,NY
                     SUM2(J,L)=0.5*(T(1,J,L)+T(NX,J,L))
                  END DO
               END DO

               DO L=1,NZ
                  DO J=1,NY
                     SUM3(J,L)=DH*(SUM1(J,L)+SUM2(J,L))
                  END DO
               END DO
```

```
              DO L=1,NZ
                 SUM4(L)=0.D0
              END DO

              DO L=1,NZ
                 DO J=2,NY-1
                    SUM4(L)=SUM4(L)+SUM3(J,L)
                 END DO
              END DO


              DO L=1,NZ
                 SUM5(L)=DI*(SUM4(L)+0.5D0*(SUM3(1,L)+SUM3(NY,L)))
              END DO

              SUM6=0.D0

              DO L=2,NZ-1
                 SUM6=SUM6+SUM5(L)
              END DO
      SUM7=DZ*(SUM6+0.5D0*(SUM5(1)+SUM5(NZ)))

              WRITE(*,*)'SUM7=',SUM7

              zz1=(3.00443889604601D-019-3.00456767168399D-019)/&
                   &(3.00456767168399D-019-3.00459907779630D-019)

              zz2=log(zz1)/log(2.d0)
              write(*,*)zz2

              zzz1=(3.00456767168399D-019-3.00459907779630D-019)/&
                   &(3.00459907779630D-019-3.00460735455507D-019)

              zzz2=log(zzz1)/log(2.d0)
              write(*,*)zzz2

!-----------     END of Grid function convergence test ---------------!

     print*,'convergent result'
   end program ilay
```

Appendix B
1–D IMPLICIT FINITE–DIFFERENCE FORTRAN 90 CODE

```
!THIS IS A ONE-DIMENSIONAL FINITE-DIFFERENCE FORTRAN CODE TO COMPUTE THE
TEMPERATURE DISTRIBUTION IN A SEMI-INFINITE SLAB SUBJECT TO A SUDDEN TEMPERATURE
RISE ON ITS BOUNDARIES.

program ilay

   IMPLICIT REAL*8 (A-H,O-Z)
      PARAMETER ( MNX = 401,NMT=600 )
      DIMENSION A(MNX,3),B(MNX),T(MNX),To(MNX),Too(MNX)

  open(2,file='out',status='unknown')
!-----------Calculate grid spacing---------------------------!
print*,'enter the value for B'
read(*,*)BB

print*,'enter the value for time step dt'
read(*,*)dt

print*,'enter the value for final time beta'
read(*,*)beta

Nt=(beta/dt)+1

  Nx=401
  ax=1.D0
  bx=3.D0
  h=(bx-ax)/DFLOAT(Nx-1)

!----------initial data-------------------------------------!
  do m=1,Nx
     To(m)=0.D0
  enddo

 do m=1,Nx
   Too(m)=0.D0
 enddo

   sum=0.D0
```

```
 !----------constants----------------------------------!

  c1=1.D0
  c2=1.D0
  c3=BB
  c4=-(c3 + 0.5D0*dt )*(1.D0/h**2)
  c5=(c3 + 0.5D0*dt )*(2.D0/h**2) +(c1+(c2/dt))
  c6=(-c3 + 0.5D0*dt )*(1.D0/h**2)
  c7=(-c3 + 0.5D0*dt )*(-2.D0/h**2) +(c1+(2.D0*c2/dt))

!-----------begin time stepping-----------------------------!
  do n=1,Nt

!----------load tridiagonal matrix and right hand side------!

    ! Lftbndry

     A(1,1)=0.D0
     A(1,2)=1.D0
     A(1,3)=0.D0

!-----DIRICHLET BOUNDARY CONDITION ------------------------!
   B(1)=1.D0

     do m=2,Nx-1
        A(m,1)=c4
        A(m,2)=c5
        A(m,3)=c4

B(m)=c6*(To(m-1)+To(m+1))+c7*To(m)-(c2/dt)*Too(m)
     enddo

     A(Nx,1)=2.D0*c4
     A(Nx,2)=c5
     A(Nx,3)=0.D0

! Rhtbndry(t)

!-----NEUMAN BOUNDARY CONDITION ------------------------!
      B(Nx)=2.D0*c6*To(Nx-1)+c7*To(Nx)-(c2/dt)*Too(Nx)


!----------solve tridiagonal system-----------!
     call LUDCMP(A,B,T,Nx)
```

```
 !---------store current time level solution-----!

     do m=1,Nx
        Too(m)=To(m)
     enddo

    do m=1,Nx
        To(m)=T(m)
     enddo
!---------go to next time step---------!

  enddo
!--------end time stepping ------------!


do i=1,Nx
   WRITE(2,*)h*(i-1),T(i)
enddo

do i=2,Nx-1
 sum=sum+T(i)
 end do
!---------Grid function convergence test----------!

 sum2 =h*(sum+0.5D0*(T(1)+T(Nx)))

 write(*,*)h,'sum2',sum2
qqn=(1.1267175266327-1.12669930503795)
qqd=(1.12669930503795-1.12669474967179)
qq1=qqn/qqd
qq2=log(qq1)/log(2.D0)
  write(*,*)'q',qq2
!---------End grid function convergence test----------!

end program ilay

!_____________________________________________________________________________*

!-------------------------LU decomposition ------------------------------!
!_____________________________________________________________________________*

      SUBROUTINE LUDCMP(A,B,T,Nx)
```

```
      IMPLICIT REAL*8 (A-H,O-Z)
      PARAMETER ( MNX = 401 )
      DIMENSION A(MNX,3),B(MNX),T(MNX)

!*    Construction of L and U from elements of A
      A(1,3) = A(1,3)/A(1,2)
      B(1) = B(1)/A(1,2)

       DO I=2,Nx-1
        A(I,2) = A(I,2) - (A(I,1)*A(I-1,3))
        A(I,3) = A(I,3)/A(I,2)

!-------- Forward substitution (solve LY=B)--------------------!

       B(I) = (B(I) - A(I,1)*B(I-1))/A(I,2)
      END DO

      A(Nx,2) = A(Nx,2) - (A(Nx,1)*A(Nx-1,3))
      B(Nx) = (B(Nx) - A(Nx,1)*B(Nx-1))/A(Nx,2)

!-------- Backward substitution (solve UX=Y)-------------------!
      T(Nx)=B(Nx)
       DO I=(Nx-1),1,-1
        T(I) = B(I) - (A(I,3)*T(I+1))
      END DO

      END SUBROUTINE LUDCMP

!_______________________________________________________________________________*
!
```

Appendix C
1–D IMPLICIT FINITE–DIFFERENCE FORTRAN 90 CODE

```
!THIS IS A ONE-DIMENSIONAL IMPLICIT FINITE-DIFFERENCE FORTRAN CODE TO SOLVE DPL
EQUATION (WITH A DIFFERENT NUMERICAL FORMULATION) TO COMPUTE THE TEMPERATURE
DISTRIBUTION IN A THIN METAL FILM EXPOSED TO SHORT-PULSE LASER

program ilay
      IMPLICIT REAL*8 (A-H,O-Z)
      PARAMETER ( MNX = 101,NMT=1402 )
      DIMENSION A(MNX,3),B(MNX),T(MNX)
      DIMENSION To(MNX),B(MNX),U(MNX),Un(MNX),S(0:MNX,0:NMT)
      DIMENSION FR(0:1220),RE(0:1220),FRONT(0:1220),REAR(0:1220)

  tauT=90D-12
  tauq=8.5D-12
  alpha=1.2D-4 !thermal diffusivity m2s-1
  tp=96D-15
  Ra=0.93      !reflectivity dimensionless
  aJ=13.4       !laser fluence Jm-2
  delta=15.3D-9
  ac=1.992
  kapa=315    !thermal conductivity Wm-1K-1
  Temp=300.D0

  open(1,file='out.plt',status='unknown')
  open(2,file='out',status='unknown')

!-----------Calculate grid spacing--------------------------!


  Nt=1201
  dt=2.5D-12/(Nt-1)

  Nx=101
  h=0.1D-6/(Nx-1)

  r=dt/(2.D0*h*h)

  write(*,*)'r',r
  write(*,*)'dt=',dt
  write(*,*)'dh=',h
```

```
  write(*,*)'Nt',Nt
  write(*,*)'Nx',Nx

!----------initial data-----------------------------------!
  do m=1,Nx
     To(m)=300.D0
  enddo

  do m=1,Nx
     Un(m)=0.D0
  enddo

   do k=1,Nt
     FR(k)=Temp
     RE(k)=Temp
  end do

  !----------constants-----------------------------------!

  c1=tauT/h**2
  c2=2.D0*(tauT/h**2 + tauq/(alpha*dt) )
  c3=2.D0*(tauT/h**2 - tauq/(alpha*dt) )
  c4=1.D0+tauT/(r*h**2)
  c5=c2/r + 2.D0 +1.D0/(alpha*r)
  c6=c3/r + 2.D0 -1.D0/(alpha*r)
  c7=h**2/kapa +tauq/(r*kapa)
  c8=h**2/kapa -tauq/(r*kapa)
  c9=0.94D0*aj*(1-Ra)/(tp*delta)

  do n=1,Nt
    do m=1,Nx
      S(m,n)=c9*dexp(-(m*h)/delta -(1.992D0/tp) &
      &        *dabs((n*dt)-2.D0*tp))
      print*,m,n,S(m,n)
    end do
  !  pause
  end do

!-----------begin time stepping-----------------------------!
  do n=1,Nt

!----------load tridiagonal matrix and right hand side------!

   ! A(1,1)=0.D0
```

```
   ! A(1,2)=1.D0
   ! A(1,3)=0.D0

    ! Lftbndry
   ! B(1)=350.D0

     A(1,1)=0.D0
     A(1,2)=-c5
     A(1,3)=2.D0*c4

     B(1)=c6*To(1)&
     &   -2.D0*c4*To(2)-(2.D0/r)*Un(1) &
&   -S(1,n+1)*c7 -S(1,n)*c8

     do m=2,Nx-1
        A(m,1)=c4
        A(m,2)=-c5
        A(m,3)=c4

        B(m)=-c4*To(m-1) +c6*To(m)&
&   -c4*To(m+1)-(2.D0/r)*Un(m) &
&   -S(m,n+1)*c7 -S(m,n)*c8
     enddo

     A(Nx,1)=2.D0*c4
     A(Nx,2)=-c5
     A(Nx,3)=0.D0

  !   A(Nx,1)=0.D0
   !  A(Nx,2)=1.D0
   !  A(Nx,3)=0.D0

! Rhtbndry(t)

!-----NEUMAN BOUNDARY CONDITION ------------------------!
      B(Nx)=-2.D0*c4*To(Nx-1) +c6*To(Nx)&
&   -(2.D0/r)*Un(Nx)&
&   -S(Nx,n+1)*c7 -S(Nx,n)*c8

!-----DIRICHLET BOUNDARY CONDITION----------------------!
   !B(Nx)=1.D0

     do m=1,Nx
    !    T(m)=To(m)
```

```
     enddo

!----------solve tridiagonal system-----------!
     call LUDCMP(A,B,T,Nx)


         do m=2,Nx-1
           U(m)=-c1*T(m-1)+c2*T(m)-c1*T(m+1)&
                &-c1*To(m-1)+c3*To(m)-c1*To(m+1)&
                &-Un(m)
        enddo

   do m=2,Nx-1
        Un(m)=U(m)
     enddo

!---------store current time level solution-----!

     do m=1,Nx
        To(m)=T(m)
     enddo

!---------go to next time step---------!

  FR(n)=T(1)
  RE(n)=T(Nx/2)
write(1,*)T(1)
  enddo
!--------end time stepping ------------!

!--------OUTPUT-----------------------!
open (7,file='fr',status='unknown')
do k=1,Nt
write(7,*)FR(k)
end do

d=0.D0
do i=1,Nx
WRITE(2,*)(i-1)*h*1.d6,'                      ',T(i)
d=d+h
enddo


!-------------- NORMALIZED TEMPERATURE-------------------!
```

```
      T1max=FR(1)
              T2max=RE(1)

      open (25,file='front2',status='unknown')
      open (26,file='rear2',status='unknown')

              do k=1,Nt
                 if (FR(k).GE.T1max) T1max=FR(k)
                 if (RE(k).GE.T2max) T2max=RE(k)
              end do

              print*,'T1max',T1max,'T2max',T2max

              do k=1,Nt
                 if(FR(k).LE.TEMP) then

                    FR(k)=TEMP

  ELSE
                    FRONT(k)=(FR(k)-TEMP)/(T1max-TEMP)
                 endif
                WRITE(25,*)(((k-1)*dt)-2*tp)*1.D12,FRONT(k)
      end do

              do k=1,Nt
                 if(RE(k).LE.TEMP) then
                    RE(k)=TEMP

  ELSE
                    REAR(k)=(RE(k)-TEMP)/(T2max-TEMP)
                 endif
                WRITE(26,*)(((k-1)*dt)-2*tp)*1.D12,REAR(k)
              end do


!---------------  END NORMALIZED TEMPERATURE CHANGE  ---------!


end program ilay

!_____________________________________________________________________________*

!-------------------------LU decomposition -----------------------------!
```

```
!-------------------------------------------------------------------------------*
!

      SUBROUTINE LUDCMP(A,B,T,Nx)

      IMPLICIT REAL*8 (A-H,O-Z)
      PARAMETER ( MNX = 101 )
      DIMENSION A(MNX,3),B(MNX),T(MNX)

!*    Construction of L and U from elements of A
      A(1,3) = A(1,3)/A(1,2)
      B(1) = B(1)/A(1,2)

       DO I=2,Nx-1
        A(I,2) = A(I,2) - (A(I,1)*A(I-1,3))
        A(I,3) = A(I,3)/A(I,2)

!-------- Forward substitution (solve LY=B)--------------------!

       B(I) = (B(I) - A(I,1)*B(I-1))/A(I,2)
      END DO

      A(Nx,2) = A(Nx,2) - (A(Nx,1)*A(Nx-1,3))
      B(Nx) = (B(Nx) - A(Nx,1)*B(Nx-1))/A(Nx,2)

!-------- Backward substitution (solve UX=Y)-------------------!
      T(Nx)=B(Nx)
       DO I=(Nx-1),1,-1
        T(I) = B(I) - (A(I,3)*T(I+1))
      END DO

      END SUBROUTINE LUDCMP
```

BIBLIOGRAPHY

1. Allen, P. B., 1987, "Theory of thermal relaxation of electrons in metals," *Phy. Rev. Lett.*, **59**, pp. 1460-1463.

2. Alexander, J. D. Jr., 1995, "Computational fluid dynamics the basics with applications," McGraw-Hill, Inc., New York, pp. 153-161.

3. Al-Nimr, M.K., and Arpaci, V.S., 2000, "The thermal behavior of thin metal films in the hyperbolic two-step model," *International Journal of Heat and Mass Transfer*, **43**, pp. 2021-2028.

4. Anisimov, S I., Kapeliovich, B.l., and Perel'man, T. L., 1974, "Electron emission from metal surfaces exposed to ultrashort laser pulses," *Sov. Phys. JETP,* **39**, pp. 375-377.

5. Bai, C., Lavine, A. S., 1995, "On the hyperbolic heat conduction and second law of Thermodynamics," *International Journal of Heat and Mass Transfer*, **117**, pp. 256-263.

6. Barletta, A., Zanchini, E., 1997, "Hyperbolic heat conduction and local equilibrium: second law analysis," *International Journal of Heat and Mass Transfer*, **40**, pp.1007-1016.

7. Baumeister, K. J. and Hamill, T. D., 1969, "Hyperbolic heat conduction equation - A solution for the semi-infinite body problem," *ASME Journal of Heat Transfer*, **91**, pp. 543-548.

8. Baumeister, K. J. and Hamill, T. d., 1971, "Hyperbolic heat conduction equation - A solution for the semi-infinite body problem," *ASME Journal of Heat Transfer*, **93**, pp. 126-128.

9. Bertman, B. and Sandiford D.J., 1970, "Second sound solid helium," *Scient. Am.*, **222(5)**, pp. 92-101.

10. Boyd, I.W., 1989, "Laser Processing of Thin Films and Microstructures," Springer, New York.

11. Brorson, S.D., Kazeroonian, A., Moodera, J. S., Face, D.W., Cheng, T.K., Ippen, E.p., Dresselhaus, M.S., and Dresselhaus, G., 1990, "Femtosecond room temperature measurements of the electron-phonon coupling constant λ in metallic superconductors," *Phys. Rev. Lett.*, **64**, pp. 2172-2175.

12. Brorson, S.D., Fujimoto, J.G., and Ippen, E.P., 1987, "Femto-second electron heat-transport dynamics in thin gold film," *Phys. Rev. Lett.*, **59**,pp. 1962-1965.

13. Cantatore, J. L., and Kriegel, D. A., 2004, "Laser surgery: an approach to the pediatric patient," *Journal of the American Academy of Dermatology*, **50**, pp. 165-184.

14. Cattaneo, M.C., 1958, "Sur une forme de l'equation de la chaleur eliminant le paradox d'une propagation instantanee", *Comptes Rendus Hebd. Seances Acad. Sci.*, **247**, pp.431-433.

15. J.K. Chen and J.E. Beraun, 2001, "Numerical study of ultrashort laser pulse interactions with metal films," *Numerical Heat Transfer*, **40**, pp. 1-20

16. Chiu, K. S, 1999, "Temperature dependent properties and microvoid in thermal lagging," Ph. D. Dissertation, University of Missouri-Columbia, Columbia, Missouri.

17. Chryssolouris, G., 1991, "Laser Machining, Theory and Practice," Springer, New York.

18. Cimmelli, V. A., 2002, "Boundary Conditions for Diffusive Hyperbolic Systems in Non Equilibrium Thermodynamics," *Technische Mechanik, Band* **22**, Heft 3, pp. 181-186.

19. Cimmelli, V. A., Frischmuth, 1996, "Hyperbolic heat conduction at cryogenic temperatures," *Reniconti del Circolo Matematico di Palermo,* **II, 45**, pp.137-145.

20. Coleman, B. D., Fabrizio, M., and Owen, D. R., 1982, "On the thermodynamics of second sound in dielectric crystals," *Arch. Rat. Mech. Anal.,* **80**, pp. 135-158.

21. Coleman, B. D., Fabrizio, M., and Owen, D. R., 1986, "Thermodynamics and the constitutive relations for second sound in crystals," *New Perspectives in Thermodynamics,* J. serin, ed., pp. 171-185.

22. Dai, W., Shen, L., Nassar, R., and Zhu, T., 2004, "A stable and convergent three-level finite difference scheme for solving a dual-phase-lagging heat transport equation in spherical coordinates," *International Journal of Heat and Mass Transfer*, **47**, pp. 1817-1825.

23. Dai, W., Shen, L., Nassar, R., 2004, "An unconditionally stable three level finite difference scheme for solving parabolic two-step micro heat transport equations in a three-dimensional double-layered thin film," *International Journal for Numerical Methods in Engineering*, **59**, pp. 493-509.

24. Dai, W., Shen, L., and Nassar, R., 2004, "A convergent three-level finite difference scheme for solving a dual-phase-lagging heat transport equation in spherical coordinates," *Numerical Methods for Partial Differential Equations*, **20**, pp. 60-71.

25. Dai, W., and Nassar, R., 2003, "A three level finite difference scheme for solving micro heat transport equations with temperature-dependent thermal properties," *Numerical Heat Transfer, Part B*, **45**, pp. 509-523.

26. Dai, W., and Nassar, R., 2003, "An unconditionally stable hybrid FE-FD scheme for solving a 3-D heat transport equation in a cylindrical thin film with sub-microscale thickness," *Journal of Computational Mathematics*, **21**, pp. 555-568.

27. Dai, W., and Nassar, R., 2002, "An unconditionally stable finite difference scheme for solving 3-D heat transport equation in a sub-microscale thin film," *Journal of Computational and Applied Mathematics*, **145**, pp. 247-260.

28. Dai, W., and Nassar, R., 2001, "A finite difference method for solving 3-D heat transfer equations in double layered thin film with micro-scale thickness and nonlinear interfacial conditions," *Numerical Heat Transfer, Part A*, **39**, pp. 21-33.

29. Dai, W., and Nassar, R., 2001, "A finite difference scheme for solving a three dimensional heat transport equation in a thin film with micro-scale thickness," *International Journal for Numerical Methods in Engineering*, **50**, pp. 1665-1680.

30. Dai, W., and Nassar, R., 2001, "A compact finite difference scheme for solving a one-dimensional heat transport equation at the micro-scale," *Journal of Computational and Applied Mathematics*, **132**, pp. 431-441.

31. Dai, W., and Nassar, R., 2000, "A compact finite difference scheme for solving a three-dimensional heat transport equation in a thin film," *Numerical Methods for Partial Differential Equations*, **16**, pp. 441-458.

32. Dai, W., and Chen, C. D., 1989, "A three level difference schemes for two dimensional nonlinear parabolic differential equations," *Mathematica Numerica Sinica,* **11**, pp. 1-9. (Chinese)

33. Dai, W., 1992, "An unconditionally stable three level explicit difference scheme for the Schrodinger's equation with a variable coefficient," *SIAM J Numer Anal*, **29**, pp. 174-181.

34. Dai, W., and Nassar, R., 1999, "A finite difference method for solving the heat transport equation at the microscale," *Numer. Methods Partial Differential Equations*, **15**, pp. 698-708.

35. de Oliveria, J. E., Page, J. N., and Rosenberg, H. M., 1989, "Heat transfer by fracton hopping in amorphous materials," *Physical Review Letters*, **62**, pp. 780-783.

36. Douglas J., Gunn, J. E., 1964, "A general formulation of alternating direction methods," *Numer. Math.* **6**, pp. 428-453.

37. Elsayed-Ali, H.E., 1991, "Femtosecond thermoreflectivity and thermotransmissivity of polycrystalline and single-crystalline gold films," *Phys. Rev.* **B43**,pp. 4488-4491.

38. Elsayed-Ali, H.E., Norris, T. B., Pessot, M. A., and Mourou, G. A., 1987, "Time-resolved observation of electron-phonon relaxation in copper," *Phys. Rev. Lett.* **58**, pp. 1212-1215.

39. Fournier, D., and Boccara, A.C., 1989, "Heterogeneous media and rough surface: A fractal approach for heat diffusion studies," *Physica A*, **157**, pp. 587-592.

40. Fujimoto, J.G., Liu, J.M., and Ippen, E.P., 1984, "Femtosecond laser interaction with metallic tungsten and non-equilibrium electron and lattice temperature," *Phys. Rev.* **53**, pp. 1837-1840.

41. Graβmann, A., Peters, F., 1999, "Experimental investi-gation of heat conduction in wet sand," *Heat and Mass Transfer*, **35**, pp. 289-294.

42. Gefen, Y., Aharony, A., and Alexander, S., 1983, "Anomalous diffusion on percolating clusters," *Physical Review Letters*, **50**, pp. 77-90.

43. Groeneveld, R. H. M., Sprik, R., Witterbrood, M., and Lagendijk, A., 1990, "Ultrafast relaxation of electrons probed by surface plasmons at thin silver film," In *Ultrafast phenomena VII* (Edition by C. B. harris et al.), pp. 368-370.

44. Gurtin, M. E. and Pipkin, A. C., 1968, "A general theory of heat conduction with finite wave speeds," *Arch. Rat. Mech. Anal.*, **33**, pp. 113-126.

45. Guyer, R. A., and Krumhansl, J. a., 1966, "Solution of the linearized Boltzmann equation," *Physical Review*, **148**, pp. 766-778.

46. Hanreich, G., Nicolics, J., and Stangl, G., 2000, "Investigation of the thermal performance of micro-whisker structured silicon heat spreaders for power devices," *Microelectronics Journal*, **31**, pp. 969-973.

47. Herwig, H., Beckert, K., 2002, "Experimental evidence about the controversy concerning Fourier or non-Fourier heat conduction in materials with a nonhomogeneous inner structure," *Heat and Mass Transfer*, **36**, pp. 387-392.

48. Jagannathan, A., Orbach, R., and Entin-Wohlman, O., 1989, "Thermal conductivity of amorphous materials above the plateau," *Physical Review B*, **39**, pp. 13465-13477.

49. Joseph, D. D. and Preziosi, L., 1989, "Heat waves," *Reviews of Modern Physics*, **61**, pp. 41-73.

50. Joseph, D. D. and Preziosi, L., 1990, "Addendum to paper Heat waves," *Reviews of Modern Physics*, **62**, pp. 375-391.

51. Jou, D., Casas-Vazquez, J., and Lebon, G., 1988, "Extended irreversible thermodynamics," *Reports on Progress in Physics*, **51**, pp. 1105-1179.

52. Kagnov, M I., Lifshitz, I. M., and Tanatarov, M. V., 1957, "Relaxation between electrons and crystalline lattices," *Soviet Physics JETP*, **4**, pp. 173-178.

53. Kaliski, S., 1965, "Wave equation of heat conduction," *Bull. Acad. Pol. Sci.*, **XIII(4)**, pp. 211-219.

54. Kaminski, W., 1990, "Hyperbolic heat conduction equation for materials with a nonhomogeneous inner structure," *International Journal of Heat and Mass Transfer*, **112**, pp.555-560.

55. Kittell, C., 1986, "Introduction to solid state physics", 6th Edn. Wiley, New York.

56. Koshland, D.E., 1991, "Special section: Engineering a small world, from atomic manipulation to microfabrication," Science **254**, pp. 1300-1342.

57. Korner, C., Bergmann, H. W., 1998, "The physical defects of the hyperbolic heat conduction equation," *Appl. Phys. A*, **67**, pp. 397-40.

58. Lee, M., 1961, "Alternating direction and semi-explicit difference scheme for parabolic partial differential equations," *Numer Math*, **3**, pp. 398-412.

59. Lin, C.K, Hwang, C.C., and Chang, Y.P., 1997, "The unsteady solution of a unified heat conduction equation," *International Journal of Heat and Mass Transfer*, **40**, pp. 1716-1719.

60. Majumdar, A., 1992, "Role of fractal geometry in the study of thermal phenomena," *Annual Review of Heat Transfer*, **IV**, Edited by Tien, C. L., Hemisphere, Washington, D. C, pp. 51-110.

61. Mitra, K., Kumar, S., Vedavarz, S., Moallemi, M. K., 1995, "Experimental evidence of Hyperbolic Heat Conduction in Processed Meat," *ASME Journal of Heat Transfer*, **117**, pp.568-573.

62. Narayan, J., Godbole, V.P., and White, G.W., 1991, "Laser method for synthesis and processing of continuous diamond films on nondiamond substrates," *Science* **52**, pp. 416-418.

63. Özisik, M.N., and Tzou, D.Y., 1994, "On the wave theory in heat conduction," *ASME Journal of Heat Transfer*, **116**, pp. 526-536.

64. Peshkov.V., 1969, "Second sound in Helium II," *Journal of physics USSR*, **91**, pp. 543 54.

65. Qiu, T. Q., Tien, C. L., 1992, "Short-pulse laser heating on metals," *International Journal of Heat and Mass Transfer*, **35**, pp. 719-726.

66. Qiu, T. Q., Tien, C. L., 1993, "Heat transfer mechanisms during short-pulse laser heating of metals," *ASME Journal of Heat Transfer,* **115**, pp. 835-841.

67. Qiu, T. Q., Juhasz, T., Suarez, C., Bron, W. E., and Tien, C. l., 1994, "Femtosecond laser heating of multi-layered metals- II. Experiments," *International Journal of Heat and Mass Transfer*, **37**, pp. 2799-2808.

68. Kumar, R. R., Kunadian, I., McDonough J. M., Menguc, M. P., 2004, "Efficient numerical solution to 3D microscale heat transport equation," to be submitted to *Journal of Computational Physics*.

69. Taitel, Y., 1972, "On the Parabolic, hyperbolic and discrete formulation of the heat conduction equation," *International Journal of Heat and Mass Transfer*, **15**, pp.369-371

70. Tang, D.W., and Araki, N., 1999, "Wavy, wavelike, diffusive thermal responses of finite rigid slabs to high-speed heating of laser-pulses," *International Journal of Heat and Mass Transfer*, **42**, pp. 855-860.

71. Tzou, D. Y., 1996, "*Macro-to-Microscale Heat Transfer: The Lagging Behavior*," Taylor and Francis, Washington, DC.

72. Tzou, D. Y., 1995, "A unified approach for heat conduction from macro-to micro scales," *ASME Journal of Heat Transfer,* **117**, pp. 8-16.

73. Tzou, D. Y., 1995, "The generalized lagging response in small-scale and high-rate heating," *International Journal of Heat and Mass Transfer*, **38**, pp. 3231-3240.

74. Tzou, D. Y., 1995, "Experimental support for lagging behavior in heat propagation," *J. Thermophysics and Heat transfer*, **9**, pp.686-693.

75. Tzou, D. Y., and Chiu, K. S., 2001, "Temperature-dependent thermal lagging in ultrafast laser heating," *International Journal of Heat and Mass Transfer*, **44**, pp. 1725-1734.

76. Vernotte, P., 1958, "Les panadoxes de la theorie continue de l'equation de la chaleur," *C.r.acad.Sci.Paris*, **246**, pp.3154-3155.

77. Wang, L., Xu, M., and Zhou, X., 2001, "Well-posedness and solution structure of dual-phase-lagging heat conduction," *International Journal of Heat and Mass Transfer* **44**, pp. 1659-1669.

78. Wang, L., and Zhou, X., 2001, "Dual-Phase-Lagging Heat Conduction: Problems and Solutions," *Shandong University Press, Jinan.*

79. Wang, L., and Zhou, X., 2000, "Dual-Phase-Lagging Heat Conduction," *Shandong University Press, Jinan.*

80. Zhang. J., Zhao J. J., 2001, "Unconditionally stable finite difference scheme and iterative solution of 2D microscale heat transport equation," *Journal of Computational Physics*, **170**, pp. 261-275.

81. Zhang. J., Zhao J. J., 2001, "Iterative solution and finite difference approximations to 3D microscale heat transport equation," *Mathematics and Computers in Simulation*, **57**, pp. 387-404.

VITA

Illayathambi Kunadian

Born May 23rd, 1979 in Chennai, India.

Education

Master of Science, Mechanical Engineering, August 2002 - May 2004

UNIVERSITY OF KENTUCKY, Lexington, KY, USA.

Bachelor of Science, Mechanical Engineering, July 1998 - May 2002

ANNA UNIVERSITY, Chennai, India.

Professional Positions Held

Research Assistant, Fall 2002 - Summer 2004

Advanced Computational Fluid Dynamics Group

Department of Mechanical Engineering, University of Kentucky, Lexington, KY.

Teaching Assistant, Fall 2002 - Spring 2004

Department of Mechanical Engineering, University of Kentucky, Lexington, KY.

Graduate Assistant, Summer 2003

Agricultural and Biosystems Engineering, University of Kentucky, Lexington, KY.

Scholastic Honors

Teaching Assistantship, Fall 2002 - Spring 2004

University of Kentucky, Lexington, KY.

Kentucky Graduate Scholarship, Fall 2002 - Spring 2004

University of Kentucky, Lexington, KY.

Professional Society Membership

American Institute for Aeronautics and Astronautics

American Society of Mechanical Engineers

Papers and Conferences

1. Kunadian I., J. M. McDonough, K. A. Tagavi, "Numerical simulation of heat transfer mechanisms during femtosecond laser heating of nano-films using 3-D dual phase lag model," 2004 ASME Heat Transfer/Fluids Engineering Summer Conference, Charlotte, North Carolina, July 11-15, 2004.
2. Kunadian I., McDonough J. M., Tagavi K. A., "Numerical analysis of thermal transport phenomena in nano-scale metal films irradiated by pulsating laser using 3-D dual phase lag model," ASME Region VI Graduate Student Technical Conference, Lexington, Kentucky, March 27, 2004.
3. Kunadian I., J. M. McDonough, K. A. Tagavi, "Numerical simulation of heat transfer mechanisms during femtosecond laser heating of nano-films using 3-D dual phase lag model," Dayton-Cincinnati Aerospace Science Symposium, Dayton, OH, March 3, 2004.

Undergraduate Projects

1. Optimization of locating pins to produce minimum deformation of the work piece-Experimental and ANSYS simulation, May 2002.
2. Design and fabrication of *manipulator* for physically challenged people, December 2001.